

COMPUTATIONAL AND ROBOTIC MODELS OF
HUMAN POSTURAL CONTROL

by

Arash Mahboobin

B.S., Azad University, 1998

M.S., University of Illinois at Urbana–Champaign, 2002

Submitted to the Graduate Faculty of
the School of Engineering in partial fulfillment
of the requirements for the degree of

Doctor of Philosophy

University of Pittsburgh

2007

UNIVERSITY OF PITTSBURGH
SCHOOL OF ENGINEERING

This dissertation was presented

by

Arash Mahboobin

It was defended on

November 20, 2007

and approved by

P. J. Loughlin, Ph.D., Department of Electrical and Computer Engineering

M. S. Redfern, Ph.D., Department of Bioengineering

C. G. Atkeson, Ph.D., The Robotics Institute, Carnegie Mellon University

J. R. Boston, Ph.D., Department of Electrical and Computer Engineering

A. A. El-Jaroudi, Ph.D., Department of Electrical and Computer Engineering

Z-H. Mao, Ph.D., Department of Electrical and Computer Engineering

P. J. Sparto, Ph.D., Department of Physical Therapy

Dissertation Director: P. J. Loughlin, Ph.D., Department of Electrical and Computer
Engineering

Copyright © by Arash Mahboobin
2007

ABSTRACT

**COMPUTATIONAL AND ROBOTIC MODELS OF HUMAN POSTURAL
CONTROL**

Arash Mahboobin, PhD

University of Pittsburgh, 2007

Currently, no bipedal robot exhibits fully human-like characteristics in terms of its postural control and movement. Current biped robots move more slowly than humans and are much less stable. Humans utilize a variety of sensory systems to maintain balance, primary among them being the visual, vestibular and proprioceptive systems. A key finding of human postural control experiments has been that the integration of sensory information appears to be dynamically regulated to adapt to changing environmental conditions and the available sensory information, a process referred to as “sensory re-weighting.” In contrast, in robotics, the emphasis has been on controlling the location of the center of pressure based on proprioception, with little use of vestibular signals (inertial sensing) and no use of vision. Joint-level PD control with only proprioceptive feedback forms the core of robot standing balance control. More advanced schemes have been proposed but not yet implemented. The multiple sensory sources used by humans to maintain balance allow for more complex sensorimotor strategies not seen in biped robots, and arguably contribute to robust human balance function across a variety of environments and perturbations. Our goal is to replicate this robust human balance behavior in robots.

In this work, we review results exploring sensory re-weighting in humans, through a series of experimental protocols, and describe implementations of sensory re-weighting in simulation and on a robot.

TABLE OF CONTENTS

PREFACE	xi
1.0 INTRODUCTION	1
2.0 BACKGROUND	4
2.1 MOTIVATION AND SIGNIFICANCE	4
2.2 CURRENT MODELS OF HUMAN POSTURAL CONTROL	5
2.2.1 Postural Control Models I: Sensory Re-weighting	6
2.2.2 Postural Control Models II: Optimal Estimation and Control	9
3.0 POSTURAL CONTROL AND SENSORY RE-WEIGHTING I	15
3.1 POSTURAL CONTROL MODEL DESCRIPTION	15
3.1.1 Steady-state vs. Transient Conditions	18
3.2 BACKGROUND: SENSORY RE-WEIGHTING IN YOUNG ADULTS	21
4.0 POSTURAL CONTROL AND SENSORY RE-WEIGHTING II	23
4.1 EXPERIMENT I: MOVING-SCENE PERTURBATIONS	23
4.1.1 Abstract	23
4.1.2 Introduction	24
4.1.3 Methods	25
4.1.4 Results	29
4.1.5 Discussion	33
4.2 EXPERIMENT II: ATTENTION AND SENSORY INTEGRATION	36
4.2.1 Abstract	36
4.2.2 Introduction	36
4.2.3 Methods	38

4.2.4	Results	44
4.2.5	Discussion	45
5.0	A MECHANISM FOR SENSORY RE-WEIGHTING	48
5.1	INTRODUCTION	48
5.2	BACKGROUND	49
5.2.1	Human Postural Control Model with Eyes-closed	49
5.3	DYNAMIC SENSORY RE-WEIGHTING ALGORITHM	52
5.4	SIMULATIONS AND ANALYSIS	53
5.4.1	Model Simulations	53
5.4.2	Signal Analysis	54
5.5	RESULTS	55
5.6	DISCUSSION	59
6.0	ROBOT EXPERIMENTS	63
6.1	ROBOT EXPERIMENT I	63
6.2	ROBOT EXPERIMENT II	65
6.2.1	Balance Control In An Optimization Context	65
6.2.2	Model Simulations vs. Experimental Results	72
6.2.3	Discussion	74
6.3	ROBOT EXPERIMENT III	76
6.3.1	Discussion	79
7.0	CONCLUSIONS AND FUTURE WORK	81
APPENDIX A.	PENDULUM EQUATIONS OF MOTION	83
A.1	EULER-LAGRANGE METHOD	83
A.2	DERIVATION WITH RESPECT TO HORIZONTAL REFERENCE	84
A.3	DERIVATION WITH RESPECT TO VERTICAL REFERENCE	88
APPENDIX B.	SENSORY DIFFERENCE THRESHOLD	91
APPENDIX C.	POSTURAL CONTROL MODEL WITH ESTIMATION	92
APPENDIX D.	MATLAB CODES AND SIMULINK MODELS	97
D.1	MATLAB CODES	97
D.1.1	PARAMETER SETUP	97

D.1.2 ADAPTIVE SENSORY WEIGHT S-FUNCTION	98
D.1.3 PLATFORM MOTION CONTROL S-FUNCTION	101
D.1.4 SENSORY CHANNEL NOISE FILTER DESIGN	103
D.1.5 PARAMETER SETUP FOR MODEL WITH ESTIMATION	104
D.2 SIMULINK MODELS	106
BIBLIOGRAPHY	108

LIST OF TABLES

1	Postural control time delay and proprioceptive weight	45
---	---	----

LIST OF FIGURES

1	Block diagram representation of human postural control model: format I . . .	8
2	Block diagram representation of human postural control model: format II . . .	10
3	Block diagram representation of human postural control model: format III . . .	12
4	Human postural control model	17
5	Schematic representation of the sensory re-weighting hypothesis	19
6	Frequency response plots for the human postural control model	20
7	Time series and corresponding time-varying spectra of an example subject . . .	22
8	Moving-scene experimental setup and visual stimuli	27
9	Ensemble average time series of AP-COP velocity	31
10	Ensemble average peak-squared velocity of AP-COP	32
11	Human postural control model for eyes-closed stance	39
12	Platform motion used in attention and sensory integration experiment	41
13	Normal change in time delay and proprioceptive weight	46
14	Human postural control model including sensory difference strategy	50
15	Example model simulations for fast and slow weight adjustments	56
16	Time-varying spectra of example experimental data	57
17	High- to low-frequency energy ratios	58
18	Model simulations using alternative sensory difference strategy	61
19	Experimental setup and robot simulations	64
20	Model for standing balance	66
21	External disturbance applied to the ankle	72
22	Model simulations using the model for standing balance	74

23	Experimental setup for robot experiment III	76
24	Control trial with constant sensory weights	77
25	Robot simulations using the sensory difference strategy	78
26	High- to low-frequency energy ratios for robot experiments	79
27	Frequency response plots using robot parameters	80
28	Single-link inverted pendulum with respect to horizontal reference	85
29	Single-link inverted pendulum with respect to vertical reference	88
30	Human postural control model with estimation	93
31	Energy ratios with nominal neural controller values	95
32	Energy ratios with increased neural controller values	96
33	Simulink implementation of the human postural control model	106
34	Platform control subsystem	106
35	Proprioceptive and graviceptive channel noise subsystems	107
36	Simulink implementation of the human postural control model with estimation	107

PREFACE

I would like to express my deepest gratitude to all the members of the dissertation committee – Profs. Atkeson, Boston, El-Jaroudi, Loughlin, Mao, Redfern and Sparto – for their encouragement and guidance. I am particularly grateful to Dr. Chris Atkeson of Carnegie Mellon University for providing me with the opportunity to work at the Robotics Institute at CMU, and for his enthusiastic input on this work. Also, I am profoundly grateful to Stuart Anderson at CMU for putting a tremendous amount of time into helping me with the robot experiments. Quite frankly, without Stuart the robot experiments would have not been possible.

My thanks and gratitude also goes to Dr. Mark Redfern for his confidence in me and most of all his generosity towards me. Thank you for all your kindness in the past five years.

I am also grateful to Dr. Patrick Sparto for his assistance and guidance on the human experiments, and helpful comments on my dissertation.

Thanks as well to Drs. Boston, El-Jaroudi and Mao for their service on my PhD committee and their valuable feedback on my dissertation.

Last but not least I would like to thank Dr. Patrick Loughlin, my advisor, for all the contributions, help, and encouragement that he continually and magnanimously provided in the past five years. I will always cherish the work-related advice and fondly remember the Monty Python-related jokes.

This research was funded in part by grants from the National Institutes of Health, and the Pittsburgh Claude D. Pepper Older Americans Independence Center.

1.0 INTRODUCTION

This work describes mechanisms used by humans to stand on moving platforms, and to combine body orientation and motion information from multiple sensors including vision, vestibular, and proprioception. A key finding of human postural control experiments has been that the integration of sensory information appears to be dynamically regulated to adapt to changing environmental conditions and the available sensory information, a process sometimes referred to as “sensory re-weighting” [24, 82, 84, 102, 49, 36, 76, 50]. This simple mechanism has been proposed to explain how human subjects learn to reduce the effects of a moving support platform on balance. Our goal is to replicate this robust balance behavior using a computational model of postural control in bipedal (humanoid) robots, during quiet stance, and experimentally validate the model.

Sensory re-weighting provides a way to combine many sensory systems. As just mentioned, humans use proprioception, inertial sensing (vestibular), and vision to stand robustly. Robots typically rely on only one or two sensory systems. Another function of sensory re-weighting is to handle inconsistent or malfunctioning sensors. To date, models of this process are conspicuously absent from work on human balance control, and are necessary for robot balance control. An important step towards robust robot behaviour is developing mechanisms to handle erroneous, inconsistent, or malfunctioning sensors.

In this dissertation we explore sensory re-weighting in humans, simulation, and in a robot implementation. Results from three human experiments that investigate sensory re-weighting are presented. In the first experiment, performed by Peterka and Loughlin [84], transient periods of low- or high-frequency oscillations in the body sway of healthy young adults were observed under conditions where the sensory input to the postural control system was deliberately altered [84]. Simulations obtained from a simple feedback postural control

model of these experimental conditions resulted in a good match between model predictions and experimental results inspiring confidence in the model capturing important attributes of sensorimotor integration (i.e., sensory re-weighting) in postural control. This work provides a foundation for our research and is summarized in Section 3.2.

In an experiment that we performed, the effect of continuous moving-scene perturbations on postural responses was investigated [50]. It was observed that exposure to prolonged continuous visual perturbation while standing on a moving platform (proprioceptive perturbation) would cause sensory re-weighting resulting in reduced reliance on visual sensory information.

In another experiment, we examined the impact of attention on balance in young and older adults. The interaction between attention and sensory integration was explored through a dual-task experiment involving information processing (IP) tasks concurrent with postural perturbations [54]. The novel idea about this experiment is its attempt to quantitatively model the effects of performing a concurrent cognitive task on balance control. This was achieved by applying a computational model of postural control incorporating attention to test specific hypotheses. Changes in sensory re-weighting was observed during postural challenges with concurrent IP tasks, compared to baseline (i.e., no IP task) conditions, in the older adults.

While no single model currently explains all aspects of human postural control, the feedback postural control model presented in the first experiment has been shown to accurately fit experimental data. Moreover, the model provides a conceptually simple, yet experimentally supported, concept of sensory re-weighting. However, the model doesn't describe how sensory weights change under different environmental conditions. An important question to be addressed is how sensory re-weighting might be accomplished. By extending this feedback postural control model, we discuss one possible strategy that we believe is physiologically plausible. The approach is based on a comparison between sensory channels, in order to determine disagreement between the channels with respect to sensed body sway. Model simulations using this strategy are compared to experimental data reported in [84].

To date, no bipedal robot exhibits fully human-like characteristics in terms of its postural control and movement. Our aim is to develop a bipedal robot that implements a sensory

integration strategy similar to that believed to occur in humans, resulting in postural sway characteristics that mimic human sway under a variety of experimental conditions. We present a series of three robot experiments by first implementing a preliminary manual sensory re-weighting control strategy similar to that described in [82, 84], a manual sensory re-weighting control strategy in an optimal filtering and control context [55], and finally an automatic sensory re-weighting control strategy based on the proposed sensory difference approach.

2.0 BACKGROUND

2.1 MOTIVATION AND SIGNIFICANCE

Humans utilize a variety of sensory systems to maintain balance, primary among them being the visual, vestibular (graviceptive), and proprioceptive systems. Several studies have demonstrated that human standing posture is affected by perturbations to these sensory systems [17, 24, 31, 34, 42, 80], suggesting that feedback control, based on perceived body motion, contributes to postural stability. There is redundancy across these sensory systems and the organization of these feedback control mechanisms is not fully known. Also, there is some question as to whether feedback alone is sufficient for human postural control [20, 66], although recent studies have shown that a postural control strategy based solely on sensory feedback can account for experimental findings involving a variety of proprioceptive and visual perturbations to postural control [82, 84].

A key finding of human postural control experiments has been that the integration of sensory information appears to be dynamically regulated to adapt to changing environmental conditions and the available sensory information, a process sometimes referred to as “sensory re-weighting” [24, 82, 84, 102, 49, 36, 76, 50]. For example, during eyes-closed stance on a fixed, level surface, the primary sensory source for information about body orientation in space is proprioceptive, but under conditions where the platform moves, the primary source of sensory information shifts from proprioceptive to graviceptive/vestibular [82].

Current biped robots move more slowly than humans and are much less stable [73, 68, 46, 22, 32, 74]. The control algorithms are typically not designed to handle large perturbations or ambiguous sensory information, two components often seen in human balance experiments and daily activity. Instead, the floor is assumed to be level, stiff, and not in motion.

Independent and decoupled simple linear controllers for each joint (joint-level proportional-derivative (PD) control) with only proprioceptive feedback form the core of robot standing balance control, where perturbations small enough that decoupled linear control is adequate. Some robots use force control to implement a more compliant ankle [22, 33, 44] which is useful for stepping on uneven terrain, but not for standing vertically. There is only one response strategy to choose from, typically using ankle torques to adjust the center of pressure (referred to as the “ankle strategy” in human postural control jargon). One exception to this are the Honda robots, which can take a step in response to a large perturbation [22]. More advanced schemes have been proposed but not yet implemented [23, 27, 38].

We note a major difference between current robots and humans in how balance is maintained. In robotics, the emphasis has been on controlling the location of the center of pressure based on proprioception, with little use of vestibular signals (inertial sensing) and no use of vision. In humans, vestibular and visual signals are also important [82]. The multiple sensory sources allow for more complex sensorimotor strategies not seen in biped robots, and arguably contribute to robust human balance function across a variety of environments and perturbations.

2.2 CURRENT MODELS OF HUMAN POSTURAL CONTROL

Human postural control (HPC) has been studied for over fifty years, with conceptual and computational models being developed. These models have led to advances in the diagnosis and management of balance disorders. A variety of models have been proposed and continue to be developed (e.g., [31, 82, 102, 39, 101, 81, 83, 64, 40]).

Computational models can aid researchers in understanding and explaining complex systems. In fields such as human postural control, where the ultimate goal is maintaining upright balance under different external perturbations (e.g., platform movements), models can help predict possible outcomes of the human postural system that can later be evaluated experimentally. Models can also help in analyzing and explaining data obtained from experi-

ments performed on the body or can simply be used as a tool for designing new experiments. Other benefits of modeling are in allowing a systematic manipulation of certain (desired) parameters that can then be fine-tuned using experimental data.

There have been numerous modeling contributions in the field of human postural control. The current standing human postural control models mainly focus on *sensory integration* (e.g., [82, 84, 101, 102]), *motor strategy response* (namely the ankle and hip strategies [39, 40, 78]), and *cognitive interactions* [51, 52, 53, 54]. Recent work has begun to incorporate time-varying and non-linear aspects of the human postural system into these models [63, 64, 60]. However, there are few models that attempt to incorporate the dynamics of the sensory and motor systems into the postural control system. Also, current models of standing balance are incomplete and experiment-orientated, that is, they try to answer questions to specific details of a single experiment or perturbation design. There is a need for more complex, complete, and unifying models that incorporate sensorimotor dynamics.

Model of human postural control can be broadly categorized based on the type of control process they adopt: models that utilize proportional-integral-derivative (PID) control (or PD control) [30, 102, 81, 82, 84], and models that use optimal filtering and control [39, 101, 78]. A brief and in depth description of some of these models that are of interest in this work are presented in the subsequent sections and chapters, respectively.

2.2.1 Postural Control Models I: Sensory Re-weighting

Currently, the complete nature of the human postural control system is unknown and open to speculation. However, as mentioned in the preceding section, it is known that upright posture in healthy humans is maintained via control-like strategies, e.g., feedback control, based on information provided by three main sensory systems, namely, the vestibular (graviceptive), visual, and proprioceptive (ankle) sensory systems [70, 43, 48, 101, 82]. Each of these sensory systems is believed to operate in a specific frequency range with redundancies amongst them that help the body maintain an upright position under conditions where information from one or more sensory cues is either not available or inaccurate [85]. As the body deviates from an equilibrium position (upright stance) a gravity-induced torque acts to drive it further from

equilibrium in the absence of any counter torque. In order to maintain balance the body has to generate a corrective torque opposing the torque induced by the force of gravity. To generate such a corrective torque the body relies on the information provided by the sensory cues. This information is then integrated in the central nervous system (CNS), which can be thought of as the control center, to generate the required corrective torque to maintain balance.

The utility of each sensory system depends upon environmental conditions and the reliability of sensory orientation and movement information. In the absence of particular sensory information or in conditions where sensory information is inaccurate, it is hypothesized that the CNS varies the primary source of sensory information to compensate this loss [72, 58]. In other words, dynamic regulation or re-weighting of the sensory cues enables the body to maintain upright stance under different environmental conditions [24]. The relative contribution of the aforementioned sensory systems to maintaining an upright posture and the dependence of the postural control system on them under different environmental conditions are reported in various studies, e.g., [72] and [6], in which it was shown that perturbing individual sensory systems (visual and proprioceptive) in healthy adults caused a small increase in body sway compared to perturbing multiple sensory systems simultaneously, which resulted in larger body sways. Under such conditions, that is, simultaneous perturbation of the visual and proprioceptive sensory systems, in healthy adults, it is hypothesized that the body relies on the vestibular (graviceptive) system to maintain balance. This reliance was not seen in patients with vestibular deficits, and exposure to simultaneous stimuli caused loss of balance in this population. Recent studies have also supported the sensory regulation or re-weighting hypothesis that the relative contribution of the sensory systems involved in maintaining balance are adjusted according to environmental conditions that impact the accuracy or reliability of the sensory information [82, 84, 102, 12].

Figure 1 shows a schematic representation of a dynamically regulated feedback control model proposed by Peterka [82]. The model¹ purely uses feedback control to maintain upright stance. The corrective torque generated about the ankle joint is dependent upon orientation

¹A comprehensive description of this model is presented in Chapter 3.

cues provided by the various sensory systems (vestibular, visual, proprioceptive) involved in the human body. Prior to any torque generation, these sensory cues are weighted (sensory re-weighting) and summed up in the CNS.

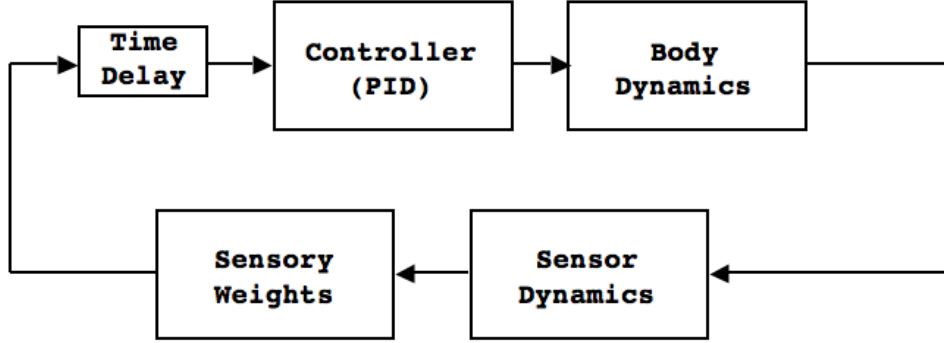


Figure 1: Block diagram of feedback control model proposed by Peterka [82]. The body is modeled as a linearized inverted pendulum. The Sensory Weights includes variable sensory weights, namely the graviceptive (vestibular), visual, and proprioceptive (W_g, W_v, W_p) that change as environmental factors change. Corrected torque about the ankle is generated by a PID controller with fixed gains

The body dynamics are modeled as a linearized single-link inverted pendulum and the corrective torque (active torque) generated about the ankle joint is provided by a PID controller with constant, that is, time-invariant, gains. To stabilize an inverted pendulum the corrective torque requires only two of the three components of a PID controller: the proportional component K_P , or the stiffness factor, which relates the output of the controller, $u(t)$, and the actuating error signal, $e(t)$, proportionally ($u(t) = K_P e(t)$), and the derivative component K_D , or the damping factor, where the rate of change of the error signal is proportional to the controller output ($u(t) = K_D \frac{de}{dt}$). The integral component K_I (swiftness factor), where the rate of change of the controller output is proportional to the error signal ($\frac{du}{dt} = K_I e(t)$ or $u(t) = K_I \int e dt$), is used for low frequency error correcting properties and it is not necessary for stability [30, 82]. To incorporate sensory transduction, neural processing and transmission, muscle activation, and force development delays, an effective overall time delay is implemented in the model.

The contribution of each sensory system is determined by variable (dynamic) sensory weights (W_g, W_v, W_p). These weights represent the relative contribution of the graviceptive (vestibular), visual, and proprioceptive (ankle) sensory systems to torque generation about the ankle joint, and are determined by utilizing system identification techniques. The model assumes that under steady-state conditions the sum of the sensory weights is unity ($W_g + W_v + W_p = 1$). When this condition is satisfied, body sway in response to an external perturbation is non-resonant, that is, there is no significant oscillatory behavior. But when this condition is not met, which can occur when sensory information is altered, oscillatory behavior presents itself in the system.

Although the model is capable of producing accurate fits of body sway in response to steady-state visual and platform conditions [82] as well as transient conditions [84], it doesn't describe how sensory weights change under different environmental conditions². Also, it is assumed that all the sensory systems included in the model have no dynamic behavior, that is, they are static over the bandwidth of body sway movement. Hence, a need for more sophisticated models is apparent. Such model that include sensor dynamics and use optimal estimation to provide a best estimate of body orientation from noisy sensors, have been proposed in the literature [101, 102, 39, 40, 78]. The next section provides a brief description of these models.

2.2.2 Postural Control Models II: Optimal Estimation and Control

The first two models considered are the models proposed by van der Kooij et al. [101, 102]. Both models consist of four main components (see Figure 2 for a schematic representation of both models³): **a) *body dynamics***: based on a three-link model (including shank, thigh, and trunk) of a standing human on a support base capable of translating and rotating about the ankle joint (model **A**), later reduced to a linearized single-link inverted pendulum (model **B**), **b) *sensory dynamics***: including transfer functions representing five different sensory system: muscle spindles, sensing joint angle and angular velocity; otolith organs, sensing

²An approach addressing this question is presented in Chapter 5.

³For ease of reference, we refer to the first model [101] as model **A** and the second model [102] as model **B**

translational acceleration of the head; semicircular canals, sensing rotational acceleration of the head; skin afferents (tactile), sensing shear and pressure forces in the sole of the foot; and the visual system, sensing the position and velocity of the head in space, **c)** *sensory integration center*: providing a best estimate of body orientation based on integration of available multisensory information; and **d)** *action control center*: providing muscle actions (corrective torque) based on information provided by the sensory integration center.

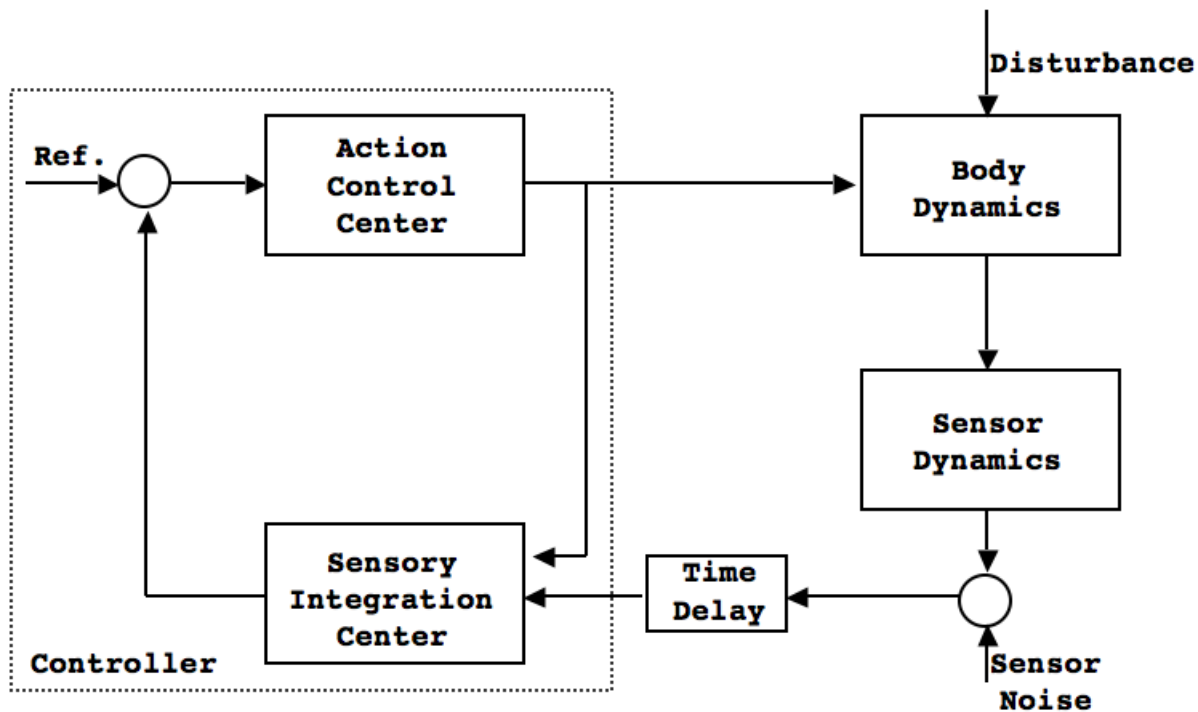


Figure 2: Block diagram of human stance control model proposed by van der Kooij et al. [101, 102]. Body dynamics describe a standing person on a support surface. Sensor dynamics relate sensory inputs to sensory outputs. The delayed sensory output plus sensor noise, and muscle actions are inputted to the sensory integration center, which makes the best estimate of body orientation. Based on this estimate, the action control center selects muscle actions in order to maintain an upright stance.

To account for inherent time delays in the human postural system the sensory integration center is subdivided into two parts: *estimation*, consisting of a Kalman filter to make a best estimate of the states for which sensory information is available, and *prediction*, a linear (least

mean-squared) predictor to make a prediction of the current state to compensate for time delays. Due to the nonlinear nature of model **A** the Kalman filter/linear predictor concept was extended to the nonlinear case by a tandem combination of an extended Kalman filter with a nonlinear predictor. In model **B**, where the system is linear, the extended Kalman filter is replaced by the standard Kalman filter and the predictor by a tapped delay line, basically a finite impulse response (FIR) filter [77]. In this model (model **B**) the statistics of the state noise (process noise) are assumed to be unknown and therefore estimated before computing the Kalman filter gain. The statistics of the sensor noise (measurement noise) are assumed to be constant and known. The controller introduced in model **A** is a linear quadratic regulator (LQR) which minimizes the usual quadratic objective (cost) function with weighting matrices Q and R . In model **B**, the LQR is replaced by a simple PD controller with constant gains. It is worth mentioning that an interesting aspect of the two models discussed is the inclusion of the dynamics of the environment in the overall human postural control model. Although, recent findings favor models that do not implicitly include internal dynamics of the environment (see e.g., [11]), more systematic examination of these concepts is essential in the development of complex models.

In the remainder of this chapter, we present two more models that utilize similar optimal estimation and control techniques used in [101, 102], but focus on incorporating the motor strategy responses identified in postural control, namely the ankle and hip strategies. In the model proposed by Kuo [39] (Figure 3), the CNS is modeled after the classical linear quadratic Gaussian (LQG) optimal controller with the usual LQR and linear quadratic estimator (LQE) components.

The design philosophy of this control system is similar to the van der Kooij model [101], where a desired state vector from higher levels of the CNS is compared with a measured state provided by the estimator which then leads to generating the motor command for maintaining an upright position. Unlike the van der Kooij models [101, 102], this model does not explicitly implement any sensor dynamics, and, the controller, that is the optimal control component, is designed independently from the estimator. The focus of this model is mainly on the optimal controller design, rather than optimal estimation, and implementation of the two main movement strategies identified in humans, namely the ankle and hip strategies

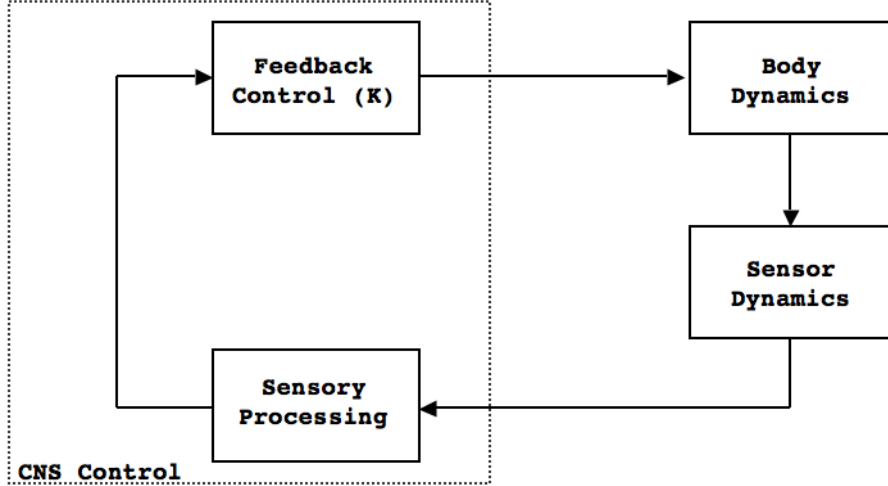


Figure 3: Block diagram of feedback control model proposed by Kou [39]. Body dynamics are modeled as a two-link inverted pendulum. The estimator uses the controller output and the sensory information to form the current state estimate, which is then fed to the controller to be compared to a desired reference state to generate a set of feedback gains.

[24, 25]. However, a newer version of this model has been introduced that includes sensor dynamics (graviceptive (vestibular), visual, proprioceptive (ankle and hip)) as well as an optimal state estimator to generate the best estimate of body’s angle and angular velocity [40].

The optimal controller u in [39] is obtained by minimizing a quadratic objective function of the form $J = \int_0^\infty x^T Q x + u^T R u$, where Q and R are the state and control weighting matrices, respectively. In this model the state weighting matrix Q is designed such that it only weights the joint angle deviations, excluding velocity terms. Also, the Q matrix is constructed in such a way that it is possible to consider biomechanical constraints on the body, such as center of mass (COM) position, upright body position, and head position. This is a nice feature of the model, where the constraints imposed are modeled such that it is still possible to remain in the LQR framework. Another feature of this model is the ability of the control selection center to choose between feedforward and feedback schemes proposed in the literature (see e.g., [71, 2]).

The body dynamics are modeled as a reduced-order four state system analogous to a two-joint system, namely a double-link inverted pendulum. To reduce the number of degrees of freedom of the system the controller is defined in the strategy space rather than joint-torque space. Since one of the constraints imposed on the body dynamics model is restriction of knee movement (basically it is assumed that the knees should be kept relatively straight), instead of being concerned with three joint torques (ankle, knee, and hip) the model is only concerned with two strategies, namely, the “ankle strategy” relating to movements predominantly about the ankle joint usually caused by small perturbations, and the “hip strategy” relating to flexion and extension of the hip joint usually caused by larger disturbances that put the COM near the perimeter of foot support.

Finally, recent work by Park et al. [78], incorporating elements of the model described above [39], has implemented a state feedback control model that includes variable gains set by the CNS depending upon the anticipated level of perturbation. The implications of this model are that the postural control system adapts to levels of perturbation, replacing the need for a library of motor responses with the need for a perturbation recognition system, which might be based on a library of experienced perturbations or perturbation templates. The model consists of body dynamics based on a three-link model (linearized) confined to the sagittal plane, a linear feedback controller (LQR) similar to the one proposed in [39], and an optimization procedure based on sequential quadratic programming (SQP) to minimize a quadratic objective function subject to nonlinear constraints that require stability of the closed-loop system at all times. The optimization procedure is utilized to determine the feedback control gain (\mathbf{K}) based on the hypothesis that the CNS is required to scale the feedback gains due to the presence of biomechanical constraints. In other words, in the absence of constraints, a set of fixed gains are sufficient to guarantee stability, or upright stance, but in the presence of constraints, gains appropriate for smaller perturbations (ankle strategy) might not be sufficient for larger perturbations (hip strategy). Hence, it is hypothesized that the CNS would scale the feedback gains as a function of the level of perturbation.

In summary, as mentioned earlier, a variety of models of human postural control have been proposed in the literature and continue to be developed. We plan to focus on *sensory*

integration (sensory re-weighting) models described above and implement these models in simulation and later apply them to a bipedal robot. However, we must note that these sensory (and motor) modeling approaches are not necessarily distinct and there can be an integration of these models.

3.0 POSTURAL CONTROL AND SENSORY RE-WEIGHTING I

In this chapter, we begin by providing a comprehensive description of the model of human postural control utilized extensively throughout the rest of this work. Then, in the following chapter (Chapter 4), we proceed by reporting experimental findings examining the sensory re-weighting hypothesis of the human postural control under different experimental conditions.

3.1 POSTURAL CONTROL MODEL DESCRIPTION

While no single model currently explains all aspects of human postural control, the model [82, 84] we consider in detail here has been shown to accurately fit experimental data in a variety of conditions, both steady-state [82] and transient [84]. Moreover, the model provides a conceptually simple, yet experimentally supported, concept of sensory adaptation/re-weighting (for which additional recent experimental evidence has been obtained [12]).

The model (Figure 4) consists of a linearized (i.e., small angle) single-link inverted pendulum representation of body dynamics (for completeness, a detailed derivation of the equations of motion is presented in APPENDIX A). Upright stance is maintained by a corrective torque applied about the ankle joint, generated by a proportional-integral-derivative (PID) controller, with fixed gain parameters K_P , K_I and K_D . Note that the model utilizes both position and velocity information to stabilize the inverted pendulum, consistent with control theory.

The parameters K_P and K_D represent the active stiffness and damping, respectively, of the postural control system. They are termed “active” because they generate corrective torque in response to an external perturbation, in contrast to passive stiffness and damping

of the muscles and tendons during quiet standing. The contributions of the passive stiffness and damping to torque generation have been found to be negligible during perturbations (a factor of ten smaller than the active torque generation) and can be dropped from the model [82, 83]. The parameter t_d in the model represents the effective time delay of the system, which includes combined delays due to sensory transduction, neural transmission, nervous system processing, muscle activation, and force development.

If all of the sensory systems are modelled as having no dynamics over the bandwidth of body sway movement (i.e., taken as unity), then

$$E(t) = W_v(VS(t) - BS(t)) + W_p(SS(t) - BS(t)) - W_g(BS(t)) \quad (3.1)$$

where BS, VS and SS are angles, with respect to earth-vertical, of the body, visual scene and support surface, respectively, as shown in the stick-figures and W_v , W_g and W_p are the sensory weights for the visual, graviceptive (vestibular), and proprioceptive sensory systems, respectively. For healthy subjects with intact sensory organs and perturbations limited in magnitude and bandwidth to those often used in experimental studies of human postural control (e.g., [82, 84]), this “no dynamics” assumption for the sensory systems is reasonable, and simplifies the sensory integration strategy, which is modelled via the sensory weights W_v , W_g and W_p . Unlike the fixed PID gains of the controller, the sensory weights can change with environmental conditions (the “sensory re-weighting” strategy). These sensory weights represent the relative contribution of each sensory channel to postural control.

For the model, the body sway (BS) in response to support surface (SS) or visual scene (VS) motion is given in the Laplace domain by

$$BS(s) = H(s)[W_p SS(s) + W_v VS(s)] \quad (3.2)$$

where s is the Laplace variable and

$$H(s) = \frac{(K_D s^2 + K_P s + K_I) e^{-s t_d}}{J s^3 - m g h s + \mathbf{W} (K_D s^2 + K_P s + K_I) e^{-s t_d}} \quad (3.3)$$

is the unity-gain transfer function of the postural control feedback model.

A key concept of the model and the sensory re-weighting hypothesis is the effective overall sensory weight, \mathbf{W} , of the system, which is the sum of the sensory weights of those channels

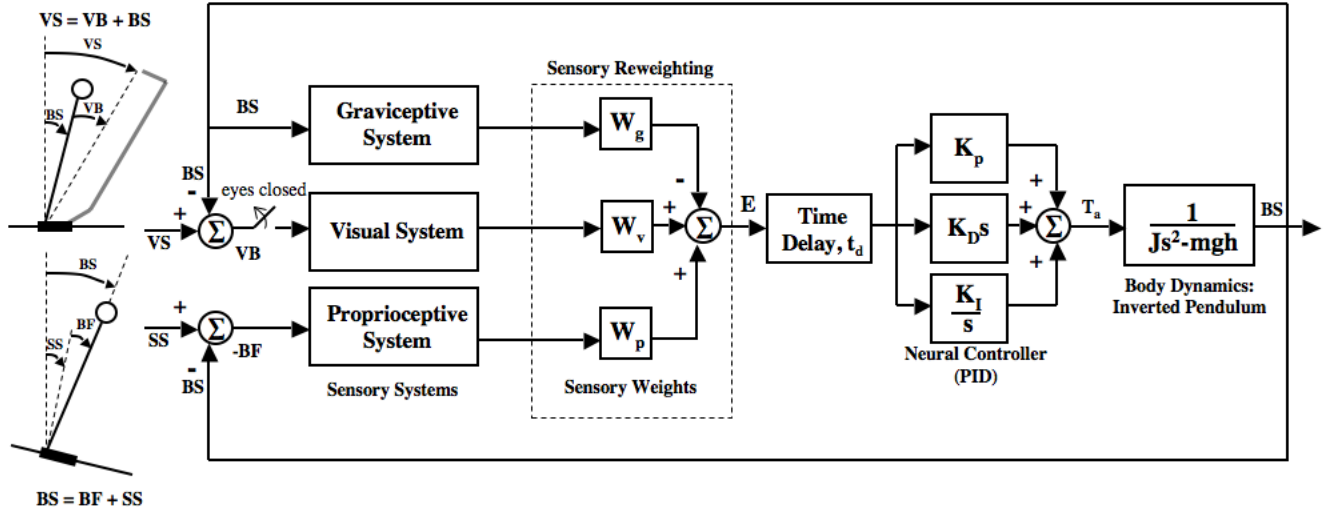


Figure 4: Feedback model of postural control. The body is modelled as a linearized inverted pendulum. The sensory pathways include variable sensory weights (W_g , W_v , W_p) that can change as environmental factors change (the “sensory re-weighting” hypothesis). BS, VS and SS are angles, with respect to earth-vertical, of the body, visual scene, and support surface, respectively, as shown in the stick-figures. VB and BF are the relative angles of the visual scene and the support surface with respect to the body. Corrective torque about the ankle, T_a , is generated by a proportional-integral-derivative (PID) controller with fixed gains K_P , K_D , K_I , acting on the combined delayed sensory error signal E. Modified from [82] and [84].

that contribute accurate sensory information about body sway. For example, the effective overall sensory weight is $\mathbf{W} = W_p + W_g + W_v$ during quiet standing on a fixed platform with eyes-open (Figure 5, left graph). But, for eyes-closed stance, the visual system does not contribute information about body sway, so the effective overall sensory weight in this case is $\mathbf{W} = W_p + W_g$ (Figure 5, middle graph). For stance on a sway-referenced platform, on which the support surface rotates in one-to-one proportion to body sway ($SS = BS$ in Figure 4), the proprioceptive channel does not contribute accurate information about body sway, so in this case the effective overall sensory weight is $\mathbf{W} = W_g + W_v$ under eyes-open condition and $\mathbf{W} = W_g$ under eyes-closed condition. Thus, the sensory weights that contribute to the effective overall sensory weight are different under different environmental conditions (i.e., under different manipulations of the sensory inputs). An important point to appreciate is that as the value of \mathbf{W} changes, the dynamics of body sway will change. In particular, during transient conditions the system can be pushed towards instability if sensory re-weighting is inadequate, causing \mathbf{W} to be too large or too small, as discussed further below.

3.1.1 Steady-state vs. Transient Conditions

As described above, the sensory re-weighting hypothesis holds that, under steady-state conditions, the effective overall sensory weight is unity, $\mathbf{W} = 1$ (this is a torque normalization constraint that results in non-oscillatory dynamics of body sway) [82]. For example, for stance with eyes closed on a fixed platform, $\mathbf{W} = W_p + W_g = 1$ during steady-state (Figure 5, middle graph). However, during transient conditions, in particular following a sudden change in the available sensory information, \mathbf{W} will differ from unity for a period of time until the sensory integration process adjusts the weights of the sensory systems to compensate for the transient change in sensory information [84]. For example, for the eyes-closed stance condition, if the platform suddenly transitions from fixed to sway-referenced, then the effective overall sensory weight becomes $\mathbf{W} = W_g$, and this is initially less than unity (Figure 5, right graph). If \mathbf{W} is not unity, then either too much or too little corrective torque will be generated and oscillatory sway will occur at specific frequencies. This oscillatory sway persists until the sensory integration process re-establishes $\mathbf{W} = 1$. The tendency of a system

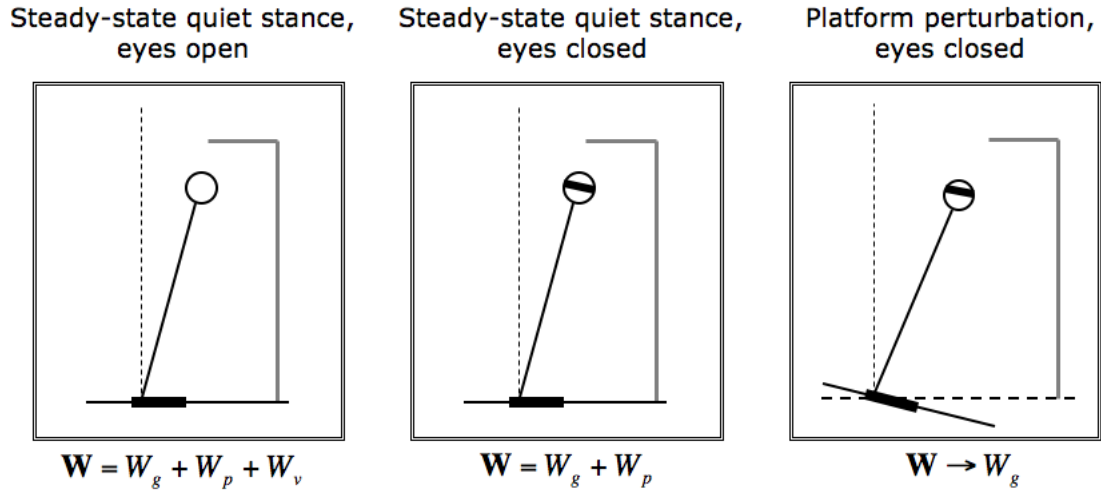


Figure 5: Schematic representation of the sensory re-weighting hypothesis and the corresponding effective overall sensory weight \mathbf{W} . The sensory re-weighting hypothesis holds that, under steady-state conditions, the effective overall sensory weight, which is the sum of the sensory weights of those channels that contribute accurate sensory information about body sway (BS), is unity. For example, for stance with eyes open on a fixed platform, $\mathbf{W} = W_p + W_g + W_v = 1$ (left graph) and under eyes closed on a fixed platform, $\mathbf{W} = W_p + W_g = 1$ during steady-state (middle graph). However, during transient conditions, in particular following a sudden change in the available sensory information, \mathbf{W} will differ from unity. For example, for the eyes-closed stance condition, if the platform suddenly transitions from fixed to sway-referenced, then the effective overall sensory weight becomes $\mathbf{W} = W_g$, and this is initially less than unity (right graph).

to oscillate at a particular frequency is called “resonance” and is reflected by a peak in the systems frequency response at that frequency; the sharper the peak, the more “resonant” is the system, meaning the stronger and more sustained are the oscillations. Increased resonance is characteristic of a system nearing instability. This effect of changes in the value of \mathbf{W} on the body sway that develops is illustrated in the frequency response magnitude plots shown in Figure 6. Note that the model predicts oscillatory body sway at specific frequencies if sensory re-weighting is inappropriate (\mathbf{W} less than or greater than one).

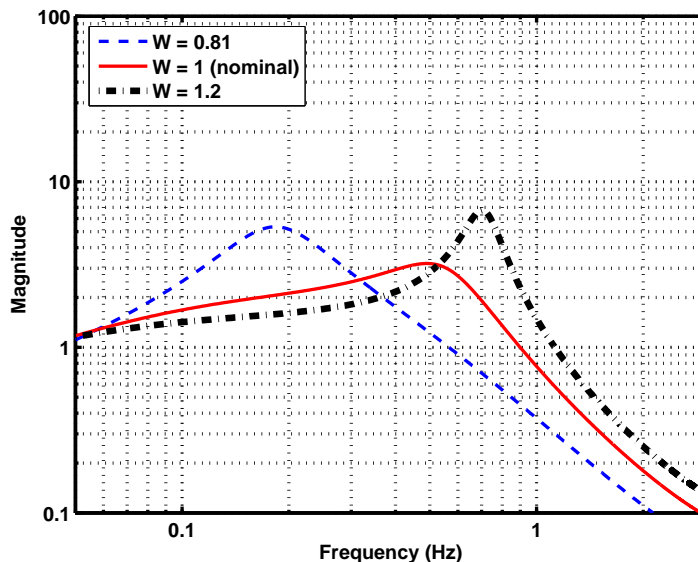


Figure 6: Frequency response plots for the postural control model, showing the effects of changes in the effective overall sensory weight, \mathbf{W} . Dotted curve is for $\mathbf{W} = 0.81$, solid is for $\mathbf{W} = 1$, dotted-dashed is for $\mathbf{W} = 1.2$. PID control parameters were the same in all cases ($K_P = 18.1 \text{ N} \cdot \text{m}/\text{deg}$, $K_I = 2.2 \text{ N} \cdot \text{m}/\text{deg} \cdot \text{sec}$, $K_D = 6.1 \text{ N} \cdot \text{m} \cdot \text{sec}/\text{deg}$), as were other physical parameters ($g = 9.8 \text{ m}/\text{s}^2$, $m = 83 \text{ Kg}$, $h = 0.9 \text{ m}$, $J = 81 \text{ Kg} \cdot \text{m}^2$). Note the changes in the frequency response as \mathbf{W} changes, and in particular the development of resonances (peaks in the frequency response) at particular frequencies for $\mathbf{W} > 1$ and $\mathbf{W} < 1$.

These results have been shown to be consistent with results obtained experimentally [84], in which transient periods of low- or high-frequency oscillations in the body sway of healthy young adults were observed (refer to Section 3.2 for details). The good match between model predictions and experimental results inspires some confidence that the model

captures important attributes of sensorimotor integration in postural control. However, the model doesn't describe how sensory weights change under different environmental conditions. An important question to be addressed is how sensory re-weighting might be accomplished. By extending this feedback postural control model, we discuss one possible strategy that we believe is physiologically plausible. The approach is based on a comparison between sensory channels, in order to determine disagreement between the channels with respect to sensed body sway. Model simulations using this strategy are compared to experimental data reported in [84].

3.2 BACKGROUND: SENSORY RE-WEIGHTING IN YOUNG ADULTS

Our final experiment reports on results obtained in a recent publication [84] in which a version of the postural control model introduced in the previous chapter is used to explain the experimental data through a sensory re-weighting hypothesis. For a detailed description of the experimental setup and analysis we refer the reader to [84]. Here, we briefly summarize the results.

Under experimental conditions where the sensory input to the postural control system was deliberately altered, transient periods of low or high frequency oscillations in the body sway of healthy young adults were observed [84], consistent with the oscillations predicted by the frequency response of the model (see Figure 6). Shown in Figure 7 are body sway measurements and the corresponding time-varying spectrum (or time-frequency distribution [TFD]) obtained during eyes-closed stance on a platform that transitioned from fixed, to sway referenced for 60 seconds, and then back to fixed. (See [84] for details of the experimental protocol, methodology and data analysis.) During the initial period of eyes-closed stance on the fixed platform, the effective overall sensory weight is $\mathbf{W} = W_p + W_g$ (see Figure 5, middle graph), and under the sensory re-weighting hypothesis, once steady-state has been reached we have $W_p + W_g = 1$. Following the transition to the sway-referenced platform (starting at 60 seconds in Figure 7), the proprioceptive channel no longer provides accurate information about body sway. Hence the effective overall sensory weight becomes $\mathbf{W} = W_g$

(see Figure 5, right graph) which will be less than unity immediately after the transition to sway-referencing. This decrease in the value of \mathbf{W} will cause a change in the frequency characteristics of body sway as predicted by the frequency response curve shown in Figure 6 (dashed curve) and seen experimentally in the time-varying spectrum of Figure 7 (note the band of energy in the TFD plot around 0.1 Hz that develops after $t = 60$ sec). As the body adjusts to the sway-referenced condition over time, sensory re-weighting brings the effective sensory weight back to unity, i.e., the graviceptive weight W_g increases to near unity. Upon the transition back to a fixed platform (at $t = 120$ sec), the effective sensory weight becomes $\mathbf{W} = W_p + W_g$, but now the graviceptive weight is higher than it was during the initial fixed platform condition ($t < 60$ sec), so that now $\mathbf{W} > 1$. According to the model, this should result in oscillatory sway near 1 Hz (see Figure 6, dot-dashed curve), which was observed experimentally (see the time-varying spectrum in Figure 7 and in particular the band of energy that develops around 1 Hz after $t = 120$ sec).

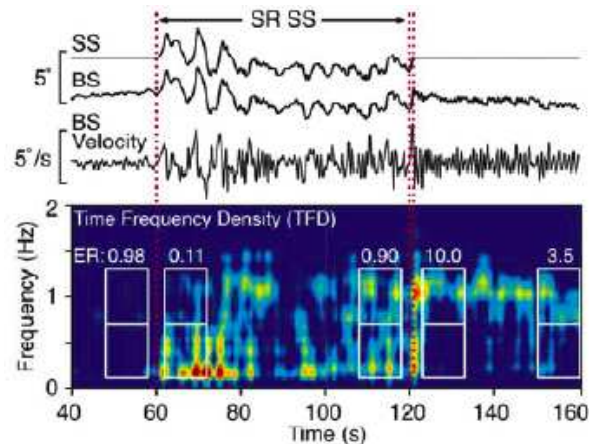


Figure 7: Time series and corresponding time-varying spectra (or time-frequency distributions (TFD), bottom plots) of postural sway from a representative subject. The support surface angle (SS) is sway-referenced (SR) during the period 60-120 sec. After rapidly returning to a fixed support surface within 1 sec (denoted by the double vertical dotted lines at 120 sec), body sway oscillations at about 1 Hz develop (orange-yellow band in the TFD around 1 Hz for $t > 120$ sec), indicative of inadequate sensory re-weighting. (Boxed areas in the TFD correspond to time-frequency regions of interest for which energy ratios (ER) of high-frequency (0.7-1.3 Hz) to low-frequency (0.1-0.7 Hz) energy were analysed; numbers above the box reflect the ER values.) Adapted from [84].

4.0 POSTURAL CONTROL AND SENSORY RE-WEIGHTING II

In this chapter we present results from two human experiments. The first experiment investigated the sensory re-weighting hypothesis by evoking anterior-posterior (AP) body sway using visual stimuli during sway-referencing of the support surface. The second experiment examined the impact of attention and sensory integration in postural control in young and older adults. Under eyes-closed stance, the proposed postural control model discussed in Chapter 3 was fit to the data to obtain desired parameters to quantify the interference of attention on postural control. The aim of this experiment was to utilize the postural control model to show that the cognitive processing and integration of sensory inputs for balance requires time, and that attention influences this processing time, as well as sensory selection by facilitating specific sensory channels (sensory re-weighting).

4.1 EXPERIMENT I: MOVING-SCENE PERTURBATIONS

4.1.1 Abstract

The aim of this study¹ was to investigate the sensory re-weighting hypothesis, by evoking anterior-posterior (AP) body sway using visual stimuli during sway-referencing of the support surface. Twelve healthy adults participated in this study. Subjects stood on the platform while looking at a visual scene that encompassed the full horizontal field of view. A sequence of scene movements was presented to the subjects consisting of multiple visual push/pull perturbations; in between the first two push/pull sequences, the scene either moved randomly

¹Published in *Experimental Brain Research* [50]

or was stationary. The peak-squared velocity of AP center-of-pressure (COP) was computed within a 6 sec window following each push and pull. The peak-squared velocity was lowest for the push/pull sequence immediately following the random moving scene. These results are consistent with the sensory re-weighting hypothesis, wherein the sensory integration process reduced the contribution of visual sensory input during the random moving scene interval. We also found evidence of habituation to moving scene perturbations with repeated exposure.

4.1.2 Introduction

Moving visual environments have been extensively used to investigate the contribution of the visual sensory information to postural control [42, 43, 95, 4, 100, 80]. In situations where there is conflicting sensory information, it has been shown that vision plays an important role in control of posture [5, 4, 95, 9]. For example, when standing on a sway-referenced platform, moving visual environments have a larger effect on postural responses [8]. The role of vision in postural control can also be assessed by examining patients with defects of the vestibular or somatosensory systems [79, 87]. It has been shown that visually-induced postural sway is significantly greater in patients with vestibular deficits than normal subjects, in particular at greater stimulus amplitudes [87, 80, 82]. In contrast, a saturation effect can be seen in healthy younger adults, such that increases in the amplitude of moving visual environments cause little or no additional postural sway [43, 7, 100, 80].

Exposure to external motion stimuli can perturb natural stance such that balance is compromised and corrective action by the body is necessary to maintain balance [43, 17, 29]. As the body deviates from an equilibrium position (upright stance), a torque due to the force of gravity acts on the body, driving it further from equilibrium in the absence of any counter-torque. In order to maintain balance, a corrective torque opposing the gravity-induced torque must be generated by the body [30]. Experiments in human balance suggest that feedback control plays a dominant (although possibly not exclusive [20, 66]) role in maintaining upright posture in humans [101, 82, 84]. Recent studies suggest that the source of sensory information used for torque generation depends upon environmental conditions

and the reliability of sensory orientation and movement information [82, 84]. A feedback control model to explain these findings was developed, wherein orientation and movement information from the senses is weighted in a negative feedback control strategy (“sensory re-weighting”), with decreased reliance on sensory information that is unreliable [82, 84].

In this study, we hypothesized that exposure to prolonged continuous visual perturbations (random moving scene) while standing on a sway-referenced platform would cause sensory re-weighting resulting in reduced reliance on visual sensory information. To assess this, we chose to use step response-like perturbations (moving scene push/pull sequence), common in engineering systems analysis, preceding and following a period of random anterior-posterior (AP) visual scene motion. We hypothesized that during the period of prolonged random scene motion, sensory re-weighting would occur, resulting in decreased reliance on visual information for balance. Accordingly, we would expect to see a decrease in the push/pull response following exposure to the random moving scene compared to the response to the first push/pull sequence. To control for habituation to the push/pull sequences, we also included a control group that was subjected to the same push/pull sequences, but not to the prolonged random moving scene between the push/pull sequences. For this group, we would not expect sensory re-weighting like that of the random scene group, such that their response to the second push/pull sequence would not be as diminished compared to the response of the first group. While visual adaptation has been analyzed previously using prolonged sinusoidal or noise-like perturbations (e.g., [76, 82]), which are also commonly used excitations in engineering systems analysis, responses to step-like inputs have not been as widely investigated, and thus our protocol provides new experimental evidence with regard to sensory adaptation and the sensory re-weighting hypothesis.

4.1.3 Methods

Subjects: Data were collected from twelve healthy, young adults (5 male, 7 female, age 21 to 31 years, average age 24 years). The experimental protocol was approved by the Institutional Review Board of the University of Pittsburgh Medical Center, and all subjects gave their informed consent prior to participating in the study. Of the twelve subjects, six

(1 male, 5 female, age 21 to 25 years, average age 23 years) participated in an experiment where the visual push/pull was combined with a random moving scene, and the other six (4 male, 2 female, age 21 to 31 years, average age 25 years) participated in an experiment where the visual push/pull was presented without a random moving scene as a control condition. These groups are hereafter labeled as RANDOM and STATIONARY, respectively. Subjects were assigned randomly to each group.

Experimental setup: A 6 degree-of-freedom electromagnetic tracking device (Polhemus Fastrak, Colchester, VT) was placed on the top of the head and the back of the pelvis at the level of the iliac crest. Subjects stood on a custom-designed posture platform while looking at a visual scene that encompassed the full horizontal field of view (180 degrees horizontal, 70 degrees vertical). Subjects were instructed to stand in a relaxed manner, looking straight ahead at the scene, located at a distance of 1.5 meters away from the subject, with their arms crossed in front of their chest. The visual environment was projected contiguously across three screens using three LCD projectors. The visual scene directly in front of the subject consists of a target (bull’s eye) pattern of alternating black and white concentric rings, and the sides of the visual surround were checkerboards with alternating black and white rectangles; see Figure 8(a). Simulated motion of the scenes was computer controlled and synchronized.

At the onset of each trial, the platform was allowed to rotate in direct one-to-one proportion to body sway, about an axis colinear with the subject’s ankle (“sway-referencing” of the platform), so that sensory information from ankle proprioception about body position was rendered less reliable than when standing on a fixed, level platform. The AP translation of the pelvis tracker, which approximates the movement of the lower extremities in an inverted pendulum model of sway, was converted to an angular measure which was used to provide the signal used for sway-referencing the platform at 20 Hz. Although it is recognized that the signal may not directly keep the ankle angle fixed at 90 degrees, the ability of the ankle to provide an accurate reference to the world is disrupted during sway-referencing [69, 72, 80, 24]. The sequence of scene movements was then presented to the subjects in each group. For both groups, the visual scene movement consisted of three push/pull sequences starting at 30, 114, and 158 sec, respectively. The start time of 30 sec into the trial was

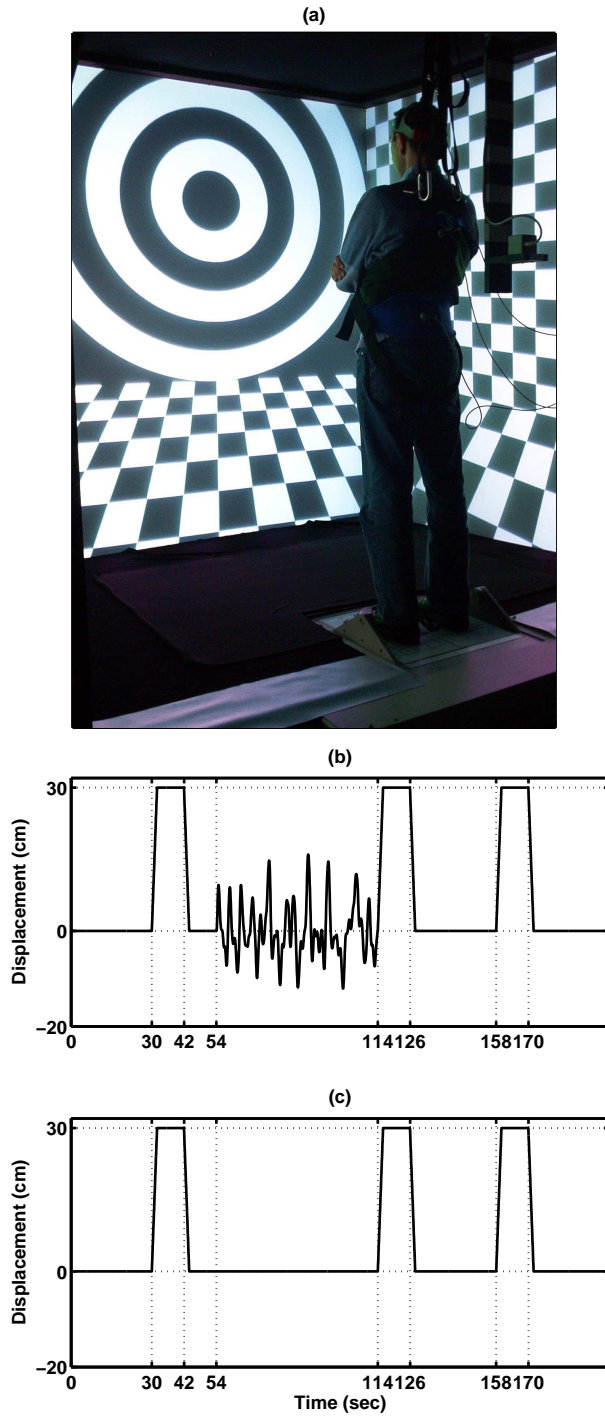


Figure 8: Experimental setup. (a) Subject standing on a movable platform while viewing AP optic flow on three back-projected screens encompassing full horizontal field of view. (b) visual stimuli consisted of three push/pull sequences (where onset of each push and pull is at (30, 114, 158 sec), and (42, 126, 170 sec), respectively) with random movement (54-114 sec) included or (c) three push/pull sequences with no random motion of the scene (54-114 sec).

chosen to allow subjects to acclimate to standing on the sway-referenced platform prior to subjecting them to visual perturbations. The push/pull sequence contained a 30 cm push over 2 sec (i.e., the scene moved 30 cm towards the subject over 2 sec, and then stopped), followed by a 30 cm pull 10 sec later (i.e., the scene moved 30 cm away from the subject over 2 sec, back to its original position, and stopped). Hence, the duration of each push/pull sequence from the start of the push to the end of the pull was 14 sec. The first push/pull ended at $t = 44$ sec, and was followed by 10 sec of no scene movement to allow for settling following the first pull. Then, a 60 sec random moving scene (0.05-0.5 Hz white Gaussian noise, 8 cm root-mean-square (RMS) power, beginning at 54 sec) was presented to half of the subjects (RANDOM Group), ending at 114 sec. A second push/pull sequence was then presented to subjects, beginning at $t = 114$ sec and ending at $t = 128$ sec. After the second push/pull sequence, we allowed 30 sec to pass before a third final push/pull was presented, starting at $t = 158$ sec. The third push/pull was given to see if sensory re-weighting occurred over the 30 sec of no scene movement following the second push/pull. See Figure 8(b) and 8(c).

The velocity of the visual push/pull sequence was chosen because it is within the linear region of the relationship between the amplitude of visual responses and the logarithm of the scene velocity [43]. In addition, it is of the same order of magnitude as the peak velocity of sinusoidal optic flow stimuli that are known to induce postural responses [80, 8]. For example, a 0.3 Hz sinusoidal moving scene with amplitude ± 8 cm has a peak velocity of approximately 15 cm/sec, which corresponds to the velocity of our push/pull sequences (30 cm/2 sec). Similarly, for the random noise signal, the RMS power was chosen to be consistent with previous studies utilizing sinusoidal perturbations (e.g., [8, 96]) and the bandwidth was chosen as such to span the spectral range over which visual information is known to elicit postural responses and thus is presumably relevant to postural control [4, 82].

Anterior-posterior center-of-pressure (AP-COP) was recorded for the duration of each 200 sec trial. Each subject performed three trials with 2 min of rest between each trial. For subject safety, a harness was used to prevent falls; the harness was sufficiently slack so as to not impede normal upright stance and sway, or provide significant proprioceptive or tactile feedback.

Data analysis: Center-of-pressure (COP) was used as the outcome variable because it represents the neuromuscular response in the control of body sway [104]. At low frequencies, COP approximates the horizontal translation of center-of-mass (COM). The COP data were recorded at a sampling rate of 100 samples/sec. Spectral analysis of these data revealed that over 99% of the power was contained below 1.5 Hz, consistent with previous findings [94, 87]. Accordingly, the COP data were down-sampled off-line to 4 samples/second (pre-filtered with a digital IIR filter with corner frequency at 1.5 Hz and 25 dB attenuation at 2 Hz, using the “filtfilt” command in Matlab). The mean was then removed from these down-sampled, filtered COP data, and the first difference (COP velocity) was computed. For analysis, the peak of the squared velocity of AP-COP was computed within a 6 s window following the end of each push and pull, to quantify the movement response to the visual perturbations. In our examinations of pilot data, the peak velocity was always reached well within this 6 s interval. We chose the peak, rather than for example the mean, as a more sensitive measure of the initial sway response to the abrupt push/pull perturbation. As a squared quantity, the peak-squared velocity is akin to the maximum instantaneous power of velocity.

A repeated-measure ANOVA of the peak-squared velocity of AP-COP after each push and pull perturbation was conducted. To stabilize the variance and normalize the distributions, a logarithmic transformation of the data ($10 \cdot \log(COP_{vel}^2)$) was applied; accordingly, results are plotted on a decibel (dB) scale. The independent variables included: Trial (1, 2, 3), Perturbation Direction (Push, Pull), and Sequences (first, second, or third) along with all first-order interactions. This analysis was performed separately on the data collected with the random scene movement (RANDOM Group) and the data collected without the random scene movement (STATIONARY Group).

4.1.4 Results

The ensemble-average time-series of COP velocity for trial 1 is shown in Figure 9. The left column shows the average velocity time-series for the RANDOM Group (random moving scene between first and second push/pull sequences), and the right column shows the results

for the STATIONARY Group (no random moving scene). In the RANDOM and STATIONARY Groups, large perturbations in velocity were recorded during the first push/pull sequence. During the second sequence, the perturbation in COP velocity due to the pushes is less, especially for the RANDOM Group. Furthermore, the change in velocity due to the second pull is barely distinguishable from the rest of the recording. Changes in the velocity during the third sequence are larger for the RANDOM Group, as compared to the second push/pull sequence, but mixed for the STATIONARY Group, i.e., smaller push response but a larger pull response compared to the second sequence.

The RANDOM and STATIONARY Groups responded differently to the push/pull stimuli. For the RANDOM Group data (Figure 3, left column), results showed a significant effect of Trial×Pulse interaction ($F = 34.59; p = 0.02$). This Trial×Pulse interaction occurred due to a significant reduction in COP response from the first pulse to the second pulse in trial 1 ((Figure 10(a)).

For the STATIONARY Group data, significant effects were found for Trial ($F = 6.59; p = 0.01$) and Perturbation Direction ($F = 13.78; p < 0.01$). All other factors were not significant ($p > 0.05$). The Trial effect showed a decrease from trial 1 to trial 3 (see Figure 3, right column), suggesting habituation to the push/pull sequences. The Perturbation Direction showed a significantly greater response to the Push compared to the Pull.

To further test the hypothesis that exposure to the random scene created a reduction in the gain of the visual input, the change in magnitude from the first Push to the second Push in trial 1 was examined. This was done for both the RANDOM Group data (Figure 10(a)) and the STATIONARY Group data (Figure 10(d)). A significant reduction in sway from Push 1 to Push 2 for the RANDOM Group data was found ($t = 3.74; p < 0.01$). For the STATIONARY Group data, no significant change from Push 1 to Push 2 was found ($t = 1.00; p = 0.36$). Thus, during the first trial, there is a significant drop in COP response to the push immediately after the random scene exposure and there is no reduction during the control condition of no random scene exposure. A further analysis of trial 1 for the change in COP response from Pulse 2 to Pulse 3 in the RANDOM Group showed a significant increase ($t = 1.96; p = 0.04$). Thus, in the first trial there was some recovery of response.

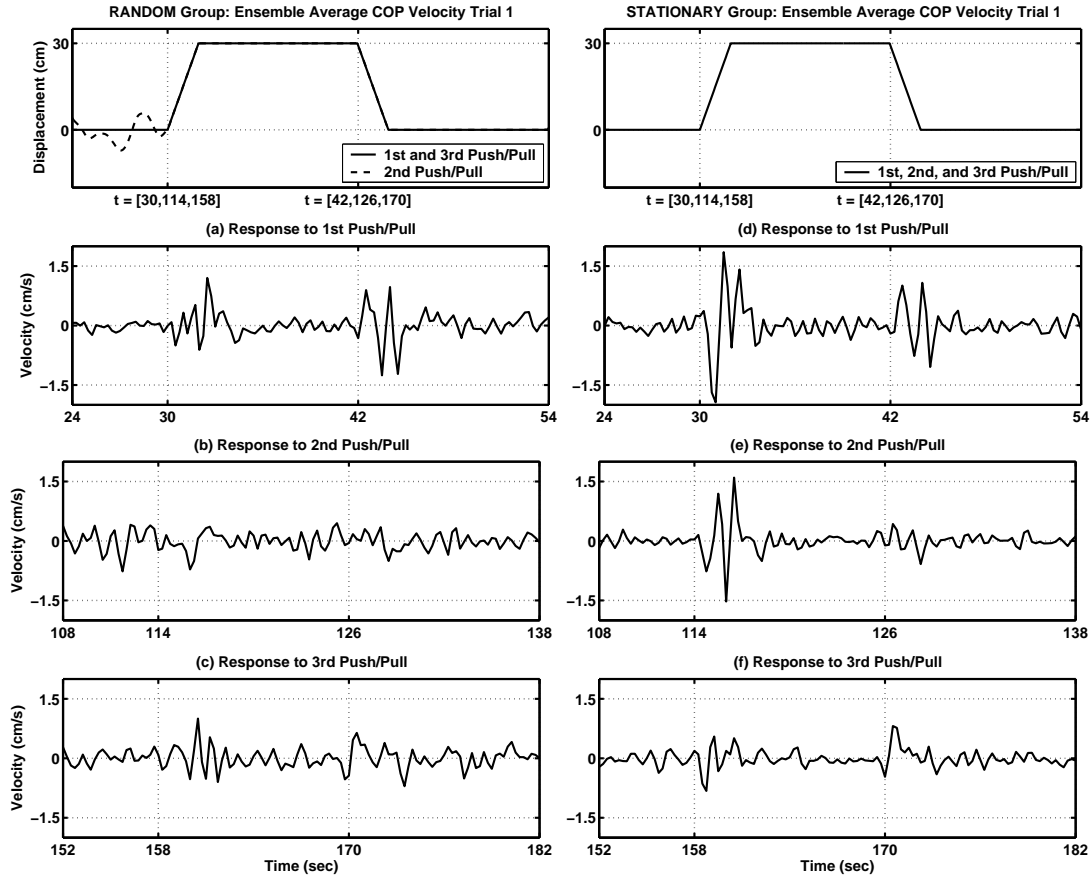


Figure 9: Ensemble average time series of AP-COP velocity for (a) RANDOM Group: Trial 1, and (b) STATIONARY Group: Trial 1. The top figures in each column plot the push/pull sequences, where for the RANDOM Group the last 6 sec of the random moving scene perturbation, prior to the second push/pull sequence, is also included. The second, third, and fourth figures in each column are ensemble average AP-COP velocity response plotted over a 30 sec period, where the plots shown in each figure include the first push/pull (24-54 sec), the second push/pull (108-138 sec), and the third push/pull sequences (152-182 s), respectively. In each plot, the first vertical dotted line indicates the onset of the push sequences, and the second dotted line the onset of the pull sequences, respectively.

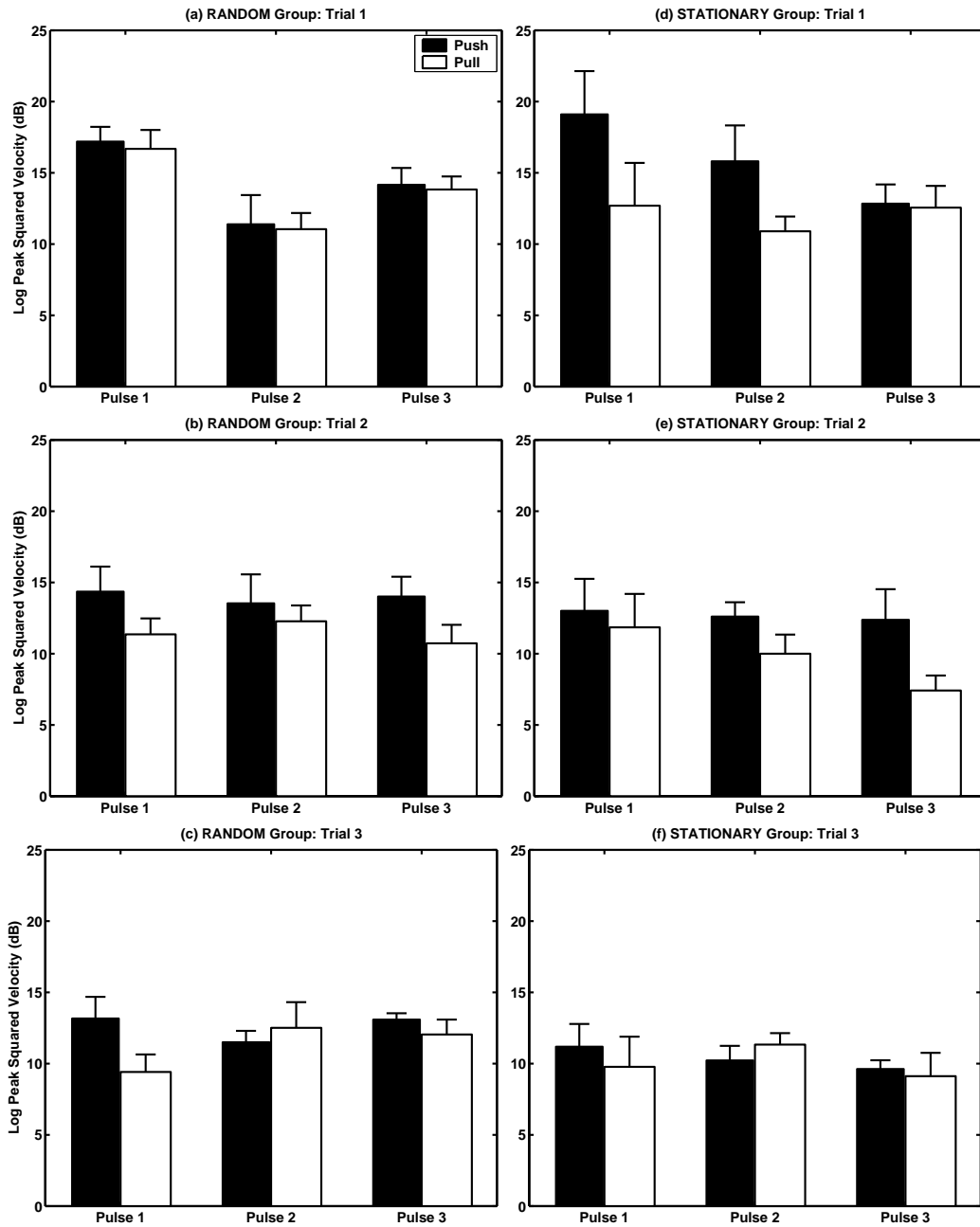


Figure 10: Ensemble average peak-squared velocity of AP-COP (dB, mean \pm sem) for (a) RANDOM Group: Trial 1, (b) RANDOM Group: Trial 2, (c) RANDOM Group: Trial 3, (d) STATIONARY Group: Trial 1, (e) STATIONARY Group: Trial 2, and (f) STATIONARY Group: Trial 3. Peak-squared velocity of AP-COP is computed within a 6 s window following each visual push and pull. For plotting purposes, 10 dB is added to the means.

4.1.5 Discussion

The aim of this study was to further investigate the sensory re-weighting hypothesis suggested in recent studies [82, 84]. In [84], sensory re-weighting was investigated by utilizing platform perturbations during eyes-closed stance. We proposed to investigate sensory re-weighting during eyes-open stance on a sway-referenced platform while exposed to moving scenes. Our hypothesis was that exposure to persistent visual perturbations (prolonged random moving scene) while standing on a sway-referenced platform would induce sensory re-weighting of the visual channel compared to the case of no random scene movement, resulting in decreased reliance on visual feedback.

We found that exposure to continuous random visual motion (RANDOM Group) prior to the second visual push was associated with a smaller COP response compared to no random visual motion (STATIONARY Group). Although having subjects perform both visual conditions (i.e., random and stationary) would have resulted in greater statistical power due to the repeated measures design, we wanted to protect against a potential habituation to the push/pull perturbations. In order to determine if both subject groups were similar at baseline, we examined the RMS magnitude of their COP velocity during the initial 30 s of the first trial, prior to any visual movement. The magnitude of COP during this period was 0.32 cm/s for the RANDOM Group and 0.33 cm/s for the STATIONARY Group, which was not significantly different ($p > 0.05$). Our results are consistent with and can be interpreted in terms of the sensory re-weighting hypothesis, as follows: standing on a sway-referenced platform renders proprioceptive feedback less reliable than during stance on a stable platform, resulting in increased reliance on visual and vestibular sensory feedback. When visual information is then simultaneously perturbed by persistent random moving scenes, the sensory integration process re-weights the incoming sensory information, placing less emphasis on the visual channel. Subsequent visual perturbations have less impact on postural response. This result is in agreement with similar studies concerned with investigating the sensory re-weighting hypothesis; see for example [76, 82], in which the role of the visual system, amongst other contributing sensory systems to posture, was analyzed using

prolonged sinusoidal [76] and noise-like perturbations [82]. This decreased visual weight, in our study, results in a smaller response to the second push sequence that occurs at the end of the random scene movement.

Visual weight also appears to increase when random visual input is turned off. This shows that the visual system is capable of adjusting its weight when the visual environment, after a prolonged perturbation, becomes stable (no moving scene). This was observed for trial 1 of the RANDOM Group, where there was a significant increase in COP response from Pulse 2 to Pulse 3. This increase suggests that the visual weight increased during the no-motion period between Pulse 2 and Pulse 3. However, it should be noted that the COP response to Pulse 3 did not reach the levels of Pulse 1, suggesting that the visual weight was still reduced compared to the beginning of the trial.

In addition to results consistent with the sensory re-weighting hypothesis, a reduction in COP response to the visual perturbations was also found across trials. This result suggests that there is a longer-term effect (i.e., habituation across trials) as well. Similar habituation effects have been observed previously in other studies of sensory re-weighting, using different sensory perturbations [84].

Visual weights do not appear to be able to be reduced to zero, i.e., visual information does not appear to be ignored totally. Numerous studies have shown sway responses to sinusoidally moving environments, even after repeated exposure [100, 80, 8]. In our results, we continued to find responses to our visual motions (both the pushes/pulls and random scene motions) in the third trial. Thus there appear to be limits to the reduction of visual gain in the postural control system. This limit is also believed to be subject-dependent, with some individuals having the capability to reduce this gain to a greater extent than others.

Pathologies influencing components of the postural control system would be expected to influence the relative contribution of these sensory weights. Patients with vestibular disorders have been found to have increased reliance on visual information (i.e., increased visual weights), even to repeated visual motions [87, 80]. Aging can also have an effect, with increased sway to moving visual environments in elderly [99, 8], and in children [41, 3]. Thus modulation of visual weights have limitations that are dependent upon the health of the vestibular system and individual differences. The ability to dynamically change the sensory

weights may be impaired in some conditions. For example, persons with Parkinson’s Disease have shown an inability to quickly change their postural set in response to changing postural demands [13, 14].

An important factor revealed by our experiment, as well as other experiments concerned with sensory re-weighting hypothesis (see for example, [76, 82]), is the ability of the postural control system to adjust its sensory weights, which contribute to balance, based on changes in environmental conditions, such as changes caused by visual perturbations. Simple [83] as well as sophisticated models [101] of human postural control have also been used to predict these changes in sensory weights as observed in experimental data. However, the source of sensory re-weighting in the human postural control system is still an open question and further research is required to understand how this phenomenon occurs.

While our results can be interpreted in terms of the sensory re-weighting hypothesis, they do not prove that sensory re-weighting occurs, and indeed other mechanisms could be responsible for the reduced response observed following the random scene movement. For example, it is possible that changes in body stiffness through increasing antagonistic muscle actions around the ankle [107] occur during the random moving scene while standing on a sway-referenced platform. In a second-order linearized inverted pendulum model of postural control, increased stiffness would result in decreased peak sway response following a push/pull perturbation. Accordingly, while sensory re-weighting is a plausible explanation of our findings, and is based on previous experimental findings, other explanations are possible.

4.2 EXPERIMENT II: ATTENTION AND SENSORY INTEGRATION

4.2.1 Abstract

In this study² we conducted a dual-task experiment that involved information processing (IP) tasks concurrent with postural perturbations to explore the interaction between attention and sensory integration in postural control in young and older adults. A postural control model incorporating sensory integration and the influence of attention was fit to the data, from which parameters were then obtained to quantify the interference of attention on postural control. The model hypothesizes that the cognitive processing and integration of sensory inputs for balance requires time, and that attention influences this processing time, as well as sensory selection by facilitating specific sensory channels. Performing a concurrent IP task had an overall effect on the time delay. Differences in the time delay of the postural control model were found for the older adults. The results suggest enhanced vulnerability of balance processes in older adults to interference from concurrent cognitive IP tasks.

4.2.2 Introduction

Falls are a significant problem in older adults, resulting from a complex interaction of sensory, motor and cognitive loss. Recent research has found that attention plays a role in postural control [28, 88, 89, 93, 103], as does dynamic regulation of sensory integration [24, 75, 76, 82, 84]. Environmental changes that alter sensory orientation information tend to have a greater destabilizing effect on older adults, and older adults appear to require greater attentional resources for balance control. However, the interaction between attention and sensory integration is an open question. Studying how these two factors interact, and developing a model of that interaction, will improve our understanding of their impact on balance control and predisposing conditions for falls in older adults. This paper addresses the incorporation of the interaction of attention and the dynamic regulation of

²Published in *Neuroscience Letters* [54]

sensory integration into models of postural control. In particular, we quantitatively investigated, through experiments and model-based analysis, the influence of attention-requiring tasks on the dynamics of sensory integration and postural control in older adults.

Studies suggest that balance engages attentional processes to varying degrees, depending upon the postural challenge and the age and capabilities of the individual [10, 28, 35, 57, 59, 86, 88, 89, 90, 93, 98, 103]. Many studies use a dual-task paradigm to examine interference between a cognitive task and a balance task. Dual-task paradigms explore attentional processes involved in sensorimotor function by requiring subjects to perform two tasks simultaneously. Different cognitive tasks have been used in dual-task paradigms involving standing and walking, including mental arithmetic [10, 98], visuospatial tasks (e.g. [35]), auditory and visual reaction time tasks [59, 88, 89, 93], word recall [45], and visuospatial memory tasks [1]. Degradation in performance of either the balance task or the cognitive (or information processing (IP) task) is believed to reflect competition for cognitive resources (i.e., attention). As challenge is varied in one task, the amount of interference created in the other task is thought to reflect the degree of attention required to perform the task. If two tasks are processed in parallel, then the interference would be nonexistent. However, dual-task interference is suggestive of the two tasks sharing some common attentional resources. This concept of attention is employed in this study of balance and concurrent information processing (IP) tasks. The hypothesis is that this sharing of attentional resources affects balance by slowing the postural control system, and would be reflected in an increased delay in our model of sensory integration.

Dual task interference between reaction time tasks and standing posture as the postural tasks varied included sensory conflicts [88, 89, 90]. Auditory simple and choice reaction times increased as the postural task included sway referencing, with greater interference [88, 90]. In a recent dual-task study by Redfern et al. [89] involving IP tasks (auditory and visual choice reaction time tasks) and postural perturbations, the investigators found evidence suggesting that attention shifted away from the IP tasks while a balance-stabilizing response to the postural perturbation (sudden platform translations) was made. Moreover, the study found greater interference for the auditory task than the visual task. The present study

uses similar auditory IP tasks to further examine attentional influences on postural control by examining changes in parameters of a postural control model during dual-task paradigms, particularly comparing older adults to young adults.

An experimentally validated postural control model [82, 84] sets forth a quantitative framework for exploring this hypothesis. We explicitly incorporate a cognitive component (i.e., attention) into the model (Figure 11), whereby attention influences sensory integration primarily through the time delay parameter t_d and the sensory weights of the model. This model hypothesizes that the processing and integration of sensory inputs for balance requires time, and that attention influences this processing time.

In this study, a dual-task experiment was conducted to examine competition for cognitive resources and its impact on a model of postural control through increase in sensory processing time, quantified by the time delay parameter in the model. Least-squares model fits to subject data were made to quantify differences between young and older adults. We hypothesized that attentional processes would play a greater role in postural control during concurrent IP tasks, resulting in longer cognitive processing times of balance sensory information, manifest in the time delay parameter of the postural control model when fit to the experimental data. We further hypothesized that this effect would be greater in older adults.

4.2.3 Methods

Subjects: Ten healthy young adults (M = 5, F = 5, 25 ± 3 yrs., range: 22-33 yrs.) and ten older adults (M = 4, F = 6, 73 ± 8 yrs., range: 61-85 yrs.) participated in this study, after giving their informed, written consent. The experimental protocol was approved by the Institutional Review Board of the University of Pittsburgh Medical Center, and was performed in accordance with the Declaration of Helsinki. All subjects had no history of auditory, vestibular or neurological disorders, and were screened for normal vestibular function through caloric and rotational vestibular testing. In addition, a neurologist performed a neurological examination to confirm normal neurological function. All subjects also had a Mini-Mental Status Exam (MMSE) score of greater than 24.

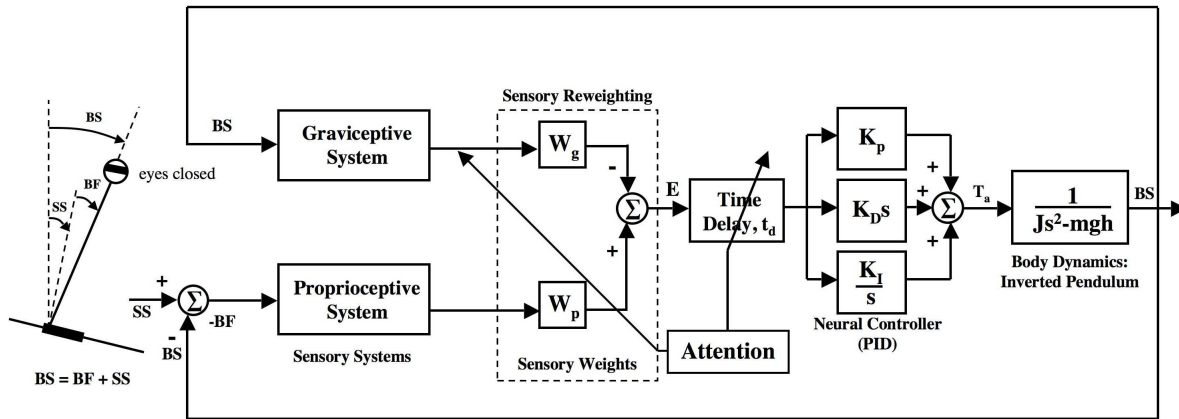


Figure 11: Feedback model of postural control for eyes-closed stance. The body is modeled as a linearized inverted pendulum. Sensory pathways include weights (W_g , W_p) that can change as environmental factors change (the “sensory re-weighting” hypothesis). Corrective ankle torque, T_a , is generated by a fixed-gain proportional-integral-derivative controller acting on the combined delayed error signal E from the sensory systems. Attentional tasks that interfere with balance are hypothesized to increase cognitive processing time involved in balance, manifest in the model as an increase in the time delay of the system. Attention may also influence sensory integration, as manifest in the model via the sensory weights (W_g , W_p). Modified from [82, 84].

Experimental protocol: A dual-task paradigm was performed that combined postural perturbations with concurrently performed information processing (IP) tasks. Based on our past findings showing interference between postural control and auditory IP tasks, auditory stimuli were used for the IP tasks (see below). Postural challenge was provided by rotating a posture platform (EquiTest, Neurocom, Inc.) during eyes-closed stance about an axis collinear with the ankle angle in a random manner for 121 sec, at a peak-to-peak amplitude of 2 degrees. The platform was driven by computer interface using custom software. Platform motion was preceded and followed by 30 sec of no movement.

The signal used to randomly rotate the platform consisted of two consecutive 60.5 second pseudorandom ternary sequence (PRTS) time series, with peak-to-peak amplitude of 2 degrees. A plot of the platform position time series, including the 30 sec of no movement before and after the PRTS motion, is shown in Figure 12. This platform perturbation has been used in previous studies (e.g., [82]). The 2 degree peak-to-peak amplitude was selected based on [82] to avoid saturation effects in the postural response. The PRTS has a wide spectral bandwidth, with the velocity waveform having spectral and statistical properties approximating a white noise stimulus. Hence, any concerns about subjects adapting to the platform motion, such as can occur with sinusoidal perturbations, are ameliorated by using this platform perturbation. The duration of random platform motion (2 cycles of the PRTS sequence, as shown in Figure 12) was chosen to ensure adequate steady-state conditions for estimation of experimental transfer functions and model parameter fits, while at the same time keeping trials short enough to avoid fatigue effects, especially in the older subjects.

The IP tasks were: 1) None, 2) an auditory choice reaction task (CRT), in which subjects had to click a hand-held microswitch with either the left hand or right hand depending on whether they heard a high- or low-pitched tone (980 Hz vs. 560 Hz, 250 msec duration, 80 dB SPL (Sound Pressure Level), mean inter-stimulus interval of 4 sec (range 2-6 sec)), and 3) an auditory vigilance task (VT), in which subjects experienced the same tone stimuli as in the CRT task but rather than pushing a button in response to the tone, for the VT task subjects had to remember the number of high or low tones they heard during the trial. Auditory stimuli were presented throughout the entire 3 minute trial every 2-6 seconds via Etymotic Research model 3A insert earphones. Note that, although the IP tasks are discrete,

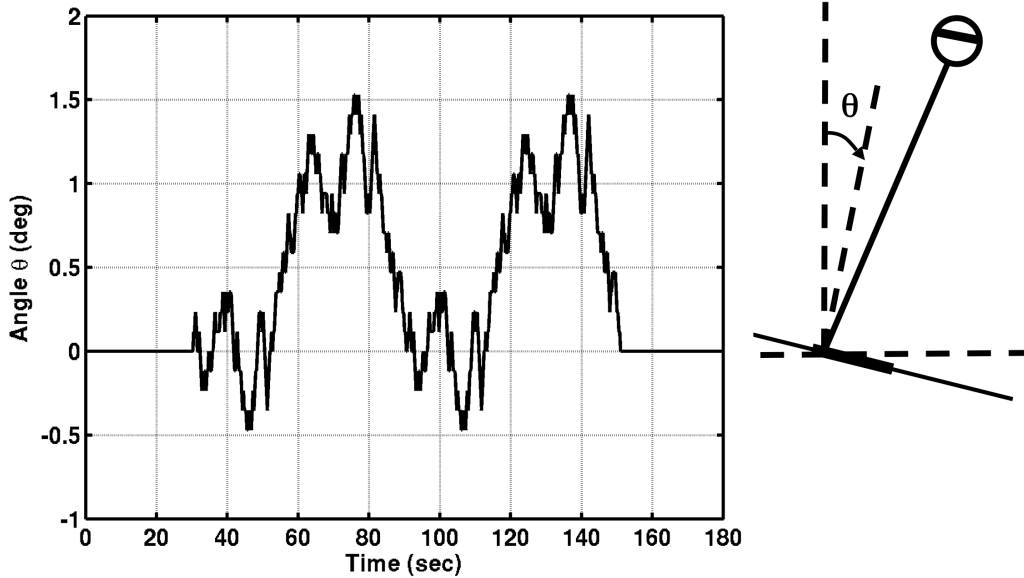


Figure 12: Platform motion (position) used in the experimental protocol, consisting of two 60.5 second cycles of a pseudorandom ternary sequence (PRTS) with 2 degree peak-to-peak amplitude, preceded and followed by 30 seconds of no platform motion.

occurring randomly every 2-6 seconds throughout the trial, subjects need to attend to the auditory channel to listen for the stimulus, and hence attentional focus is continuous. The IP tasks were selected based on past research and to explore specific processing that might interfere with posture adjustment. The CRT task requires auditory stimulus detection, a choice decision, and a fast reaction. The emphasis is on simple, but fast, processing. Slowing of processing speed is a common finding with age [92]. In contrast, the VT emphasizes accuracy of detection and provides a sensory focus, with a memory requirement and no musculo-skeletal reaction (unlike the CRT task).

Subjects stood, with eyes closed and arms folded across their chest, on the posture platform while performing the IP task conditions, which persisted throughout the entire trial duration. The eyes closed condition was chosen to enhance the postural challenge, to simplify the sensory integration and sensory re-weighting strategy for modeling (presumably limited to proprioceptive and vestibular channels), and to focus attentional resources on

fewer sensory channels. Three trials for each IP task were performed, with one IP task per visit, selected randomly. The tasks were completed within 4 weeks, with 2-7 days between visits. The IP tasks were performed on separate days rather than in one visit in order to minimize any possible fatigue effects across the conditions, particularly in our older subjects.

A training session prior to testing was conducted to familiarize subjects with the IP tasks; subjects were seated for the training session. Subjects were naïve to the posture platform condition prior to the first testing session. Instructions to the subjects during testing were: With your eyes closed and arms folded across your chest, maintain a relaxed upright stance position while reacting as fast as possible to the tone for the CRT task and With your eyes closed and arms folded across your chest, maintain a relaxed upright stance position while mentally counting the number of (high or low) tones you hear for the VT IP task.

Data measurement and analysis: Anterior-posterior (AP) body sway (center-of-pressure (COP) under the feet) was recorded at 100 Hz from the force platform. COP were collected with two load cells (one anterior and one posterior) and then combined to estimate AP-COP. For small body angles and velocities of motion as obtained here, AP-COP tracks AP center-of-mass but has more high frequency power [106]. Therefore, we approximated AP body center-of-mass ($C\hat{O}M$) by digitally low-pass filtering the AP-COP data at 0.5 Hz using a zero-phase first-order Butterworth filter, then down-sampled to 20 Hz to match the platform motion sampling rate. Assuming a linearized (small angle) inverted pendulum model, AP body angle (in radians) was estimated from the processed AP-COP data by computing $\theta = \frac{C\hat{O}M}{h}$, where h is the height of the subjects center-of-mass, determined from anthropometric measurements [105].

A steady-state analysis using linear systems techniques was applied to the estimated body angle data to quantify postural responses and estimate model parameters. Specifically, experimental transfer functions of body sway angle to support surface motion were computed, and fit to a feedback model of postural control. For the eyes-closed stance, the model transfer function is [82]

$$\begin{aligned}
 M(s) &= \frac{BS(s)}{SS(s)} \\
 &= \frac{W_p(K_D s^2 + K_P s + K_I)e^{-st_d}}{Js^3 - mghs + \mathbf{W}(K_D s^2 + K_P s + K_I)e^{-st_d}},
 \end{aligned} \tag{4.1}$$

where s is the Laplace variable; BS and SS denote body sway and support surface angles, respectively, in the Laplace domain; W_p is the proprioceptive sensory weight, which according to the sensory re-weighting hypothesis can change with environmental conditions; t_d is the overall time delay that includes neural conduction times as well as cognitive processing time; and K_P , K_I and K_D are the fixed gains of a PID controller that generates the corrective ankle torque T_a to maintain upright balance. The parameters K_P and K_D represent the active stiffness and damping, respectively, of the postural control system. The parameter \mathbf{W} represents the total sensory contribution, which during eyes-closed stance is $W_p + W_g$, and under steady-state is taken to be $\mathbf{W} = 1$ [82].

Experimental transfer functions were computed by taking a Discrete Fourier transform (DFT) of each 60.5 second cycle of each trial’s platform stimulus and the corresponding measured body sway (filtered AP-COP). The DFT was calculated at 150 equi-spaced frequencies ranging from $f = 0.0165$ Hz to $f = 2.48$ Hz. A property of the PRTS stimulus is that all even frequency components have zero amplitude [82], therefore, these even frequencies are discarded leaving 75 frequency points. Power and cross-power spectral densities were computed for each 60.5 second cycle and then averaged together. High-frequency portions of these spectra were further smoothed, by averaging adjacent spectral points as in [82], to produce the final spectra at 16 frequencies ranging from 0.0165 to 1.90 Hz.

Model fits to the experimental transfer functions were made via a constrained minimization of the cost function

$$C = \sum_{i=1}^N |M(j\omega_i) - H(j\omega_i)|^2 \quad (4.2)$$

where $H(j\omega)$ is the computed frequency response of the body sway to surface motion, and $M(j\omega)$ is the frequency response of the model, obtained from Eq. (1) with $s = j\omega$ and $\mathbf{W} = 1$. N is the number of frequency points ($N = 16$) over which the transfer function curve fits were made (ranging from 0.0165 to 1.9 Hz). Experimental transfer functions were smoothed as in [82] by averaging neighboring frequency bins. Each IP condition produced three experimental transfer functions (one per trial) per subject, and these three were averaged to obtain the mean experimental transfer function per IP condition per subject. This experimental transfer function was then fit by the model transfer function via the least squares procedure above.

The model fits produced five parameters [W_p, K_P, K_D, K_I, t_d] per subject per IP condition. Statistical analysis of the parameters was performed to test the impact of concurrent information processing tasks. The within-subject differences between the no-task condition and the IP task conditions were found. Then, a repeated-measures ANOVA was conducted on the differences with the independent variables being: AGE (YOUNG, OLD), TASK (CRT, VT), and TASK \times AGE. The overall mean was included in each statistical model to examine the overall effect of performing the task on the model parameters. Secondary analyses were performed within group using t-tests to determine if the time delays within group were greater than zero during the IP tasks. A p -value of 0.05 was used for significance.

4.2.4 Results

Effects were found on the time delay and proprioceptive weight parameters, shown in Table 1, for the two age groups during each IP task condition. Figure 13 (left graph) shows the changes in time delay (t_d) from the no-task condition for each group and task. Results of the ANOVA for the time delay showed that performing a concurrent IP task had an overall increase on the time delay ($p = 0.02, t - ratio = 2.56$). There was no significant effect of TASK, AGE, or their interaction (TASK \times AGE). The overall mean increase in time delay when performing the IP tasks compared to no-task across groups was 5 msec. Secondary t-tests were performed to test whether the time delay was significantly greater than zero within each age group. This analysis showed that the increase in time delay during IP tasks for the elderly (mean increase of about 7 msec) was significantly greater than zero ($p = 0.028, t - statistic = 2.04, df = 19$), but not for the young.

Analysis of the proprioceptive weight indicated that there was an overall decrease in W_p across groups when the IP tasks were performed ($p < 0.01, t - Ratio = 3.92$). The AGE effect was significant ($p = 0.04, F(1, 18) = 4.0$). There was no significant TASK effect or TASK \times AGE interaction. Secondary analyses within AGE showed that the decrease in W_p for the older subjects was significantly different from zero ($p < 0.02, t - Ratio = 2.82$), while

Table 1: Postural control time delay and proprioceptive weight for YOUNG and OLDER adults during IP tasks vs. no task (mean \pm sd)

IP Task	t_d [msec], YOUNG	t_d [msec], OLDER	W_p , YOUNG	W_p , OLDER
NONE	153 \pm 13	153 \pm 10	0.52 \pm 0.09	0.62 \pm 0.12
CRT	153 \pm 18	160 \pm 18	0.50 \pm 0.10	0.56 \pm 0.07
VT	162 \pm 13	158 \pm 18	0.54 \pm 0.10	0.57 \pm 0.12

there was no significant difference from zero for the young subjects. Thus, W_p decreased for the older subjects but not for the younger subjects. This decrease was approximately 5 percent of the original values (see Table 1 and Figure 13, right graph).

Analysis of the neural controller parameters (K_D , K_P , and K_I) showed no significant effects of TASK, AGE, or TASK \times AGE. Accordingly, we pooled individual subject values across TASK and AGE to obtain the mean values of these parameters: $K_D = 143.2$ [N.m.s/rad] (± 60.2 SD), $K_P = 1012.0$ [Nm/rad] (± 212.5 SD), and $K_I = 288.6$ [N.m/s.rad] (± 73.0 SD).

4.2.5 Discussion

These results suggest that our model of postural control, including attentional influences in the time delay, are sensitive to the effect of dual-task interference. The model implies that the time for sensorimotor processing involved in maintaining balance is impacted by dual-task interference. The similarities and differences between age groups in time delay changes suggest that healthy older adults have similar postural control function as young adults during mild postural challenges without concurrent IP tasks, but different postural control function during dual-task conditions. These differences likely reflect the enhanced vulnera-

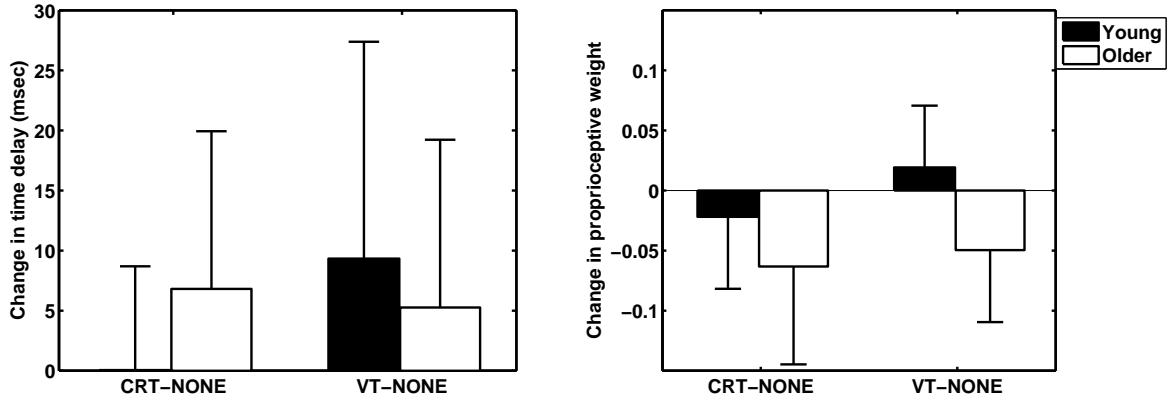


Figure 13: Normal change in postural control time delay (top graph) and proprioceptive weight (bottom graph) (mean \pm sd) during IP tasks relative to no-IP task condition (CRT-NONE and VT-NONE), for young (black) and older (white) subjects.

bility of balance processes in the older adults to interference from cognitive processes. The results also suggest that certain perceptual-motor tasks requiring speeded motor responses (i.e. pushing a button in response to a stimulus) slows balance processing in the old but not the young.

The increase in time delay with a concurrent IP task of about 7 msec for the older adults represents about 5 percent of the total time delay of the postural control system. Although this seems to be a small increase, it was statistically significant. Moreover, much of the time delay is fixed due to peripheral neural conduction velocity limitations, which is presumably not impacted by IP task. The total time delay includes this peripheral (sensory and motor) conduction delay, and central processing delay. It is the central processing delay that is hypothesized to be affected by interference from the IP tasks. The peripheral time delay is approximately 80 msec, assuming a conduction velocity of 50 m/sec [18] and a height of 2 m from ankle proprioceptors to the brain. Thus, approximately 70 msec of the total time delay is estimated to be due to central nervous processing (cortical and sub-cortical), such that the increase of 7 msec seen in the time delay represents roughly 10 percent of the central processing delay.

The changes in sensory weighting suggest a potentially significant strategic shift in posture control in the elderly that calls for further investigation. This finding regarding sensory re-weighting during IP task in the older subjects but not the young subjects can be interpreted in terms of the idea proposed in [89], that attention influences sensory selection. In particular, attentional resources drawn to the auditory task serve to enhance the auditory channel. If older adults have greater limits on cognitive resources compared to young adults as evidence suggests, then this shifting of attention to enhance one sensory channel comes at the expense of other sensory channels, namely the proprioceptive channel in this case. This decrease in the proprioceptive weight would also have a stabilizing effect, as it would reduce the influence of the platform perturbation coming in through the proprioceptive channel (SS in Figure 11). This, too, is consistent with previous findings that older adults are challenged to a greater degree to postural perturbations compared to young adults [89].

In conclusion, this initial study supports the main postulate of our model, that attention, in part, impacts processing speed of the sensory integration process. This effect appears to be true across ages under some conditions (i.e. during our VT task), but greater in older adults under other conditions (i.e. during our CRT task). Further studies in a larger population are warranted.

5.0 A MECHANISM FOR SENSORY RE-WEIGHTING

A key finding of human balance experiments has been that the integration of sensory information utilized for postural control appears to be dynamically regulated to adapt to changing environmental conditions and the available sensory information, a process referred to as “sensory re-weighting.” We consider a postural control model that includes sensory feedback, which has been shown to accurately fit experimental data in a variety of conditions, both steady-state and transient. However, this model does not automatically perform sensory re-weighting nor does it describe how sensory re-weighting is achieved. In this chapter, we adapt this model and provide a method to achieve sensory re-weighting that is physiologically plausible and readily implemented. Model simulations are compared to previously reported experimental results to demonstrate the automated sensory re-weighting strategy of the modified model.

5.1 INTRODUCTION

As already discussed, while no single model currently explains all aspects of human postural control, the model we consider here [82] has been shown to accurately fit experimental data in a variety of conditions, both steady-state [82] and transient [84]. Of special interest are the results obtained experimentally [84], in which transient periods of low- or high-frequency oscillations in the body sway of healthy young adults were observed during sway-referencing of the support surface, as described in Chapter 3. Additional experimental support for the model has recently been obtained [12]. The model provides a conceptually simple concept of sensory adaptation/re-weighting. However, it does not describe how sensory weights

change or actually implement an automatic sensory re-weighting strategy. In this chapter, we develop and implement a simple mechanism of sensory re-weighting, based on sensory difference comparisons, to extend the model and interpretation of experimental results on a sway-referenced platform reported in [84].

5.2 BACKGROUND

5.2.1 Human Postural Control Model with Eyes-closed

A comprehensive description of this postural control model was provided in Chapter 3. For completeness, we repeat some of the description here.

The model (Figure 14) consists of a linearized (i.e., small angle) single-link inverted pendulum representation of body dynamics. Upright stance is maintained by a corrective torque applied about the ankle joint, generated by a proportional-integral-derivative (PID) controller, with fixed gain parameters K_P , K_I and K_D . Note that the model utilizes both position and velocity information to stabilize the inverted pendulum, consistent with control theory. The parameter t_d in the model represents the effective time delay of the system, which includes combined delays due to sensory transduction, neural transmission, nervous system processing, muscle activation, and force development.

For eyes-closed stance, as considered here, body sway is sensed by the proprioceptive and graviceptive channels in the model. Referring to Figure 14, this sensory information is combined to yield

$$E(t) = W_p(SS(t) - BS(t)) - W_g(BS(t)) \quad (5.1)$$

where W_p and W_g are the proprioceptive and graviceptive gains or “weights.” These sensory systems have no dynamics in the model (i.e., their frequency response is constant over frequency). For healthy subjects with intact sensory organs and perturbations limited in magnitude and bandwidth to those often used in experimental studies of human postural control (e.g., [82, 84]), this “no dynamics” assumption for the sensory systems is reasonable,

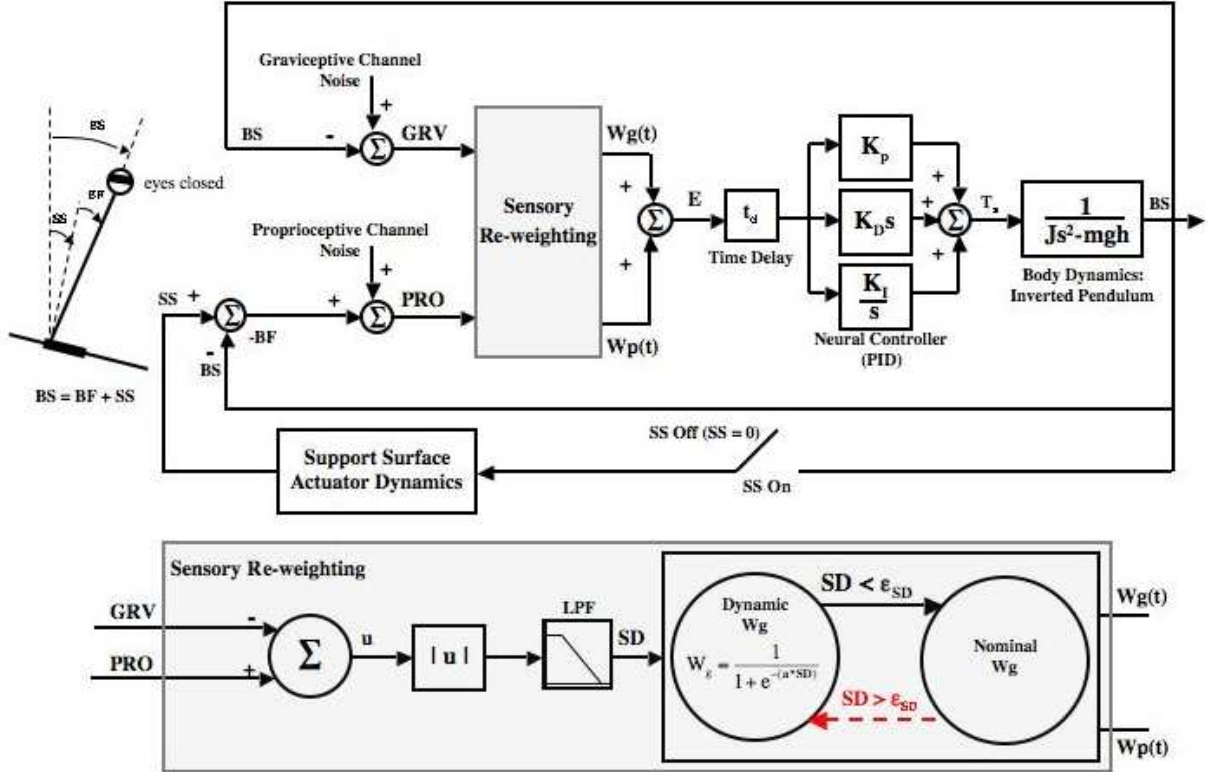


Figure 14: Feedback model of postural control. The body is modelled as a linearized inverted pendulum. The sensory pathways include variable sensory weights (W_g , W_p) that can change as environmental factors change (the “sensory re-weighting” hypothesis). BS and SS are angles, with respect to earth-vertical, of the body and the support surface, respectively, as shown in the stick-figure. BF is the relative angle of the support surface with respect to the body. Corrective torque about the ankle, T_a , is generated by a proportional-integral-derivative (PID) controller with fixed gains K_P , K_D , K_I , acting on the combined delayed sensory error signal E . To generate spontaneous body sway, filtered Gaussian white noise is added to both the graviceptive and proprioceptive channels. Also presented is a schematic representation of the dynamic sensory re-weighting algorithm. As long as the sensory difference (SD) signal remains below a predefined threshold (ϵ_{SD}) the graviceptive weight remains at its nominal value. When SD exceeds the threshold, the graviceptive weight is altered according to a nonlinear function that is dependent on SD. Modified from [82] and [84].

and simplifies the sensory integration strategy, which is modelled via the sensory weights W_g and W_p for eyes-closed stance. Unlike the fixed PID gains of the controller, the sensory weights can change with environmental conditions (the “sensory re-weighting” strategy). These sensory weights represent the relative contribution of each sensory channel to postural control. The model assumes that under steady-state conditions the sum of the sensory weights is unity ($W_g + W_p = 1$), which amounts to a torque normalization constraint [82]. When this condition is satisfied, body sway in response to an external perturbation is non-resonant, that is, there is no strong oscillatory behavior at a specific frequency. But when this condition is not met, which can occur when sensory information is altered, oscillatory behavior arises in the system and sway at a particular frequency is observed [82, 84].

For the model, the body sway (BS) in response to support surface (SS) motion is given in the Laplace domain by

$$BS(s) = H(s)[W_p SS(s)] \quad (5.2)$$

where s is the Laplace variable and

$$H(s) = \frac{(K_D s^2 + K_P s + K_I) e^{-st_d}}{Js^3 - mghs + \mathbf{W}(K_D s^2 + K_P s + K_I) e^{-st_d}} \quad (5.3)$$

is the unity-gain transfer function of the postural control feedback model.

Finally, as mentioned in the preceding chapters, a key concept of the model and the sensory re-weighting hypothesis is the effective overall sensory weight, \mathbf{W} , of the system, which is the sum of the sensory weights of those channels that contribute accurate sensory information about body sway. Thus, the sensory weights that contribute to the effective overall sensory weight are different under different environmental conditions (i.e., under different manipulations of the sensory inputs). An important point to appreciate is that as the value of \mathbf{W} changes, the dynamics of body sway will change. In particular, during transient conditions the system can be pushed towards instability if sensory re-weighting is inadequate, causing \mathbf{W} to be too large or too small, as discussed previously.

5.3 DYNAMIC SENSORY RE-WEIGHTING ALGORITHM

Our sensory re-weighting algorithm is based on two assumptions: 1) that the graviceptive channel provides veridical orientation information, and 2) the CNS can monitor differences between the sensory channels, and alters sensory weights when the difference exceeds a threshold. To develop the sensory re-weighting strategy, consider the model depicted in Figure 14. Ignoring sensory noise for the moment, the proprioceptive (PRO) and graviceptive (GRV) channels measure body sway (BS) relative to the support surface (SS), and body sway relative to earth vertical, respectively,

$$PRO = SS - BS \quad ; \quad GRV = -BS \quad (5.4)$$

Hence, the magnitude of the sensory difference, $|SD|$, is given by

$$|SD| = |PRO - GRV| \quad (5.5)$$

$$= |SS + noise| \quad (5.6)$$

where we have taken into account sensory noise. Hence, when the platform is not moving ($SS = 0$), the sensory difference is a low-level noise signal, which defines a threshold (ϵ_{SD}) below which no change to the sensory weights is made (see APPENDIX B for details on derivation of this threshold). However, when the platform moves, as in the sway-referenced condition considered here, then the sensory difference will exceed the noise threshold. When that occurs, it is assumed that the information from the proprioceptive channel is corrupted, and more emphasis is placed on the graviceptive channel by increasing the sensory weight W_g . Because of the sensory noise, the sensory difference signal is low-pass filtered (1st order filter with cut-off frequency of 0.24 Hz) in order to provide a smoother, less variable, threshold,

$$|SD|_{LP} = |SD| * h_{LP}(t) \quad (5.7)$$

where $*$ denotes convolution and $h_{LP}(t)$ is the impulse response of the filter.

In our implementation, we augment W_g according to a nonlinear (sigmoidal) function,

$$W_g = \frac{1}{1 + e^{(-5 \cdot |SD|_{LP})}} \quad (5.8)$$

which ensures that it can not exceed a specified range. In addition, to avoid abrupt jumps in W_g , the dynamic graviceptive weight (W_g) is low-pass filtered (first order filter with cutoff frequency of 0.04 Hz) after the initiation of sway-referenced platform condition until the end of sway referencing. At the end of sway-referencing and beginning of the final fixed condition, to simulate the observed experimental data reported in [84], W_g is either rapidly (no resonant behavior) or slowly (resonant behavior) returned to its nominal value (see Results), modeling fast or slow adjustments to the new environmental condition sensed by the CNS. This was achieved by filtering the graviceptive weight with either a first-order filter with a time constant of 4 sec (cutoff frequency of 0.04 Hz), to simulate fast adjustments, or with a first-order filter with a time constant of 8 sec (cutoff frequency of 0.02 Hz), to simulate slow adjustments.

5.4 SIMULATIONS AND ANALYSIS

5.4.1 Model Simulations

The parameter values used in the model were: mass $m = 85$ Kg; moment of inertia $J = 81$ Kg·m²; height to center-of-mass $h = 0.9$ m; stiffness $K_P = 970$ N·m·rad⁻¹, damping $K_D = 344$ N·m·s·rad⁻¹; swiftness $K_I = 86$ N·m·s⁻¹·rad⁻¹; and time delay $t_d = 175$ msec. These values are the same as reported in [84].

To generate spontaneous body sway in the model, filtered Gaussian white noise was added to both the graviceptive and proprioceptive channels (Figure 1). The filter specifications are the same as described in [84]. In brief, the sensory channel noise is band-pass filtered at 0.05–0.2 Hz and 0.2–2 Hz for graviceptive and proprioceptive channels, respectively, then low-pass filtered at 0.16 Hz using a first-order (Butterworth) IIR digital filter.

Analogous to the experimental platform motion described in [84], the external perturbation to the model is a sway-referenced platform motion [72], for which $SS = BS$. Each

simulation lasted 180 seconds, consisting of 60 seconds of no movement, i.e., a fixed support surface ($SS = 0$), followed by 60 seconds of sway-referenced movement ($SS = BS$), and then another 60 seconds of fixed surface. During the initial fixed support surface condition (prior to sway-referencing), the initial values of the proprioceptive and graviceptive weights were set to $W_p = 0.8$ and $W_g = 0.2$, respectively [84].

5.4.2 Signal Analysis

The model was implemented on a digital computer such that body sway position was output every 0.01 seconds. The difference between successive samples was computed to generate a body sway velocity time series. This time series was then low-pass filtered at 5 Hz and down-sampled to 10 Hz for further analysis, similar to the data analysis described in [84]. The time-varying spectrum of the down-sampled body sway velocity was estimated by computing a positive time-frequency distribution (TFD) (see [84, 15, 47] for details).

From these TFDs, energy levels were computed over distinct frequency bands (high: 0.7–1.3 Hz; low: 0.1–0.7 Hz) at five different 10 second time intervals: end of fixed platform, start of sway-referencing, end of sway-referencing, start of final fixed platform condition, and end of trial [84]. Energy ratios of high to low frequency bands were computed for each time interval to demonstrate changes in the body sway response to transient environmental conditions.

For each of the weight conditions, that is, fast and slow adjustments, ten simulations with different noise seeds for both the graviceptive and proprioceptive sensory channels were performed. Energy ratios extracted from each TFD per simulation were first averaged over each weight condition ($N = 10$), then ensemble averaged across weight conditions ($N = 20$) for comparison with experimental data [84].

All simulations were performed using Simulink with Matlab version 7 (R14) (The MathWorks, Natick, MA). For details on the model, implemented in Simulink, and accompanied Matlab codes please refer to [APPENDIX D](#).

5.5 RESULTS

Example model simulation results for fast (top) and slow (bottom) adjustments to transient environmental conditions are shown in Figure 15. Plotted in the figure are the effective sensory weight \mathbf{W} ; the individual weights W_g and W_p ; the support surface (SS) and body sway (BS) angles, and the difference between them; body sway velocity (BS Vel); and the corresponding BS Vel time-frequency distribution.

Figure 15 shows that the graviceptive weight W_g adaptively changes from its initial value (set to 0.2 at the beginning of the trial) to a value slightly higher than 0.8 when the support surface condition goes from fixed to sway-referenced (dash-dotted line at 60 sec). The proprioceptive weight W_p is kept constant at its initial value (0.8) throughout the entire trial duration, consistent with the assumptions in [84]. Note that even though W_p stays constant during sway-referencing, the proprioceptive channel does not contribute to torque generation during this period since no change in body sway relative to support surface is sensed when the body is sway-referenced.

After the platform is returned to the fixed condition over a 1 s interval (dash-dotted lines at 120 s), the graviceptive weight decays either in a fast (top) fashion causing the overall effective sensory weight \mathbf{W} to stay at 1, resulting in no resonant behavior in the system, or in a slow (bottom) fashion causing \mathbf{W} to stay at a value greater than 1, inducing an oscillatory (i.e., resonant) behavior as indicated in the time-frequency distribution plots at around 1 Hz and as observed experimentally (see Figure 16).

At the onset of sway-referencing, the change in W_g is slightly delayed (~ 0.85 sec for fast and ~ 1.2 sec for slow). This delay is an artifact of the sensory difference strategy. For some trials, at the onset of sway-referencing the value of the sensory difference signal was below the defined threshold ($\epsilon_{SD} = 0.44^\circ$), hence the change in W_g came slightly later than the onset of platform change. This, as evident from the slow adjustment model simulations (bottom), causes a spike at the onset of sway-referencing. This behavior was not observed in experimental data and is addressed in the Discussion section.

The high- to low-frequency energy ratios (ER), extracted from the time-frequency distribution, for the 10 sec time windows are plotted in Figure 17 along with ERs obtained

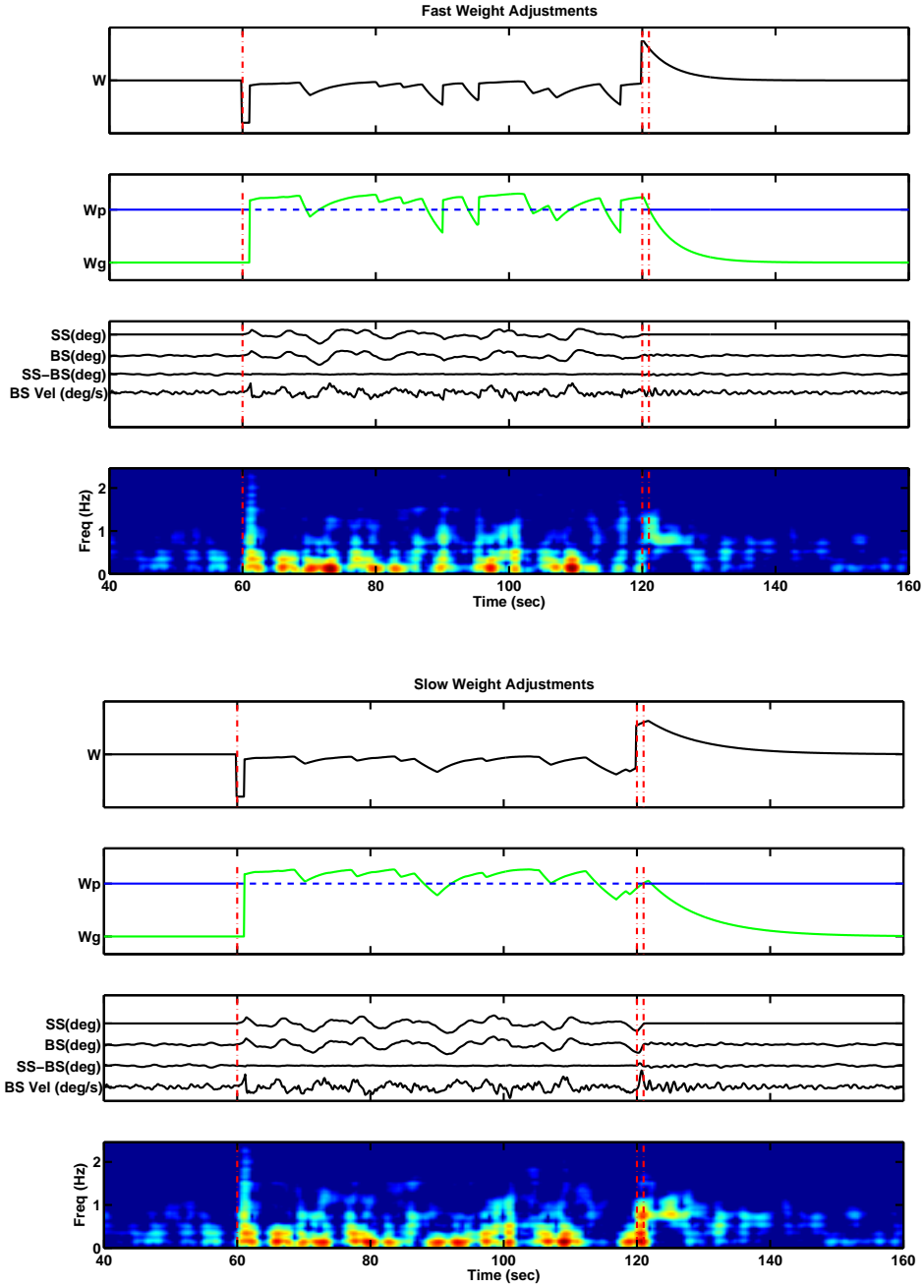


Figure 15: Example model simulations for fast (top) and slow (bottom) weight adjustments according to the sensory re-weighting hypothesis, where the top two panels show the effective sensory weight \mathbf{W} along with the individual weights W_p and W_g , set to 0.8 and 0.2 at the beginning of the trial, respectively, middle panel shows traces for the support surface (SS), body sway (BS) angle, the difference between these two (SS-BS), and body sway velocity (BS Vel), and bottom panel shows the corresponding time-frequency distribution for BS Vel.

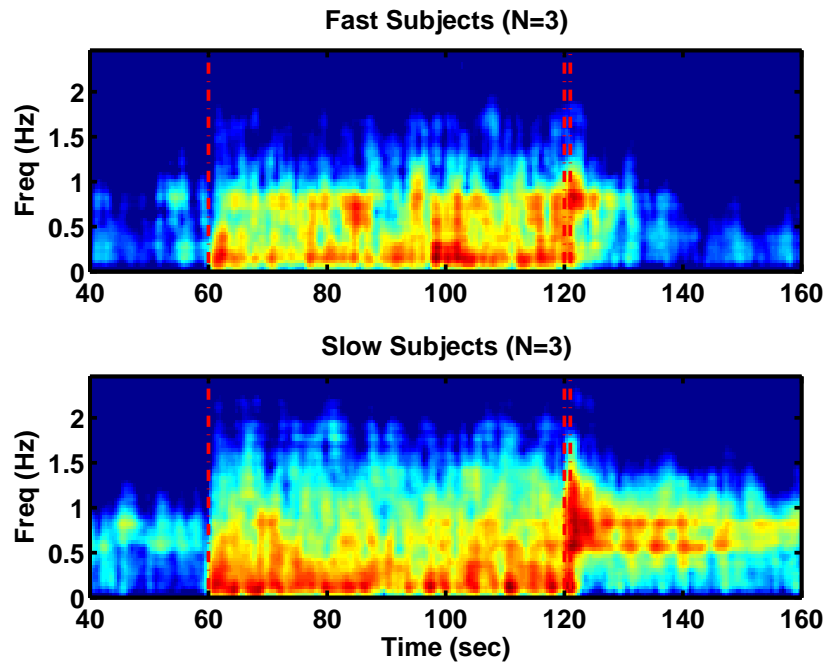


Figure 16: Example experimental time-frequency distributions (TFD) for fast (top) and slow (bottom) weight adjustments. Each subject performed three trials for which individual TFDs were computed. The TFDs were then averaged to result in one representative TFD for each subject. Three subjects were selected based on their final ER value, extracted from their respective TFD. The TFDs in each case were averaged across subjects to render the final results. The support surface angle (SS) is sway-referenced (SR) during the period 60–120 sec. After rapidly returning to a fixed support surface within 1 s (denoted by the double vertical dotted lines at 120 s), body sway oscillations at around 1 Hz develop (orange-yellow band in the TFD around 1 Hz for $t > 120$ sec in bottom graph), indicative of inadequate sensory re-weighting.

experimentally [84], reproduced here for comparison. Each bar indicates the mean \pm SE for 20 model simulations (black bars) averaged across 10 fast and 10 slow weight adjustments and 12 subjects over all trial repetitions (white bars). As evident from the graph, the sensory difference strategy is capable of producing similar patterns observed experimentally with small differences in the first three 10 sec time windows. We observed that changing the cutoff frequency (from 0.16 to 0.25 Hz) of the low-pass filter for the sensory channel noise sequences increased the first three ERs but at the cost of also increasing the fourth energy ratio.

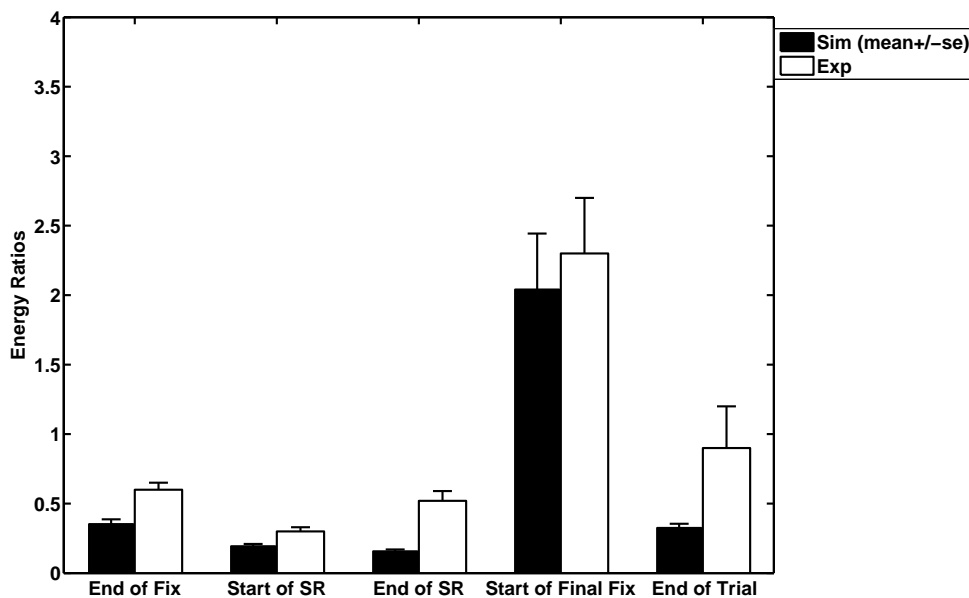


Figure 17: Bar graphs of the high- to low-frequency energy ratios (ER), extracted from the time-frequency distribution, for the 10 sec time windows. Each bar indicates the mean \pm se for 20 model simulations (black bars) averaged across 10 fast and 10 slow weight adjustments and 12 subjects over all trial repetitions (white bars).

5.6 DISCUSSION

In [84], Peterka and Loughlin showed that a simple feedback postural control model is capable of accurately fitting experimental data in a variety of conditions, both steady state [82] and transient [84]. Furthermore, the model proposed provided a conceptually simple, yet experimentally supported concept of sensory adaptation/re-weighting as discussed earlier. However, the model in [84] did not describe how sensory weights change under different environmental conditions. Our goal was to address this question.

We chose to base our sensory re-weighting scheme on the difference between the proprioceptive and graviceptive sensory channels, which we referred to as the sensory difference (SD) signal. The reason behind this is that the difference between the channels according to the model provides information about existence of an external disturbance applied to the body. If we assume that the central nervous system monitors the difference between the available sensory channels, in our case the difference between the proprioceptive and graviceptive channels since we have the eyes closed throughout the trial duration, then as long as there are no external disturbances applied to the body the difference between the channels (i.e., SD) should remain small, in other words, the difference should only reflect the amount of spontaneous sway generated by internal sources of noise in the body, which are in the form of sensory channel noise sequences in the model. But when the difference between the channels gets large, the sensory difference signal (according to the model) provides information about the external world, whether in the form of a platform motion or galvanic stimulation. This additional information, along with the individual sensory channel information provided to the central nervous system, helps in deciding which sensory channel the body need to rely on under different environmental conditions. Since the algorithm proposed is not yet sophisticated enough to distinguish between types of external disturbance, we assumed the central nervous system has knowledge of the type of perturbation applied, in our case it being in the form of a platform motion. Devising more sophisticated algorithms is left for future studies.

As shown in the Results section, the proposed sensory difference strategy was able to detect and differentiate between the two types of platform conditions modeled, namely fixed

and sway-referenced. An undesired result observed in the simulations was the existence of a velocity spike at the onset of sway-referenced platform condition caused by a small delay in switching reliance on the graviceptive channel weight (Figure 15). The reason for this phenomenon is the level of the sensory difference threshold being dependent on the sensory channel noise variances. During the initial fixed platform condition, the body relies more on the proprioceptive sensory channel as compared to the graviceptive channel [82]. To model this, we kept the respective weights constant during this time using a threshold that ensured no triggering of sensory difference. The delay observed at the onset of sway-referencing is caused by this threshold detection. Lowering the value of the sensory difference threshold resulted in body sway angle and velocity traces not observed during quiet stance in experimental data.

We did not observe this velocity spike in any of the experimentally collected data that we were trying to match, indicating the ability of humans to rapidly shift sensory reliance (sensory adaptation/re-weighting) to sudden environmental changes. One way of correcting this discrepancy is to introduce a second reference signal, along with the sensory difference (SD) signal, to be monitored by the central nervous system. Assuming that we know where the source of the external perturbation is coming from, in this case, through the proprioceptive channel, an alternative sensory re-weighting scheme proposed is to continuously monitor the proprioceptive channel (PRO) and indicate whether the information provided by that channel is deemed inaccurate or not. If the information is inaccurate, in other words, the channel does not contribute to torque generation during sway-referencing, attention is paid to the sensory difference signal for additional information. If SD is not indicating existence of an external perturbation (the difference is lower than the threshold), the weights remain constant. If there is an external perturbation detected, then the graviceptive sensory weight changes according to the same nonlinear function introduced earlier.

It was observed that this alternative approach eliminates the small delay seen in our original model simulations (Figure 15). We also noted the dependence of the delay on ϵ_{SD} , that is, the value of ϵ_{SD} had to be fixed at 0.1° in order to generate simulations matching experimental data. Figure 18 shows an example trial for the fast weight adjustments using this approach. As observed, the delay noticed in Figure 15 (top) is now corrected for by

using a smaller threshold value and introduction of the proprioceptive channel signal as another source of reference. It should be noted that using the proprioceptive signal forced us to make some modifications to the model that diverted from the original specifications indicated in [84], namely, not using the actuator dynamics (that is, only simulating the *ideal* sway-referencing case [84]), and using a very small variance for the proprioceptive channel noise sequence.

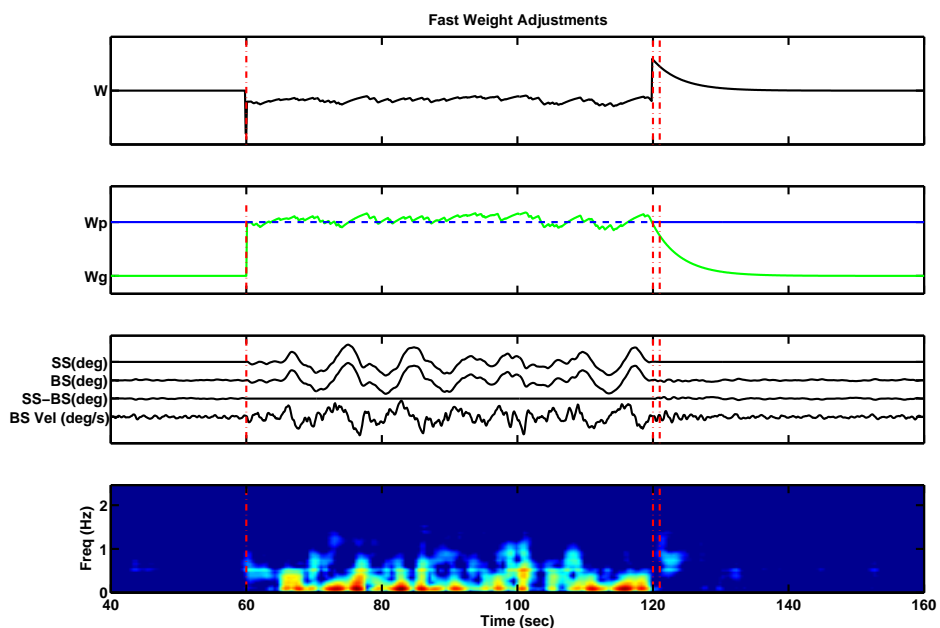


Figure 18: Example model simulation for fast weight adjustments based on the alternative sensory difference strategy, where the top two panels show the effective sensory weight \mathbf{W} along with the individual weights W_p and W_g , set to 0.8 and 0.2 at the beginning of the trial, respectively, middle panel shows traces for the support surface (SS), body sway (BS) angle, the difference between these two (SS-BS), and body sway velocity (BS Vel), and bottom panel shows the corresponding time-frequency distribution for BS Vel. Note the absence of a velocity spike at the start of sway-referencing (indicated by dash-dotted line at 60 sec).

In conclusion, our results showed that a simple adaptive sensory re-weighting scheme based on the difference between the available sensory channels is capable of reproducing

results obtained experimentally as reported in [84]. One drawback of the proposed sensory re-weighting scheme is that it is partial and depends on a specific experiment and perturbation design. More sophisticated and elaborate schemes are required to help design more complex, complete, and unifying models to address other aspects of postural control.

6.0 ROBOT EXPERIMENTS

In this chapter we present results from three robot experiments.

6.1 ROBOT EXPERIMENT I

We have implemented a preliminary sensory re-weighting control strategy similar to that described in [82, 84] in a biped robot. This preliminary implementation used the robot sensors directly, rather than attempting to simulate biological signals. To test the model, the robot was placed on a standard clinical balance testing platform (Figure 19, middle graph), and controller gains were set to maintain stability, with proprioceptive (ankle angle) and graviceptive (inertial) sensory weights initially set to 0.6 and 0.4, respectively (Figure 19, right graph). The proprioceptive and graviceptive gains are consistent with reports in the literature that during quiet standing with eyes closed, proprioception seems to be the dominant source of sensory information for standing balance in humans.

The platform is initially fixed, and at a certain point (10 seconds in Figure 19, right graph) begins sway referencing: rotating in direct 1:1 proportion to body angle about an axis collinear with the ankle joint of the robot. This behaviour has the effect of eliminating reliable ankle proprioception, because the ankle angle remains at approximately 90 degrees, independent of body sway. A feedback control strategy that utilizes primarily ankle proprioception would result in the robot falling shortly after the platform transitions to the sway-referenced condition, as indeed occurred when re-weighting was not used (Figure 19, right graph). We note that it is not unusual for human subjects to also lose their balance the first time they experience a sway-referenced platform with eyes closed.

To maintain balance, the source of sensory information must be rapidly switched from ankle proprioception to the graviceptive sensors, which provides a measure of body angle with respect to earth vertical. We manually implemented sensory re-weighting in the robot model, so that at the transition of the platform from fixed to sway-referenced, the graviceptive gain increased and the proprioceptive ankle gain decreased. This strategy resulted in stable stance for the robot on the sway-referenced platform (Figure 19, right graph). Thus, we have demonstrated that sensory re-weighting is a feasible control solution that can be implemented on a physical system with its real world noise and unmodelled dynamics.

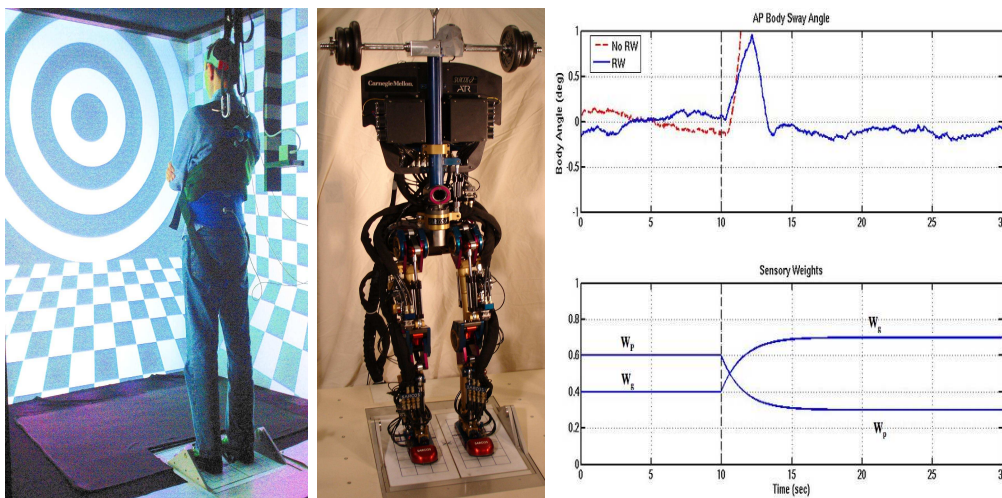


Figure 19: Left: An experimental subject standing on a clinical balance platform (Equitest) in a visual “cave”. Middle: Our bipedal robot standing on an identical balance platform. Right: Preliminary results on robot balancing during sway referencing, which tilts the support platform to keep the ankle angle at 90° . The top graph plots body angle in two trials, and the vertical dashed line indicates the onset of sway-referencing. The first trial (dashed red line) is with fixed feedback gains, and the robot quickly falls. The second trial (solid blue line) is with sensory re-weighting where the weight on the now misleading ankle sensor is reduced. The bottom graph plots the manually specified sensor weightings for proprioception (W_p) and graviception (W_g) during sensory re-weighting. When sensory re-weighting is not used the weights are held constant at their initial values (0.6, 0.4).

6.2 ROBOT EXPERIMENT II

6.2.1 Balance Control In An Optimization Context

In this section we put sensory re-weighting in an optimal filtering and control context. Figure 20 is a block diagram of a model for standing balance in a humanoid robot. For simplicity, the robot dynamics are modelled as a single link inverted pendulum, where the states (angle and angular velocity) of the inverted pendulum are defined with respect to vertical. To maintain an upright position a controlling torque (u_c) is applied at the ankle joint. The torque is generated by state feedback $u_c = -\mathbf{K}\hat{x}_d$, where \mathbf{K} is the state feedback matrix and \hat{x}_d is the state estimate. State estimates are obtained from a Kalman filter, where the inputs are the noisy sensory channels as well as the ankle torque (Figure 20).

The model includes two sensory channels: the proprioceptive (ankle) and graviceptive (vestibular) channels. It is assumed that each sensory channel senses both position and velocity of the robot and that the channels have no dynamics over the bandwidth of body sway movement. To simulate spontaneous sway, we have included process noise (w) with variance Q_w . To perturb the proprioceptive sensory system we have included an external disturbance u_s which moves the foot. Since we model the ankle as a pure torque source, this perturbation does not affect the body directly, but only affects the proprioceptive measurement of joint angle and joint angular velocity. A description of the individual components of the model is provided below.

Robot dynamics: Robot dynamics are modeled as a single link inverted pendulum with a controlling torque applied at the ankle joint. The full derivation of the equations of motion are given in the APPENDIX A. In state space notation, the robot dynamics are written as

$$\dot{x}_d = A_d x_d + B_d u_c + G w \quad (6.1)$$

where $x_d = [\theta \ \dot{\theta}]^T$ represents the states (angle and angular velocity) of the system, u_c is a controlling torque applied at the ankle joint, and w is a zero-mean white Gaussian noise representing the process noise in the system. A_d , B_d , and G are the state, input, and

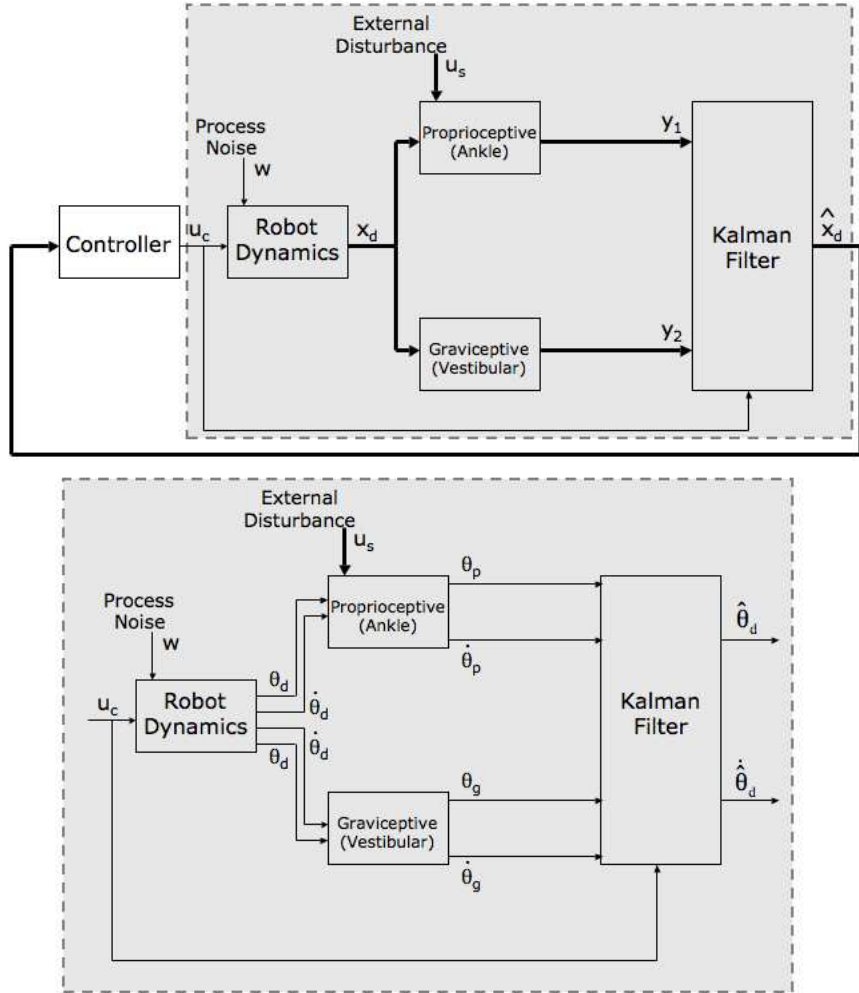


Figure 20: Model for standing balance, where vector elements are represented by bold lines. The robot dynamics are modeled as a single-link inverted pendulum. The model includes two sensory channels, namely the proprioceptive (ankle) and graviceptive (vestibular), where both channels are assumed to sense position and velocity. The ankle torque u_c is generated by state feedback. State estimates are obtained from a Kalman filter.

process noise matrices, respectively. The controlling torque is generated by state feedback $u_c = -\mathbf{K}\hat{x}_d$, where \mathbf{K} is the state feedback matrix and \hat{x}_d is the state estimate. State estimates are obtained from a Kalman filter (see below), where the inputs are the noisy sensory channels as well as the ankle torque (Figure 20).

Sensory channels: The state space representation of the sensory channels is written as

$$\dot{x}_s = A_s x_s + B_s u_s, \quad (6.2)$$

where x_s and u_s are the sensor's states and input, respectively. In addition to the state equation, each channel has an output equation of the form

$$y_s = C_s x_s + D_s u_s + v, \quad (6.3)$$

associated with it, where v is a zero-mean white Gaussian noise representing sensor noise in the model. Since in our modeling we assume that the sensory channels have no dynamics over the bandwidth of sway movement, we can omit the sensory states (x_s) equation (Equation (6.2)) and re-write Equation (6.3) as

$$y_s = C_s x_d + D_s u_s + v, \quad (6.4)$$

where we have substituted the sensor's state vector (x_s) with the robot's state vector (x_d). Together, Equations (6.1) and (6.4) represent the *body-sensor* model

$$\begin{aligned} \dot{x}_d &= A_d x_d + B_d u_c + Gw \\ y_s &= C_s x_d + D_s u_s + v. \end{aligned} \quad (6.5)$$

As mentioned earlier, the model includes two sensory channels: the proprioceptive (ankle) and graviceptive (vestibular). The third sensory channel contributing to balance is the visual channel, where for simplicity it is excluded from the LQG model (as in models of eyes-closed stance). We assume that both the proprioceptive and graviceptive channels sense the robots angle and angular velocity. We perturb the proprioceptive sensory system via an

external disturbance, which affects only the proprioceptive measurement of the joint angle and angular velocity and does not affect the body dynamics. Accordingly, the matrices C_s and D_s have the following forms, respectively

$$\begin{bmatrix} 1 & 0 \\ 0 & 1 \\ 1 & 0 \\ 0 & 1 \end{bmatrix}, \begin{bmatrix} 1 & 0 \\ 0 & 1 \\ 0 & 0 \\ 0 & 0 \end{bmatrix}. \quad (6.6)$$

In this case the sensory outputs are $y_s = [\theta_p \ \dot{\theta}_p \ \theta_g \ \dot{\theta}_g]^T$, where the first two components represent the *relative* joint angle and angular velocity contributed by the proprioceptive channel and the last two components represent the *relative* joint angle and angular velocity contributed by the graviceptive channel.

Controller: For simplifying the derivation, and eventually writing the overall closed loop system in the conventional form, $\dot{x} = Ax + Bu$, we will re-write Equation (6.5), the *body-sensor* equation, as

$$\begin{aligned} \dot{x}_d &= A_d x_d + B_d u_c + 0u_s + Gw \\ y_s &= C_s x_d + 0u_c + D_s u_s + v. \end{aligned} \quad (6.7)$$

As mentioned earlier, the controlling torque applied at the ankle joint is in state feedback form

$$u_c = -\mathbf{K}\hat{x}_d, \quad (6.8)$$

where \mathbf{K} is the state feedback gain and \hat{x}_d is the state estimate obtained from a Kalman filter. The state feedback gain \mathbf{K} can be designed in two ways: Approach 1: linear quadratic regulator (LQR) design, or Approach 2: via Peterka model [82] natural frequency and damping ratio matching. If using Approach 1, the factors involved in designing the state feedback gain are the state and input weighting matrices $Q_{\mathbf{K}}$ and $R_{\mathbf{K}}$, respectively. The state feedback gain is then obtained from the following equation

$$\mathbf{K} = R_{\mathbf{K}}^{-1} B_d^T P_{\mathbf{K}} \quad (6.9)$$

In Equation (6.9), $P_{\mathbf{K}}$ is a positive definite matrix (a matrix with positive eigenvalues) and is the solution to the following equation referred to as the algebraic Riccati equation (ARE)

$$0 = A_d^T P_{\mathbf{K}} + P_{\mathbf{K}} A_d + Q_{\mathbf{K}} - P_{\mathbf{K}} B_d R_{\mathbf{K}}^{-1} B_d^T P_{\mathbf{K}}. \quad (6.10)$$

If using Approach 2, the state feedback gain is obtained from

$$\mathbf{K} = \begin{bmatrix} K_P & K_D \end{bmatrix} \quad (6.11)$$

with

$$\begin{aligned} K_P &= \omega_n^2 J + m l_{cm} g \\ K_D &= 2\zeta \omega_n J, \end{aligned} \quad (6.12)$$

where ω_n and ζ are the natural frequency and damping ratio obtained from the Peterka model [82], respectively.

Kalman filter: The Kalman filter or the estimator has the same basic structure as the robot dynamics but with an additional input $y_s - \hat{y}_s$

$$\begin{aligned} \dot{\hat{x}}_d &= A_d \hat{x}_d + B_d u_c + 0u_s + \mathbf{L}(y_s - \hat{y}_s) \\ \hat{y}_s &= C_s \hat{x}_d + 0u_c, \end{aligned} \quad (6.13)$$

where \mathbf{L} is referred to as the Kalman filter gain. The Kalman filter gain \mathbf{L} is determined in a similar fashion as the state feedback gain \mathbf{K} : instead of the state and input weighting matrices ($Q_{\mathbf{K}}$ and $R_{\mathbf{K}}$) we have the process (w) and sensor (v) noise covariance matrices $Q_{\mathbf{L}}$ and $R_{\mathbf{L}}$, respectively. The process noise covariance matrix is obtained from $Q_{\mathbf{L}} = G Q_w G^T$, where Q_w represents the noise variance of w . Depending on the number of output measurements, $R_{\mathbf{L}}$ is a square diagonal matrix where each element on the diagonal represents the noise variance of the corresponding sensor channel. The Kalman filter gain is then obtained from

$$\mathbf{L} = P_{\mathbf{L}} C_s^T R_{\mathbf{L}} \quad (6.14)$$

where $P_{\mathbf{L}}$ is a positive definite matrix that is the solution to the filtered ARE

$$0 = A_d P_{\mathbf{L}} + P_{\mathbf{L}} A_d^T + Q_{\mathbf{L}} - P_{\mathbf{L}} C_s^T R_{\mathbf{L}}^{-1} C_s P_{\mathbf{L}}. \quad (6.15)$$

Augmented controller-estimator: To derive the overall closed-loop system, the controller and estimator can be combined into an augmented system according to the following derivations: substituting for u_c in the state equation (Equation (6.1)) gives

$$\dot{x}_d = A_d x_d - B_d \mathbf{K} \hat{x}_d + 0u_s + Gw. \quad (6.16)$$

Similarly, substituting for u_c , y_s and \hat{y}_s in the Kalman filter state equation (Equation (6.13)) yields

$$\begin{aligned} \dot{\hat{x}}_d &= A_d \hat{x}_d - B_d \mathbf{K} \hat{x}_d + 0u_s + \mathbf{L}(C_s x_s + 0u_c + D_s u_s + v) \\ &\quad - \mathbf{L}(C_s \hat{x}_s + 0u_c) \\ &= (A_d - B_d \mathbf{K} - \mathbf{L}C_s) \hat{x}_d + \mathbf{L}C_s x_d + \mathbf{L}D_s u_s + \mathbf{L}v. \end{aligned} \quad (6.17)$$

Equations (6.16) and (6.17) can be written in an augmented form as

$$\begin{aligned} \begin{bmatrix} \dot{x}_d \\ \dot{\hat{x}}_d \end{bmatrix} &= \begin{bmatrix} A_d & -B_d \mathbf{K} \\ \mathbf{L}C_s & A_d - B_d \mathbf{K} - \mathbf{L}C_s \end{bmatrix} \begin{bmatrix} x_d \\ \hat{x}_d \end{bmatrix} + \begin{bmatrix} G \\ 0 \end{bmatrix} w \\ &\quad + \begin{bmatrix} 0 \\ \mathbf{L}D_s \end{bmatrix} u_s + \begin{bmatrix} 0 \\ \mathbf{L} \end{bmatrix} v \end{aligned} \quad (6.18)$$

or more compactly as the following equation, where all the inputs to the system are lumped together

$$\begin{aligned} \begin{bmatrix} \dot{x}_d \\ \dot{\hat{x}}_d \end{bmatrix} &= \begin{bmatrix} A_d & -B_d \mathbf{K} \\ \mathbf{L}C_s & A_d - B_d \mathbf{K} - \mathbf{L}C_s \end{bmatrix} \begin{bmatrix} x_d \\ \hat{x}_d \end{bmatrix} \\ &\quad + \begin{bmatrix} G & 0 & 0 \\ 0 & \mathbf{L}D_s & \mathbf{L} \end{bmatrix} \begin{bmatrix} w \\ u_s \\ v \end{bmatrix}. \end{aligned} \quad (6.19)$$

As an extra step, and for the purpose of computing the overall closed loop transfer function of the system, representing the state vector x , input vector u , state matrix A , and input matrix B as

$$x = \begin{bmatrix} x_d \\ \hat{x}_d \end{bmatrix}, \quad (6.20)$$

$$u = \begin{bmatrix} w \\ u_s \\ v \end{bmatrix}, \quad (6.21)$$

$$A = \begin{bmatrix} A_d & -B_d\mathbf{K} \\ \mathbf{L}C_s & A_d - B_d\mathbf{K} - \mathbf{L}C_s \end{bmatrix}, \quad (6.22)$$

$$B = \begin{bmatrix} G & 0 & 0 \\ 0 & \mathbf{L}D_s & \mathbf{L} \end{bmatrix}, \quad (6.23)$$

respectively, allows us to write Equation (6.19) as

$$\begin{aligned} \dot{x} &= Ax + Bu \\ y &= Cx \end{aligned} \quad (6.24)$$

Using this equation, one can then obtain the overall closed loop transfer function from input to output given by

$$\frac{Y(s)}{U(s)} = C(sI - A)^{-1}B \quad (6.25)$$

6.2.2 Model Simulations vs. Experimental Results

We now present a simulation for the model described above. For the design of the state feedback gain we chose Approach 2, that is the state feedback gain is designed to match the natural frequency ($\omega_n = 2 \text{ rad/s}$) and damping ratio ($\zeta = 1$) found in human experiments [82]. The robot's mass multiplied by the height of its center of mass is $ml_{cm} = 34.29 \text{ Kg} \cdot \text{m}$, and its moment of inertia about the ankle is $J = 52.39 \text{ Kg} \cdot \text{m}^2$. The position and velocity gains are provided by using Equation (6.12), resulting in $K = \begin{bmatrix} 551.3 & 225.4 \end{bmatrix}$.

To simulate spontaneous sway, we have included process noise (w) with variance $Q_w = 0.002$. The external disturbance (platform perturbation, u_s) applied to the ankle has a total duration of 181 seconds and consists of two cycles of a pseudorandom ternary sequence (PRTS: random sequence of 0,-n,+n) preceded and followed by 30 seconds of no disturbance (Figure 21). Each cycle of the PRTS is 60.5 seconds with a 2-degree peak-to-peak amplitude.

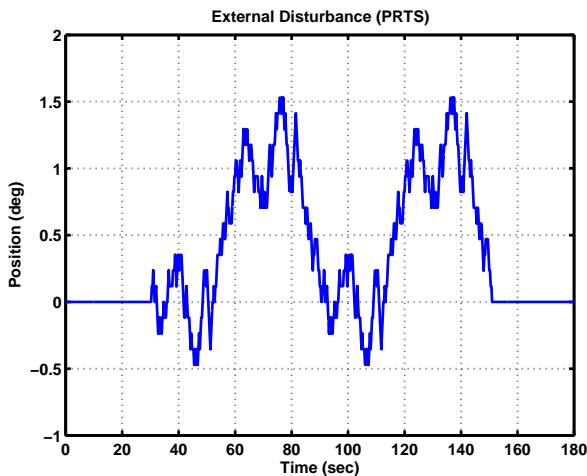


Figure 21: External disturbance applied to the ankle in the simulation.

To design the Kalman filter, the covariance on the sensor noise is

$$R_{L_1} = \begin{bmatrix} 0.14 & 0 & 0 & 0 \\ 0 & 0.14 & 0 & 0 \\ 0 & 0 & 65 & 0 \\ 0 & 0 & 0 & 0.21 \end{bmatrix}, \quad (6.26)$$

where the noise covariance for the graviceptive channel is as reported in [102]. This design leads to Kalman filter gains of

$$L_1 = \begin{bmatrix} 0.0043 & 0.0110 & 0.0000 & 0.0073 \\ 0.0110 & 0.0278 & 0.0000 & 0.0185 \end{bmatrix}. \quad (6.27)$$

We chose the ratio of the velocity elements of R to get a ratio of 60/40 in the proprioceptive vs. graviceptive elements of L_1 , which roughly matches human sensor weightings [82]. We have found that scaling R as a whole has little effect on the Kalman filter gains, probably due to the fact that the controlled system is unstable. To handle proprioceptive perturbations, we design a second Kalman filter with sensor noise covariance and gains:

$$R_{L_2} = \begin{bmatrix} 0.49 & 0 & 0 & 0 \\ 0 & 0.49 & 0 & 0 \\ 0 & 0 & 65 & 0 \\ 0 & 0 & 0 & 0.21 \end{bmatrix}, \quad (6.28)$$

$$L_2 = \begin{bmatrix} 0.0023 & 0.0057 & 0.0000 & 0.0134 \\ 0.0057 & 0.0145 & 0.0000 & 0.0339 \end{bmatrix}. \quad (6.29)$$

In this case the estimate of the strength of proprioceptive sensor noise was increased, so that the ratio of proprioceptive to graviceptive velocity elements in L is roughly 30/70, matching human sensor weightings during ankle perturbations.

The body sway angle resulting from the external disturbance to the model is plotted in Figure 22 (left graph), where the vertical black dashed line indicates onset of sensory re-weighting (switching Kalman filter gains from L_1 to L_2). As evident from the graph, after about 70 seconds into the perturbation, where sensory re-weighting has occurred, the model

is able to lower the amount of body sway and rely more on the less noisy channels available. The right graph in Figure 22 shows this experiment applied to the robot. The gains had to be changed slightly from the simulation to compensate for additional damping in the actuation and other unmodelled dynamics $K = \begin{bmatrix} 700 & 150 \end{bmatrix}$. We see that both graphs show similar performance improvements due to sensory re-weighting.

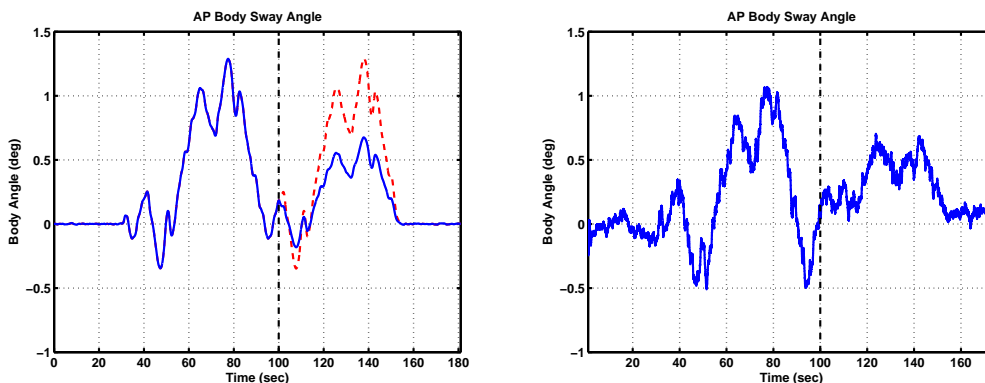


Figure 22: Model response (left graph) to a 2° peak-to-peak PRTS for no sensory re-weighting (dashed red trace) versus sensory re-weighting (solid blue trace). Robot response (right graph) to the same 2° peak-to-peak PRTS with sensory re-weighting. The vertical dashed line indicates onset of sensory re-weighting.

6.2.3 Discussion

We have described our work in modelling human balance control by applying sensory re-weighting to robots. Our long term goal is to develop computational theories of how the weights in sensory re-weighting are chosen. Models of this process are conspicuously absent from work on human balance control, and are necessary for robot balance control.

One lesson from human balance control is that sensory re-weighting is a simple mechanism to handle a wide variety of perturbations: standing on a moving bus, watching a moving scene, or handling the effects of self motion on inertial sensing. Different sensory channels are more or less sensitive to different types of perturbations, and thus different

types of perturbations can be compensated for by weighting the various sensory channels. An accurate model of the disturbance, sensors, or dynamics of the system is not needed. For example, it is not necessary to accurately estimate the platform angle in order to stand during ankle perturbations.

Sensory re-weighting provides a way to combine many sensory systems. Humans use proprioception, inertial sensing, and vision to stand robustly. Robots typically rely on only one or two sensory systems. Another function of sensory re-weighting is to handle inconsistent or malfunctioning sensors. An important step towards robust robot behaviour is developing mechanisms to handle erroneous, inconsistent, or malfunctioning sensors.

6.3 ROBOT EXPERIMENT III

Analogous to the experiment presented in Section 6.1, we implemented the automatic sensory re-weighting control strategy in a biped robot. The robot was placed on a standard clinical balance testing platform (Figure 23, right graph). Initial proprioceptive (ankle angle) and graviceptive (inertial) sensory weights were set to 0.8 and 0.2, respectively. PID controller gains were set to maintain stability on a fixed platform, with values of $K_P = 19.1$ N·m/deg, $K_D = 0.26$ N·m·sec/deg, and $K_I = 0.35$ N·m/sec·deg. In the results reported here, the platform remained level and fixed for 60 seconds, then switched to sway-referencing for 60 seconds, and then returned back to the fixed condition. As described before, sway referencing has the effect of eliminating reliable ankle proprioception, because the ankle angle remains at approximately 90 degrees, independent of body sway.

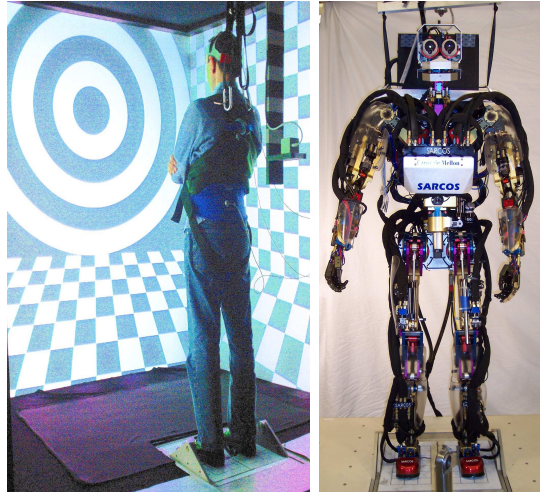


Figure 23: Left: An experimental subject standing on a clinical balance platform (Equitest) in a visual “cave”. Right: Our bipedal robot standing on an identical balance platform.

Figure 24 shows an example trial in which the robot was unable to maintain its balance during the sway-referenced platform condition when the sensory weights remained at their fixed initial values – i.e., in the absence of sensory re-weighting, the robot falls. In this experiment, the platform switched to sway referencing at 10 seconds. Therefore, using a feedback control strategy that utilized primarily ankle proprioception resulted in the robot

falling during sway-referencing. We also performed experiments with different initial sensory weights, including (W_p, W_g) values of $(0.8, 0.2)$, $(0.6, 0.4)$, $(0.4, 0.6)$, $(0.2, 0.8)$, and $(0, 1)$. In all trials except one, the robot was unable to maintain balance with fixed sensory weights.

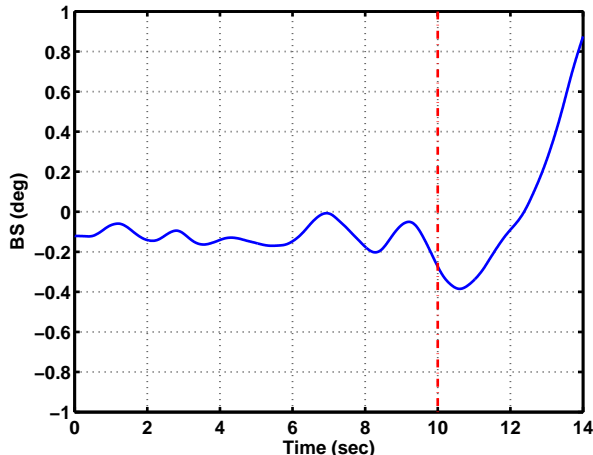


Figure 24: Example trial with fixed sensory weights held constant at their initial values $(1, 0)$ for the proprioceptive and graviceptive, respectively. The platform transition from fixed to sway-referenced is indicated by the dashed vertical line. With no sensory re-weighting, the robot is unable to maintain balance during sway-referencing.

To maintain balance, the source of sensory information must switch from ankle proprioception to the graviceptive sensors. We implemented the sensory difference strategy described in Chapter 5 in the robot model, so that at the transition of the platform from fixed to sway-referenced, the control strategy would increase the graviceptive weight while keeping the proprioceptive weight unaltered. This strategy resulted in stable stance for the robot on the sway-referenced platform (Figure 25).

Example robot experiments for fast (left graph) and slow (right graph) weight adjustments to transient environmental conditions are shown in Figure 25. Plotted in the figure are the effective sensory weight \mathbf{W} , individual weights W_g and W_p , body sway velocity (BS Vel), and corresponding BS Vel time-frequency distribution. In both cases, the graviceptive weight W_g adaptively changes from its initial value (0.2) to a value slightly higher than 0.8 when the support surface condition goes from fixed to sway-referenced (dash-dotted line at 30 sec). The proprioceptive weight W_p is kept constant at its initial value (0.8) throughout the

entire trial duration, although this channel provides little if any sensory information during sway referencing. Because of this, the effective sensory weight during sway referencing is just the graviceptive weight, $\mathbf{W} = W_g$, which increases via the sensory reweighting algorithm, to maintain stability. After the platform is returned to the fixed condition over a 1 sec interval (dash-dotted lines at 90 sec), the effective sensory weight suddenly becomes $\mathbf{W} = W_g + W_p$, which is greater than 1 because W_g has increased during the sway-referencing condition and W_p remained at 0.8. In order to return \mathbf{W} to its nominal value of 1, the sensory reweighting strategy decreases the graviceptive weight W_g . To mimic results seen in human experiments, this decrease occurs in either a rapid fashion, resulting in little resonant behavior in the system (left graph), or in a slow fashion, resulting in oscillatory (i.e., resonant) behavior as indicated in the time-frequency distribution plots at around 0.5 Hz (right graph).

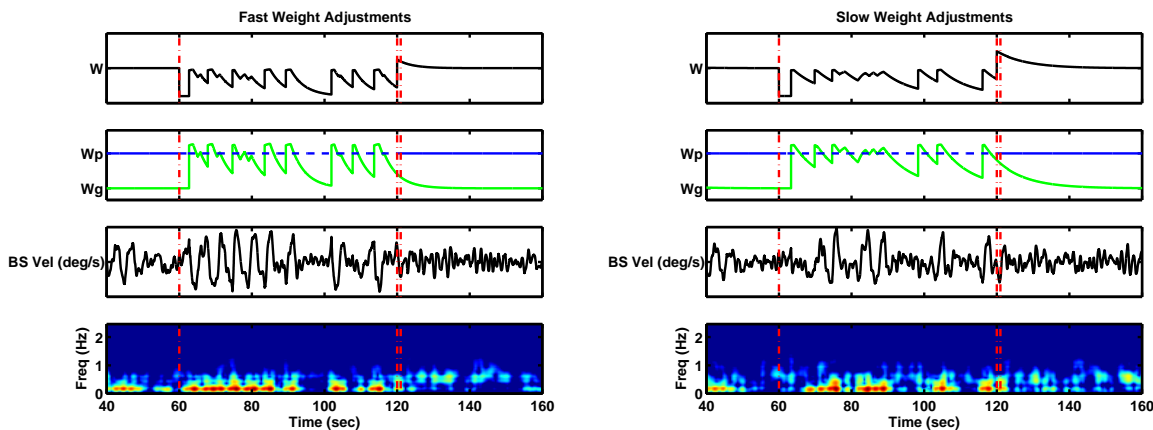


Figure 25: Example robot experiments for fast (left) and slow (right) weight adjustments according to the sensory re-weighting hypothesis, where the top two panels show the effective sensory weight \mathbf{W} along with the individual weights W_p and W_g , set to 0.8 and 0.2 at the beginning of the trial, respectively, middle panel shows traces for the body sway velocity (BS Vel), and bottom panel shows the corresponding time-frequency distribution for BS Vel.

Similar analysis to that described in Chapter 5 was applied to these data. Specifically, energy ratios were computed over distinct frequency bands at five different 10 second time intervals: end of fixed platform, start of sway-referencing, end of sway-referencing, start of final fixed platform condition, and end of trial. Energy ratios of high- to low-frequency bands, as shown in Figure 26, were computed for each time interval to demonstrate changes in

the body sway response to transient environmental conditions. As evident from the graph, the sensory difference strategy is capable of generating body sway patterns qualitatively similar to ones observed in humans (Figure 17, white bars) with an exception being the last 10 sec interval, which in the robot experiments resulted in a higher energy ratio. The robot oscillations were mainly observed around 0.5 Hz, rather than 1 Hz seen in human data. Therefore, the frequency bands over which the energy ratios were computed were changed from those used to analyze human data [84] to match the robot frequency range. The high and low frequency bands were 0.3–0.7 Hz, and 0.1–0.3 Hz, respectively.

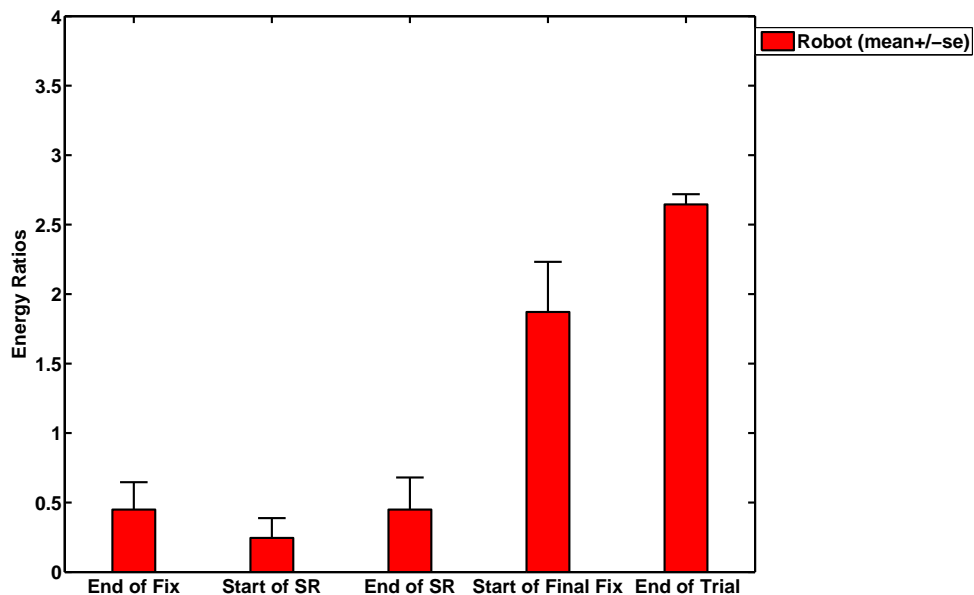


Figure 26: Bar graphs of the high- to low-frequency energy ratios (ER), extracted from the time-frequency distribution, for the 10 sec time windows. Each bar indicates the mean±se for 2 robot experiments averaged across rapid and slow weight adjustments

6.3.1 Discussion

On a fixed platform with fixed sensory weights, the robot was stable, but following the transition to a sway referenced platform, the robot became unstable if the weights remained fixed. By implementing the automatic sensory re-weighting algorithm on the robot, stability

was maintained during the transition to sway referencing, and back to the fixed platform condition. Patterns of sway similar to that observed in human experimental data were observed, although the resonance of the robot was around 0.5 Hz, unlike the human data which exhibits a resonance around 1 Hz.

The difference in resonances could be due to differences in the stiffness and damping of the robot compared to humans. As given above, the stiffness and damping for the robot were $K_P = 19.1 \text{ N}\cdot\text{m}/\text{deg}$, $K_D = 0.26 \text{ N}\cdot\text{m}\cdot\text{sec}/\text{deg}$, while in the human data, these values ranged over $K_P = 16.9\text{--}17.6 \text{ N}\cdot\text{m}/\text{deg}$ and $K_D = 2.5\text{--}6 \text{ N}\cdot\text{m}\cdot\text{sec}/\text{deg}$. Referring to the transfer function in Equation (3.3), taking $K_I = 0$ and $t_d = 0$ gives us the transfer function for a second order inverted pendulum, the characteristic equation for which is

$$s^2 + \frac{\mathbf{W}K_D}{J}s + \frac{\mathbf{W}K_P - mgh}{J} = 0. \quad (6.30)$$

Substituting the stiffness and damping of the robot in this equation results in the system having a resonant frequency at 0.4 Hz when $\mathbf{W} = 1$; this resonance increases in frequency for $\mathbf{W} > 1$, as observed in the frequency response plot below, which is about half the resonant frequency observed in human experiments.

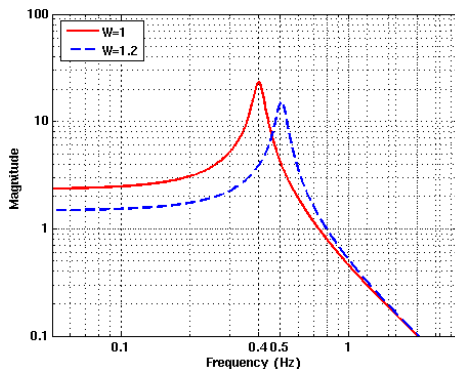


Figure 27: Frequency response plots for the robot, showing the effects of changes in the effective overall sensory weight, \mathbf{W} . Solid curve is for $\mathbf{W} = 1$, and dotted curve is for $\mathbf{W} = 1.2$. PD control parameters were the same in both cases ($K_P = 19.1 \text{ N}\cdot\text{m}/\text{deg}$, $K_D = 0.26 \text{ N}\cdot\text{m}\cdot\text{sec}/\text{deg}$), as were other physical parameters ($g = 9.8 \text{ m}/\text{s}^2$, $m = 95 \text{ Kg}$, $h = 0.8 \text{ m}$, $J = 59 \text{ Kg}\cdot\text{m}^2$). Note the changes in the frequency response as \mathbf{W} changes, and in particular the development of resonances (peaks in the frequency response) at particular frequencies for $\mathbf{W} = 1$ and $\mathbf{W} > 1$.

7.0 CONCLUSIONS AND FUTURE WORK

In this dissertation, the sensory re-weighting hypothesis and models of postural control were further investigated and developed. Chapter 4 reports on human balance experiments conducted during eyes-open stance on a sway-referenced platform while exposed to moving scenes. The hypothesis was that exposure to persistent visual perturbations (prolonged random moving scene) while standing on a sway-referenced platform would induce sensory re-weighting of the visual channel compared to the case of no random scene movement, resulting in decreased reliance on visual feedback. Results obtained from this study were consistent with the sensory re-weighting hypothesis, wherein the sensory integration process reduced the contribution of visual sensory input during the random moving scene interval. An important factor revealed by this experiment, as well as other experiments concerned with sensory re-weighting hypothesis (see for example, [76, 82, 84]), is the ability of the postural control system to adjust its sensory weights, which contribute to balance, based on changes in environmental conditions, such as changes caused by visual perturbations. Simple [83] as well as sophisticated models [101] of human postural control have also been used to predict these changes in sensory weights as observed in experimental data. However, the source of sensory re-weighting in the human postural control system is still an open question and further research is required to understand how this phenomenon occurs.

In Chapter 4, the effects of performing concurrent cognitive tasks on balance control were quantitatively modeled, building on and extending a previously experimentally validated postural control model [82, 84]. A dual-task experiment that involved information processing (IP) tasks concurrent with postural perturbations was conducted to examine competition for cognitive resources and its impact on the model through increase in sensory processing time, quantified by the time delay parameter in the model. The postural control model

hypothesizes that the processing and integration of sensory inputs for balance requires time, and that attention influences this processing time. Performing a concurrent IP task had an overall effect on the time delay, suggesting that the model of postural control, including attentional influences in the time delay, is sensitive to the effect of dual-task interference. This initial study supports the main postulate of the postural control model, that attention, in part, impacts processing speed of the sensory integration process. This effect appears to be true across ages under some conditions, but greater in older adults under other conditions. Further studies in a larger population are warranted.

Finally, Chapters 5 and 6 described our work in developing a physiologically plausible mechanism by which sensory re-weighting could be accomplished. Our goal was to develop a computational method by which the weights in sensory re-weighting are chosen. We proposed a sensory re-weighting strategy based upon a comparison between sensory channels, in order to determine disagreement in sensed body sway. Disagreement between the sensors was detected by comparing the (rectified) difference signal to some threshold, after which changes in the sensory gains were initiated. An algorithm was implemented in computational and bipedal robotic models. The sensory difference strategy generated simulation results consistent with human experimental observations. Furthermore, implementation of this automatic sensory re-weighting algorithm in a bipedal robot was successful in generating body sway patterns qualitatively similar to ones observed in humans. A limitation of the proposed sensory re-weighting strategy is that it applies to a specific experiment and perturbation design, namely sway referencing during eyes-closed stance. Extension of this sensory difference strategy to other postural situations is a subject for further investigation.

APPENDIX A

PENDULUM EQUATIONS OF MOTION

For completeness, the full derivation of equations of motion (EOM) for a single link inverted pendulum, using the method of Euler-Lagrange, is provided below. We begin by a brief introduction of the Euler-Lagrange method, then proceed to derive the EOM for a single-link pendulum.

A.1 EULER-LAGRANGE METHOD

The Lagrangian is defined as the difference between the kinetic and potential energies

$$L = K - V. \tag{A.1}$$

The kinetic energy, K , defined as the sum of translational and rotational energies, is written as

$$K = \frac{1}{2}mv^T v + \frac{1}{2}\omega^T I\omega, \tag{A.2}$$

where v and ω are the linear and angular velocities, respectively. The gravitational potential energy, V , the force required to raise an object, is defined as the applied force multiplied by the distance through which the object is raised

$$V = mgy, \tag{A.3}$$

where m represents the mass of the object, g the gravitational force, and y the height to which the object is raised. The Euler-Lagrange equations of motion is then defined as

$$\frac{d}{dt} \left(\frac{\partial L}{\partial \dot{\mathbf{q}}} \right) - \frac{\partial L}{\partial \mathbf{q}} = \tau, \quad (\text{A.4})$$

where \mathbf{q} is a vector of generalized coordinates, for example joint angles.

In the following sections we will derive the EOM for a single-link inverted pendulum. The equations are derived with respect to horizontal and vertical references, respectively.

A.2 DERIVATION WITH RESPECT TO HORIZONTAL REFERENCE

As shown in Figure 28, the position and velocity of the center of mass in 2-dimensional coordinates, that is, (x,y) , can be written as

$$\begin{bmatrix} x \\ y \end{bmatrix} = \begin{bmatrix} h \cos \theta(t) \\ h \sin \theta(t) \end{bmatrix} \quad (\text{A.5})$$

$$\begin{bmatrix} \dot{x} \\ \dot{y} \end{bmatrix} = \begin{bmatrix} -h \sin \theta(t) \\ h \cos \theta(t) \end{bmatrix} \dot{\theta}(t) \quad (\text{A.6})$$

For simplicity and ease of notation, the symbol t is omitted hereafter.

The translational and rotational energies of the pendulum can be written as

$$\begin{aligned} \frac{1}{2} m v^T v &= \frac{1}{2} m \dot{\theta}^T J^T J \dot{\theta} \\ &= \frac{1}{2} m h^2 \dot{\theta}^2, \end{aligned} \quad (\text{A.7})$$

$$\begin{aligned} \frac{1}{2} \omega^T I \omega &= \frac{1}{2} \dot{\theta}^T I \dot{\theta} \\ &= \frac{1}{2} I \dot{\theta}^2, \end{aligned} \quad (\text{A.8})$$

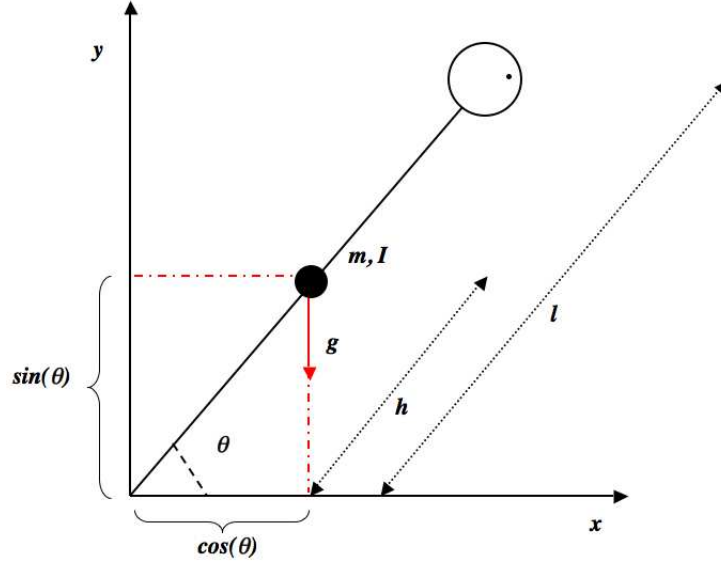


Figure 28: Single-link inverted pendulum diagram with angle and angular velocity taken with respect to horizontal reference.

where $\omega = \dot{\theta}$ is the angular velocity, I is the moment of inertia, and J is the Jacobian matrix

$$J = \begin{bmatrix} -h \sin \theta \\ h \cos \theta \end{bmatrix} \quad (\text{A.9})$$

Based on the above equations, the kinetic and potential energies can now be derived as

$$K = \frac{1}{2}(mh^2 + I)\dot{\theta}^2 \quad (\text{A.10})$$

$$V = mgh \sin \theta. \quad (\text{A.11})$$

As mentioned earlier, the Lagrangian is the difference between these two energy quantities, hence we have

$$\begin{aligned} L &= K - V \\ &= \frac{1}{2}(mh^2 + I)\dot{\theta}^2 - mgh \sin \theta. \end{aligned} \quad (\text{A.12})$$

Now the Euler-Lagrange equations of motion can be written as

$$\frac{d}{dt} \frac{\partial L}{\partial \dot{\theta}} = (mh^2 + I)\ddot{\theta} \quad (\text{A.13})$$

$$\frac{\partial L}{\partial \theta} = -mgh \cos \theta \quad (\text{A.14})$$

$$\frac{d}{dt} \frac{\partial L}{\partial \dot{\theta}} - \frac{\partial L}{\partial \theta} = (mh^2 + I)\ddot{\theta} + mgh \cos \theta \quad (\text{A.15})$$

Finally, the nonlinear equations of motion for a single-link inverted pendulum, using the above derivations, can be written as

$$(mh^2 + I)\ddot{\theta} + mgh \cos \theta = \tau, \quad (\text{A.16})$$

where τ represents a corrective torque applied at the (ankle) joint.

One way of representing the equations of motion is to use state space notation. State equations are collections of first-order differential equations. Together, these equations represent exactly the same information as the original larger-order differential equation. It is apparent that with an n^{th} order differential equation, n first-order differential equations need to be used. However, the variables used to write these first-order equations, referred to as state variables, are not unique.

The state variables for the single-link inverted pendulum are defined as the angle and angular velocity

$$\begin{aligned} x_1 &= \theta \\ x_2 &= \dot{\theta} \end{aligned} \quad (\text{A.17})$$

Using these state variables, the first order differential equations representing equations of motion of the inverted pendulum can be written as

$$\begin{aligned} \dot{x}_1 &= x_2 \\ \dot{x}_2 &= -\frac{mgh}{J} \cos x_1 + \frac{1}{J}\tau \end{aligned} \quad (\text{A.18})$$

Since the equations of motion are nonlinear, we can linearize them around a nominal point using the Taylor series expansion

$$\begin{aligned}
f(x_1, x_2, \dots, x_n) &= f(x_1^*, x_2^*, \dots, x_n^*) + \frac{\partial f}{\partial x_1} \Big|_{x_1^*} (x_1 - x_1^*) + \frac{\partial f}{\partial x_2} \Big|_{x_2^*} (x_2 - x_2^*) \\
&\quad + \dots + \frac{\partial f}{\partial x_n} \Big|_{x_n^*} (x_n - x_n^*)
\end{aligned} \tag{A.19}$$

If we define

$$\begin{aligned}
f_1(x_1, x_2, \tau) &= x_2 \\
f_2(x_1, x_2, \tau) &= -\frac{mgh}{J} \cos x_1 + \frac{1}{J} \tau
\end{aligned} \tag{A.20}$$

and let the nominal point or the equilibrium point of the inverted pendulum to be

$$\begin{aligned}
x_1^* &= \frac{\pi}{2} \\
x_2^* &= 0
\end{aligned} \tag{A.21}$$

then we can write the linearized equations of motion as

$$\begin{aligned}
\dot{x}_1 &= x_2 \\
\dot{x}_2 &= \frac{mgh}{J} (x_1 - \frac{\pi}{2}) + \frac{1}{J} \tau
\end{aligned} \tag{A.22}$$

The above equation can be represented in matrix form

$$\begin{bmatrix} \dot{x}_1 \\ \dot{x}_2 \end{bmatrix} = \begin{bmatrix} 0 & 1 \\ \frac{mgh}{J} & 0 \end{bmatrix} \begin{bmatrix} x_1 - \frac{\pi}{2} \\ x_2 \end{bmatrix} + \begin{bmatrix} 0 \\ \frac{1}{J} \end{bmatrix} \tau \tag{A.23}$$

and in a more compact form as

$$\dot{\mathbf{x}} = A\mathbf{x} + B\tau \tag{A.24}$$

where

$$A = \begin{bmatrix} 0 & 1 \\ \frac{mgh}{J} & 0 \end{bmatrix} \tag{A.25}$$

$$B = \begin{bmatrix} 0 \\ \frac{1}{J} \end{bmatrix} \tag{A.26}$$

A.3 DERIVATION WITH RESPECT TO VERTICAL REFERENCE

The derivation in this section is similar to the previous section with the exception that the reference point is now with respect to vertical (Figure 29).

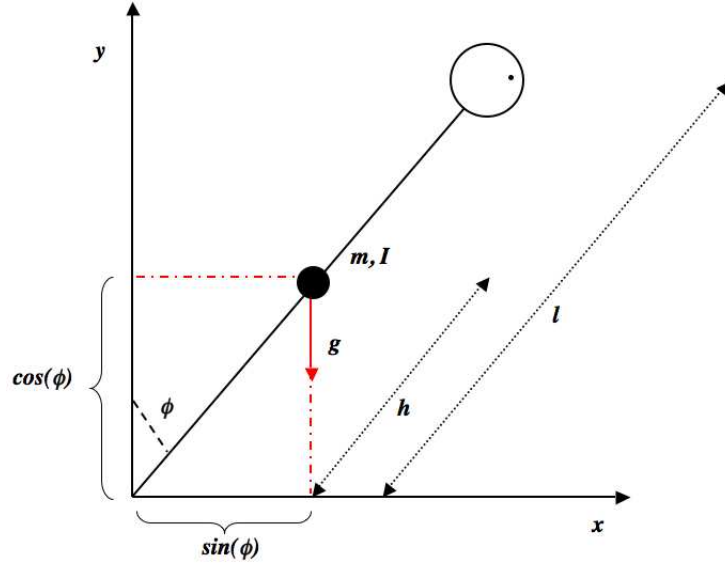


Figure 29: Single-link inverted pendulum with angle and angular velocity taken with respect to vertical reference

The position and velocity of the center of mass in this instance are written as

$$\begin{bmatrix} x \\ y \end{bmatrix} = \begin{bmatrix} h \sin \phi(t) \\ h \cos \phi(t) \end{bmatrix} \quad (\text{A.27})$$

$$\begin{bmatrix} \dot{x} \\ \dot{y} \end{bmatrix} = \begin{bmatrix} h \cos \phi(t) \\ -h \sin \phi(t) \end{bmatrix} \dot{\phi}(t) \quad (\text{A.28})$$

The translational and rotational energies are given by

$$\begin{aligned} \frac{1}{2} m v^T v &= \frac{1}{2} m \dot{\phi}^T J^T J \dot{\phi} \\ &= \frac{1}{2} m h^2 \dot{\phi}^2, \end{aligned} \quad (\text{A.29})$$

$$\begin{aligned}\frac{1}{2}\omega^T I \omega &= \frac{1}{2}\dot{\phi}^T I \dot{\phi} \\ &= \frac{1}{2}I\dot{\phi}^2,\end{aligned}\tag{A.30}$$

where $\omega = \dot{\phi}$ is the angular velocity, I is the moment of inertia, and J is the Jacobian matrix

$$J = \begin{bmatrix} -h \sin \phi \\ h \cos \phi \end{bmatrix}\tag{A.31}$$

Similar to the previous section, the kinetic and potential energies can then be written as

$$K = \frac{1}{2}(mh^2 + I)\dot{\phi}^2,\tag{A.32}$$

$$V = mgh \cos \phi,\tag{A.33}$$

and the Lagrangian as

$$\begin{aligned}L &= K - V \\ &= \frac{1}{2}(mh^2 + I)\dot{\phi}^2 - mgh \cos \phi.\end{aligned}\tag{A.34}$$

The Euler-Lagrange equations of motion are then

$$\frac{d}{dt} \frac{\partial L}{\partial \dot{\phi}} = (mh^2 + I)\ddot{\phi}\tag{A.35}$$

$$\frac{\partial L}{\partial \phi} = mgh \sin \phi\tag{A.36}$$

$$\frac{d}{dt} \frac{\partial L}{\partial \dot{\phi}} - \frac{\partial L}{\partial \phi} = (mh^2 + I)\ddot{\phi} - mgh \sin \phi\tag{A.37}$$

In this case, the nonlinear equations of motion and the linearized equations around the equilibrium point can be written as

$$(mh^2 + I)\ddot{\phi} - mgh \sin \phi = \tau\tag{A.38}$$

$$\begin{aligned}\dot{x}_1 &= x_2 \\ \dot{x}_2 &= \frac{mgh}{J}x_1 + \frac{1}{J}\tau\end{aligned}\tag{A.39}$$

respectively, with the equilibrium defined as

$$\begin{aligned}x_1^* &= 0 \\ x_2^* &= 0\end{aligned}\tag{A.40}$$

Finally, the matrix form of the above equations is given as

$$\begin{bmatrix} \dot{x}_1 \\ \dot{x}_2 \end{bmatrix} = \begin{bmatrix} 0 & 1 \\ \frac{mgh}{J} & 0 \end{bmatrix} \begin{bmatrix} x_1 \\ x_2 \end{bmatrix} + \begin{bmatrix} 0 \\ \frac{1}{J} \end{bmatrix} \tau\tag{A.41}$$

where

$$A = \begin{bmatrix} 0 & 1 \\ \frac{mgh}{J} & 0 \end{bmatrix}\tag{A.42}$$

$$B = \begin{bmatrix} 0 \\ \frac{1}{J} \end{bmatrix}\tag{A.43}$$

APPENDIX B

SENSORY DIFFERENCE THRESHOLD

For a Gaussian process $x \sim N(0, \sigma^2)$ with probability distribution $f(x) = \frac{e^{-\frac{x^2}{2\sigma^2}}}{\sigma \cdot \sqrt{2\pi}}$, would like to find the probability that $1 - P(-\epsilon_{SD} < x < \epsilon_{SD}) < \gamma$, where γ is a small number set to 5×10^{-5} and ϵ_{SD} is the desired sensory difference threshold.

Plugging in $\int_{-\epsilon_{SD}}^{\epsilon_{SD}} f(x)dx$ for $P(-\epsilon_{SD} < x < \epsilon_{SD})$ in the equation above yields

$$1 - \int_{-\epsilon_{SD}}^{\epsilon_{SD}} f(x)dx < \gamma, \quad (\text{B.1})$$

where

$$\int_{-\epsilon_{SD}}^{\epsilon_{SD}} f(x)dx = \text{erf}\left(\frac{\sqrt{2}}{2\sigma}\epsilon_{SD}\right) \quad (\text{B.2})$$

with erf denoting the error function defined as $\text{erf}(x) = \frac{2}{\sqrt{\pi}} \int_0^x e^{-t^2} dt$. Therefore,

$$1 - \text{erf}\left(\frac{\sqrt{2}}{2\sigma}\epsilon_{SD}\right) < \gamma \quad (\text{B.3})$$

which leads to

$$\epsilon_{SD} > \sqrt{2} \cdot \sigma \cdot \text{erf}^{-1}(1 - \gamma) \quad (\text{B.4})$$

Hence, the sensory difference threshold is dependent on the proprioceptive and graviceptive sensory channel noise variance.

In our model simulations, using a weighted sum of the sensory channel noise variances $\sigma = \sqrt{W_p\sigma_p^2 + W_g\sigma_g^2}$, with proprioceptive and graviceptive channel noise variances set to 1° and 6° , respectively, with $W_p = 0.8$ and $W_g = 0.2$, and $\gamma = 5 \times 10^{-5}$, we obtained $\epsilon_{SD} > 0.31^\circ$. The actual value chosen for model simulations was set to 0.45° .

APPENDIX C

POSTURAL CONTROL MODEL WITH ESTIMATION

Recent work by Jeka and colleagues [36, 37] has shown that a control strategy formulated in an optimization context and including estimation error in the body motion information provided by the sensory system can account for factors observed in human experiments. On the other hand, the Peterka model that we have predominantly used in this dissertation and which has been found to also explain human data, does not utilize an optimization and estimation framework. In this Appendix, we consider a modification of the Peterka model to put it in an optimal filtering and control context. Figure 30 shows the block diagram of the Peterka model incorporating an optimal filter (estimator) to provide the best estimate, from the noisy measurements, of body sway orientation. The model has the same features as the one presented in Chapter 5, with the exception of including an optimal filter and excluding the integral controller.

The Kalman filter provides a way to combine noisy sensors, given certain assumptions [21]. In this model, state estimates, i.e., best estimates of body sway given noisy sensors, are obtained from a Kalman filter. The Kalman filter dynamics have the same basic structure as the body dynamics but with an additional input y , i.e., the noisy sensory measurements. The Kalman filter gain was designed solely on the position information, and the noise variance (R) chosen was based on a weighted sum of the proprioceptive and graviceptive channel noise variances. The filter was designed using Matlab's **kalman** function. The regulator, or

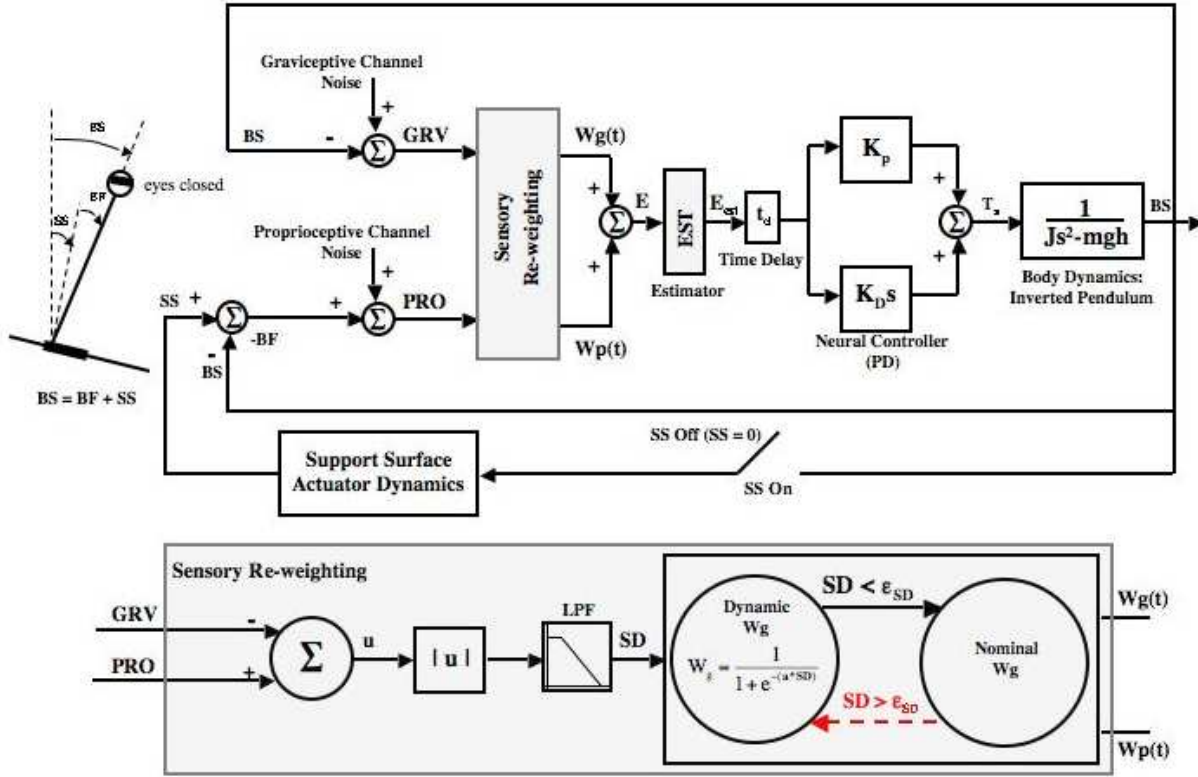


Figure 30: Feedback model of postural control with estimation. The body is modelled as a linearized inverted pendulum. The sensory pathways include variable sensory weights (W_g , W_p) that can change as environmental factors change (the “sensory re-weighting” hypothesis). BS and SS are angles, with respect to earth-vertical, of the body and support surface, respectively, as shown in the stick-figures. BF is the relative angle of the support surface with respect to the body. Corrective torque about the ankle, T_a , is generated by a proportional-integral-derivative (PID) controller with fixed gains K_P , K_D , K_I , acting on the combined delayed sensory error signal E . To generate spontaneous body sway, filtered Gaussian white noise is added to both the graviceptive and proprioceptive channels. Also presented is a schematic representation of the dynamic sensory re-weighting algorithm. As long as the SD signal remains below a predefined threshold (ϵ_{SD}) the graviceptive weight remains at its nominal value. When SD exceeds the threshold, the graviceptive weight is altered according to a nonlinear function that is dependent on SD. Modified from [82] and [84].

specifically the linear quadratic Gaussian (LQG) regulator formed by connecting the Kalman filter (estimator) and the state-feedback gain K , was then designed using Matlab's **lqgreg** function with K including the stiffness and damping factors.

The neural controller (PD) values, i.e., the stiffness and damping factors, were selected manually. The controller was first designed using optimal control techniques (linear quadratic regulator) that resulted in stiffness and damping values much higher than the nominal values presented in [84]. Simulation results using these values resulted in smaller energy ratios when compared to the experimental data (results not shown here). We then ran simulations using the nominal values presented in [84] that resulted in reasonable energy ratios (see Figure 31). We finally increased the neural controller parameters by 15 % to see the effect on the energy ratios. As seen in Figure 32, the values increased to levels closer to the ones obtained experimentally.

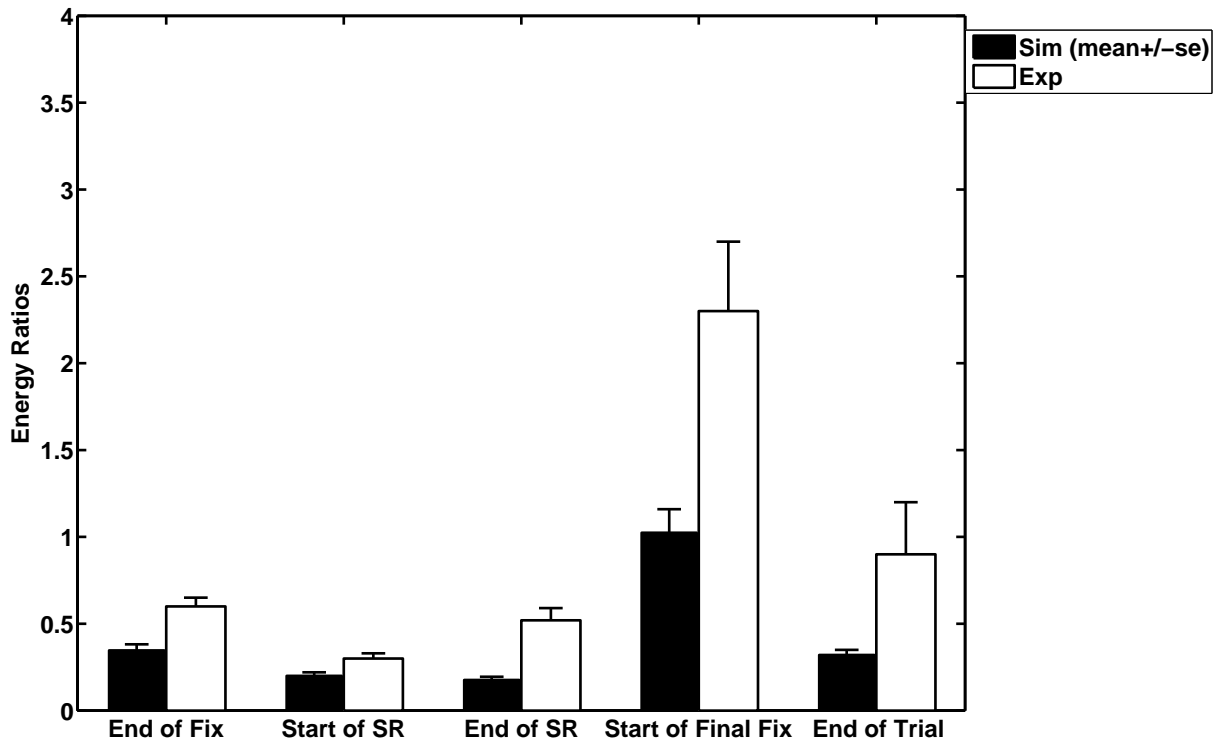


Figure 31: Bar graphs of the high- to low-frequency energy ratios (ER), extracted from the time-frequency distribution, for the 10 sec time windows. Each bar indicates the mean \pm SE for 20 model simulations (black bars), using nominal neural controller values, averaged across 10 fast and 10 slow weight adjustments, and 12 subjects over all trial repetitions (white bars).

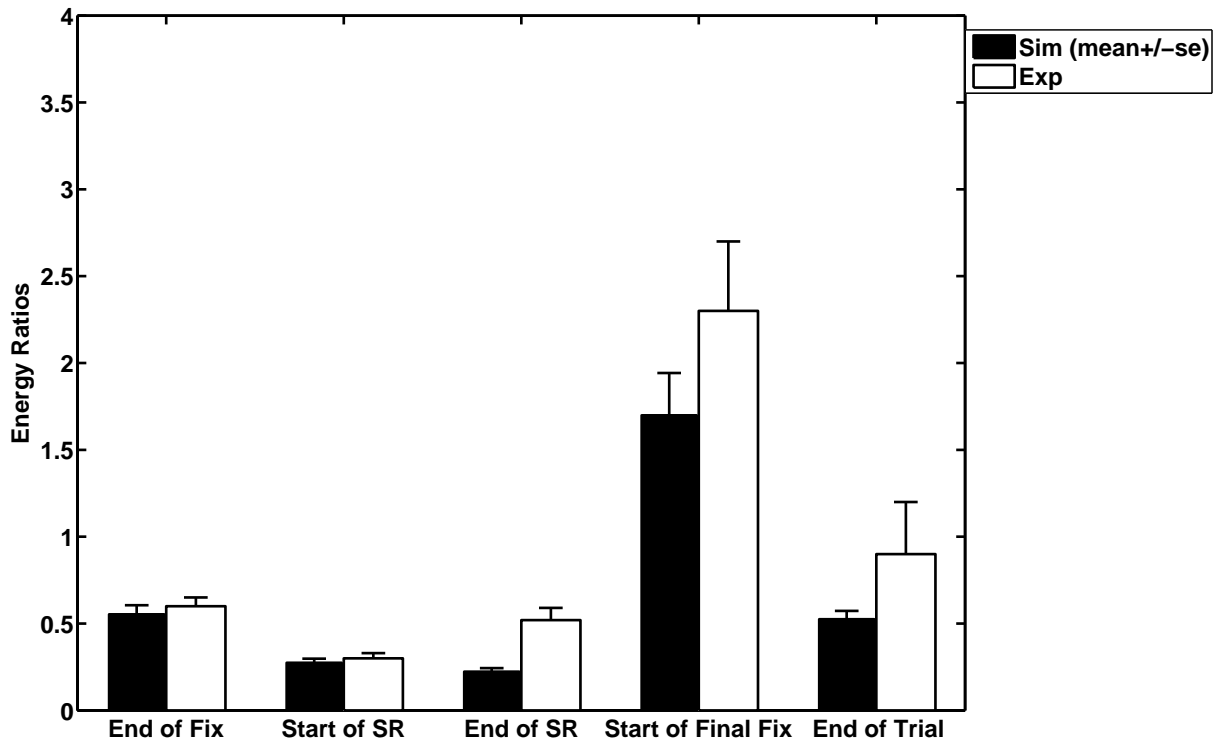


Figure 32: Bar graphs of the high- to low-frequency energy ratios (ER), extracted from the time-frequency distribution, for the 10 sec time windows. Each bar indicates the mean \pm SE for 20 model simulations (black bars), using increased neural controller values, averaged across 10 fast and 10 slow weight adjustments, and 12 subjects over all trial repetitions (white bars).

APPENDIX D

MATLAB CODES AND SIMULINK MODELS

D.1 MATLAB CODES

D.1.1 PARAMETER SETUP

```
function [Ts,trl_drt,blp,alp,tau,sdfo,epsilon,gra_ns,pro_ns]=...
    atmtcPKMdlprmsetup(choice,tc)
%ATMTCPKMDLPRMSETUP Automatic Peterka Model Parameter Setup
%
% [...] = ATMTCPKMDLPRMSETUP(CHOICE,TC) automatic Peterka model parameter
% setup with:
% CHOICE = 'fast' or 'slow', selecting fast or slow weight adjustment
% time constants, and
% TC = indicating desired graviceptive weight filter time constant

Fs=100; % sampling frequency [Hz]
Ts=1/Fs; % sampling time [sec]
trl_drt=180; % trial duration [sec]
% Sensory Difference Lowpass Filter Design (Analog)
N=1; % filter order
Fc=0.24; % cutoff frequency [Hz]
```

```

Wn=(2*pi)*Fc; % cutoff frequency [rad/sec]
[blp,alp]=butter(N,Wn,'s'); % filter coefficients
% Graviceptive Weight Filter Time Constants
switch lower(choice)
    case 'fast' % fast weight adjustments
        tau1=4; % filter time constant during sway-referencing [sec]
        tau2=tc; % filter time constant after sway-referencing [sec]
    case 'slow' % slow weight adjustments
        tau1=4; % filter time constant during sway-referencing [sec]
        tau2=tc; % filter time constant after sway-referencing [sec]
end
tau=[tau1 tau2]; % time constants
sdfo=N; % sensory difference filter order used in adptv_snsry_wghts.m
epsilon=[(pi/180)*0.45]; % sensory difference threshold [rad]
% Sensory Channel Noise Seeds
randn('state',sum(100*clock));
gra_ns=round(100*abs(randn)); % graviceptive channel noise seed
randn('state',sum(100*clock));
pro_ns=round(100*abs(randn)); % proprioceptive channel noise seed

```

D.1.2 ADAPTIVE SENSORY WEIGHT S-FUNCTION

```

function [sys,x0,str,ts]=adptv_snsry_wghts(t,x,u,flag,sdfo,epsilon,Ts,tau)
%ADPTV_SNSRY_WGHTS Adaptive Sensory Weight S-Function
%
% [...] = ADPTV_SNSRY_WGHTS(T,X,U,FLAG,SDF0,EPSILON,TS,TAU)
% dynamically generates sensory weights based on the
% difference between the sensory channels, referred to as the sensory
% difference (SD) signal

```

```

switch flag,
    case 0,
        [sys,x0,str,ts]=mdlInitializeSizes;
    case 1,
        sys=mdlDerivatives(t,x,u);
    case 2,
        sys=mdlUpdate(t,x,u,sdfo,epsilon,Ts,tau);
    case 3,
        sys=mdlOutputs(t,x,u);
    case 4,
        sys=mdlGetTimeOfNextVarHit(t,x,u);
    case 9,
        sys=mdlTerminate(t,x,u);
    otherwise
        error(['Unhandled flag = ',num2str(flag)]);
end

```

```

function [sys,x0,str,ts]=mdlInitializeSizes
size=simsizes;
sizes.NumContStates = 0;
sizes.NumDiscStates = 3; % number of discrete states
sizes.NumOutputs = 2; % number of outputs
sizes.NumInputs = 1; % number of inputs
sizes.DirFeedthrough = 1;
sizes.NumSampleTimes = 1;
sys=simsizes(sizes);
x0=[1 0.2 0.8]; % intial conditions [counter Wg Wp]
str=[];
ts=[0 0];

```

```

function sys=mdlDerivatives(t,x,u)
sys=[];

function sys=mdlUpdate(t,x,u,sdfo,epsilon,Ts,tau)
counter=x(1)+1; % counter
% Dynamic sensory re-weighting
if counter>=sdfo % sdfo=SD's filter order
    if (u>=epsilon) % u=SD [rad], epsilon=SD threshold [rad]
        u_deg=(180/pi)*(u); % u_deg=SD [deg]
        sig_fnc=1/(1+exp(-5*u_deg)); % sigmoid function
        if ((sig_fnc-x(2))~=0 & (sig_fnc-x(2))<0.3)
            % filter Wg if large jump detected
            Wg=(Ts*sig_fnc+tau(1)*x(2))/(tau(1)+Ts);
        else
            Wg=sig_fnc;
        end
    else
        sig_fnc=0.2; % initial (nominal) Wg
        if ((sig_fnc-x(2))~=0 & (sig_fnc-x(2))<0.3)
            sig_fnc=0.2;
            % filter Wg to show effect of fast or slow weight adjustments
            Wg=(Ts*sig_fnc+tau(2)*x(2))/(tau(2)+Ts);
        else
            Wg=sig_fnc;
        end
    end
end
else
    Wg=0.2; % initial (nominal) Wg
end
sys(3)=x(3);

```

```

sys(2)=Wg;
sys(1)=counter;

function sys=mdlOutputs(t,x,u)
sys=[x(2) x(3)]; % Outputs: [Wg Wp]

function sys=mdlGetTimeOfNextVarHit(t,x,u)
sampleTime=1;
sys=t+sampleTime;

function sys=mdlTerminate(t,x,u)
sys=[];

```

D.1.3 PLATFORM MOTION CONTROL S-FUNCTION

```

function [sys,x0,str,ts]=pltfrm_cntrl(t,x,u,flag,Ts)
%PLTFRM_CNTRL Control Motion of the Platform
%
% [...] = PLTFRM_CNTRL(T,X,U,FLAG,TS) controls the motion of the platform
% at the end of sway-referencing. It ensures return of the platform to
% its fixed position over a 1 second interval.

switch flag,
    case 0,
        [sys,x0,str,ts]=mdlInitializeSizes;
    case 1,
        sys=mdlDerivatives(t,x,u);
    case 2,
        sys=mdlUpdate(t,x,u,Ts);
    case 3,

```

```

        sys=mdlOutputs(t,x,u,Ts);
    case 4,
        sys=mdlGetTimeOfNextVarHit(t,x,u);
    case 9,
        sys=mdlTerminate(t,x,u);
    otherwise
        error(['Unhandled flag = ',num2str(flag)]);
end

function [sys,x0,str,ts]=mdlInitializeSizes
sizes=simsizes;
sizes.NumContStates = 0;
sizes.NumDiscStates = 3; % number of discrete states
sizes.NumOutputs = 1; % number of outputs
sizes.NumInputs = 1; % number of inputs
sizes.DirFeedthrough = 1;
sizes.NumSampleTimes = 1;
sys=simsizes(sizes);
x0=[-0.01 0 0]; % initial conditions
str=[];
ts=[0 0];

function sys=mdlDerivatives(t,x,u)
sys=[];

function sys=mdlUpdate(t,x,u,Ts)
count1=x(1)+Ts; % counter
if (count1 > 120) % end of sway-referencing=120 [sec]
    out=x(3)-x(2)*Ts;
    sys(3)=out;

```

```

        sys(2)=x(2);
        sys(1)=count1;
else
    out=u(1);
    sys(3)=out; % y previous
    sys(2)=out; % body sway (BS)
    sys(1)=count1; % counter
end

```

```

function sys=mdlOutputs(t,x,u,Ts)
sys=[x(3)];

```

```

function sys=mdlGetTimeOfNextVarHit(t,x,u)
sampleTime=1;
sys=t+sampleTime;

```

```

function sys=mdlTerminate(t,x,u)
sys=[];

```

D.1.4 SENSORY CHANNEL NOISE FILTER DESIGN

```

%SNSTRYCHNLFILTERDESIGN Sensory Channels Filter Design
%
% SNSTRYCHNLFILTERDESIGN Designs bandpass and lowpass filters for the
% graviceptive and proprioceptive sensory channels. Parameters are based
% on [Peterka and Loughlin 2004]

% Graviceptive Channel Bandpass Filter (Analog)
Fs=100; % sampling frequency [Hz]
N=1; % filter order

```

```

Fc1=0.05; % cutoff frequency [Hz]
Fc2=2; % cutoff frequency [Hz]
Wn=(2*pi)*[Fc1 Fc2]; % cutoff frequency [rad/sec]
[bg,ag]=butter(N,Wn,'s'); % filter coefficients

% Proprioceptive Channel Bandpass Filter (Analog)
Fs=100; % sampling frequency [Hz]
N=1; % filter order
Fc1=0.2; % cutoff frequency [Hz]
Fc2=2; % cutoff frequency [Hz]
Wn=(2*pi)*[Fc1 Fc2]; % cutoff frequency [rad/sec]
[bp,ap]=butter(N,Wn,'s'); % filter coefficients

% Graviceptive and Proprioceptive Lowpass Filter (Analog)
Fs=100; % sampling frequency [Hz]
N=1; % filter order
Fc=0.16; % cutoff frequency [Hz]
Wn=(2*pi)*Fc; % cutoff frequency [rad/sec]
[bl,al]=butter(N,Wn,'s'); % filter coefficients

```

D.1.5 PARAMETER SETUP FOR MODEL WITH ESTIMATION

```

function [A_body,B_body,C_body,D_body,K,A_est,B_est,C_est,D_est]=...
    atmtcPKMdlwEstprmsetup()
%ATMTCPKMDLWESTPRMSETUP Automatic Peterka Model w/ Estimator Parameter
%Setup

% Body Dynamics
g=9.81; % acceleration due to gravity [m/s^2]
m=85; % body mass [Kg]

```

```

h=0.9; % body center of mass [m]
J=81; % body moment of inertia [Kgm^2]
Fs=100; % sampling frequency [Hz]
Ts=1/Fs; % sampling time [sec]
A_body=[0 1;(1/J)*round(m*g*h) 0];
B_body=[0;(1/J)];
C_body=[1 0]; % only consider position
D_body=0;
% State Feedback Gain K
% Linear Quadratic, i.e., Optimal gains
R=1; % control weighting matrix
Q=eye(max(size(A_body))); % state weighting matrix
[P,E,K]=care(A_body,B_body,Q,R); % optimal state feedback
% Suboptimal Gains
KP_nominal=970; % stiffness [N.m/rad]
KD_nominal=344; % damping [N.m.sec/rad]
KP=round(KP_nominal+KP_nominal*0.15); % 15% increase from nominal value
KD=round(KD_nominal+KD_nominal*0.15); % 15% increase from nominal value
K=[KP KD];
% Estimator Gain L
sys=ss(A_body,B_body,C_body,D_body); % plant
s=0.8*0.0022+0.2*0.020; % noise variance (weighted sum)
RR=[s]; % sensor covariance matrix
[kest,L,P]=kalman(sys,[],RR,[],[1],1); % Kalman filter (estimator)
% Regulator Design
regulator=lqgreg(kest,K);
A_est=regulator.a;
B_est=regulator.b;
C_est=[1 0];
D_est=0;

```

D.2 SIMULINK MODELS

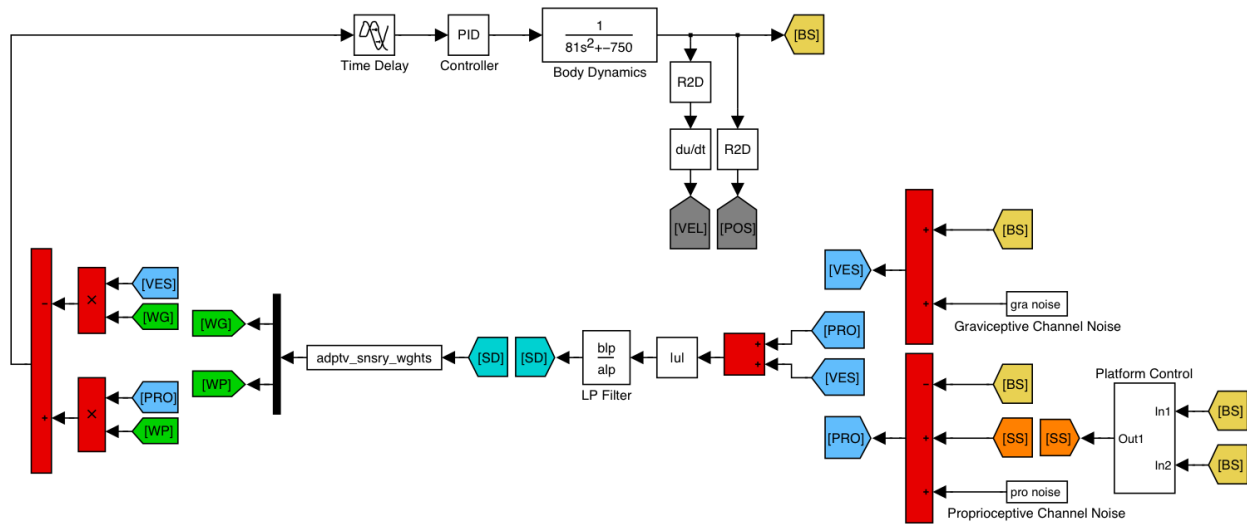


Figure 33: Simulink implementation of the human postural control model

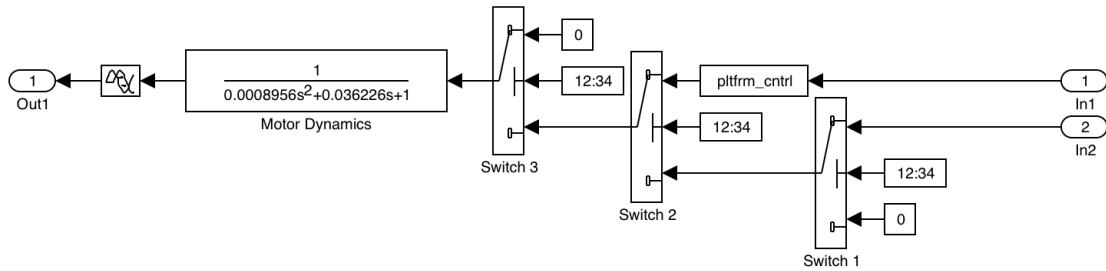


Figure 34: Platform control subsystem

BIBLIOGRAPHY

- [1] Andersson G, Yardley L, and Luxon L (1998). A dual-task study of interference between mental activity and control of balance. *American Journal of Otolaryngology* **19**[5], 632–637
- [2] Barin K (1989). Evaluation of a generalized model of human postural dynamics and control in the sagittal plane. *Biological Cybernetics*, **61**, 37–50
- [3] Bertenthal BI and Bai DL (1989). Infants sensitivity to optical flow for controlling posture. *Developmental Psychology* **25**, 936–945
- [4] Berthoz A, Lacour M, Soechting JF, and Vidal PP (1979). The role of vision in the control of posture during linear motion. *Progress in Brain Research* **50**, 197–209
- [5] Berthoz A, Pavard B, and Young RL (1975). Perception of linear horizontal self-motion induced by peripheral vision (linearvection) basic characteristics and visual-vestibular interactions. *Experimental Brain Research* **23**, 471–489
- [6] Black FO, Shupert CL, Horak FB, and Nashner LM (1988). Abnormal postural control associated with peripheral vestibular disorders. *Progress in Brain Research* **76**, 263–275
- [7] Bles W, Kapteyn TS, Brandt T, and Arnold F (1980). The mechanism of physiological height vertigo. II. Posturography. *Acta Otolaryngologica (Stockholm)* **89**, 534–540
- [8] Borger LL, Whitney SL, Redfern MS, and Furman JM (1999). The influence of dynamic visual environments on postural sway in the elderly. *Journal of Vestibular Research* **9**, 197–205
- [9] Bronstein AM (1986). Suppression of visually evoked postural responses. *Experimental Brain Research* **63**, 655–658
- [10] Brown LA, Shumway-Cook A, and Woollacott MH (1999). Attentional demands and postural recovery: the effects of aging. *The Journals of Gerontology. Series A: Biological Sciences and Medical Sciences* **54**, M165–71
- [11] Carver S, Kiemel T, van der Kooij H, and Jeka JJ (2005). Comparing internal models of the dynamics of the visual environment. *Biological Cybernetics* **92**, 147–163

- [12] Cenciarini M and Peterka RJ (2006). Stimulus-dependent changes in the vestibular contribution to human postural control. *Journal of Neurophysiology* **95**, 2733–2750
- [13] Chong RKY, Jones CL, and Horak FB (1999). Postural set for balance control is normal in Alzheimer’s but not in Parkinson’s disease. *The Journals of Gerontology. Series A: Biological Sciences and Medical Sciences* **54**[3], M129–135
- [14] Chong RKY, Horak FB, and Woollacott MH (2000). Parkinson’s disease impairs the ability to change set quickly. *Journal of the Neurological Sciences* **175**[1], 57–70
- [15] Cohen L (1995). Time-Frequency Analysis. New York: Prentice-Hall
- [16] Collins JJ and De Luca CJ (1993). Open-loop and closed-loop control of posture: A random-walk analysis of center of pressure trajectories. *Experimental Brain Research* **95**, 308–318
- [17] Day BL, Severac Cauquil A, Bartolomei L, Pastor MA, and Lyon IN (1997). Human body-segment tilts induced by galvanic stimulation: A vestibularly driven balance protection mechanism. *Journal of Physiology* **500**, 661–672
- [18] Feldman RG (2000). Peripheral Nerve Biology and Neural Conduction. *NeuroMatrix*, Cambridge, MA
- [19] Fernandez C and Goldberg JM (1971). Physiology of peripheral neurons innervating semicircular canals of the squirrel monkey ii: Response to sinusoidal stimulation and dynamics of peripheral vestibular system. *Journal of Neurophysiology* **34**, 661–675
- [20] Fitzpatrick R, Burke D, and Gandevia SC (1996). Loop gain of reflexes controlling human standing measured with the use of postural and vestibular disturbances. *Journal of Neurophysiology* **76**, 3994–4008
- [21] Grewal MS and Andrews AP (2001). Kalman filtering: Theory and practice using Matlab, 2nd edition. *John Wiley & Sons*
- [22] Hirai K, Hirose M, Haikawa Y, and Takenaka T (1998). The development of Honda humanoid robot. In *Proceedings of IEEE International Conference on Robotics and Automation*, 1321–1326
- [23] Hofmann A, Massaquoi S, Popovic M, and Herr H (2004). A sliding controller for bipedal balancing using integrated movement of contact and non-contact limbs. In *IEEE/RSJ International Conference on Intelligent Robots and Systems*, 1952–1959
- [24] Horak FB and Macpherson JM (1996). Postural orientation and equilibrium. In: Shepard J, Rowell L (eds) *Exercise: Regulation and Integration of Multiple Systems*. (Handbook of physiology, Sect 12) Oxford University Press, New York, 255–292
- [25] Horak FB (2006). Postural orientation and equilibrium: what do we need to know about neural control of balance to prevent falls? *Age and Aging* **35**[S2], ii7–ii11

- [26] Houk JC and Henneman E (1967). Response of Golgi tendon organs to forces applied to muscle tendon. *Journal of Neurophysiology* **30**, 466–481
- [27] Ito S, Nishigaki T, and Kawasaki H (2001). Upright posture stabilization by ground reaction force control. In *Proceeding of the International Symposium on Measurement, Analysis and Modeling of Human Functions (ISHF2001)*, 515–520
- [28] Jamet M, Deviterne D, Gauchard GC, Vançon G, and Perrin PP (2004). Higher visual dependency increases balance control perturbation during cognitive task fulfillment in elderly people. *Neuroscience Letters* **359**, 61–64
- [29] Jeka J, Oie KS, and Kiemel T (2000). Multisensory information for human postural control: integrating touch and vision. *Experimental Brain Research* **134**, 107–125
- [30] Johansson R, Magnusson M, and Akesson M (1988). Identification of human postural dynamics. *IEEE Transactions on Biomedical Engineering* **35**[10], 858–869
- [31] Johansson R and Magnusson M (1991). Human postural dynamics. *Biomedical Engineering* **18**, 413–437
- [32] Kaneko K, Kanehiro F, Kajita S, Hirukawa H, Kawasaki T, Hirata M, Akachi K, and Isozumi T (2004). Humanoid robot HRP-2. In *Proceedings of IEEE International Conference on Robotics and Automation*, 1083–1090
- [33] Kajita S, Yokoi K, Saigo M, and Kazuo T (2001). Balancing a humanoid robot using backdrive concerned torque control and direct angular momentum feedback. In *Proceedings of IEEE International Conference on Robotics and Automation*, 3376–3382
- [34] Kavounoudias A, Gilhodes JC, Roll R, and Roll JP (1999). From balance regulation to body orientation: two goals for muscle proprioceptive information processing? *Experimental Brain Research* **124**, 80–88
- [35] Kerr B, Condon SM, and McDonald LA (1985). Cognitive spatial processing and the regulation of posture. *Journal of Experimental Psychology. Human Perception and Performance* **11**, 617–622
- [36] Kiemel T, Oie KS, Jeka JJ (2002). Multisensory fusion and the stochastic structure of postural sway. *Biological Cybernetics* **87**[4], 262–77
- [37] Kiemel T, Oie KS, Jeka JJ (2006). Slow dynamics of postural sway are in the feedback loop. *Journal of Neurophysiology* **95**, 1410–1418
- [38] Kudoh S, Komura T, and Ikeuchi K (2002). The dynamic postural adjustment with the quadratic programming method. In *Proceedings of IEEE/RSJ International Conference on Intelligent Robots and Systems*, 2563–2568
- [39] Kuo AD (1995). An optimal control model for analyzing human postural balance. *IEEE Transactions on Biomedical Engineering* **42**, 87–101

- [40] Kuo AD (2005). An optimal state estimation model of sensory integration in human postural control balance. *Journal of Neural Engineering* **2**, S235–S249
- [41] Lee DN, Aronson E (1974). Visual proprioceptive control of standing in human infants. *Perception & Psychophysics* **15**, 529–532
- [42] Lee DN and Lishman JR (1975). Visual proprioceptive control of stance. *Journal of Human Movement Studies* **1**, 87–95
- [43] Lestienne F, Soechting J, and Berthoz A (1977). Postural readjustments induced by linear motion of visual scenes. *Experimental Brain Research* **28**, 363–384
- [44] Lim H, Setiawan S, and Takanishi A (2001). Biped walking using stabilization and compliance control. In *Proceedings of IEEE-RAS International Conference on Humanoid Robots*
- [45] Lindenberger U, Marsiske M, and Baltes PB (2000). Memorizing while walking: increase in dual-task costs from young adulthood to old age. *Psychology and Aging* **15**[3], 417–436
- [46] Lofer K, Gienger M, and Pfeiffer F (2003). Sensors and control concept of walking johnnie. *International Journal of Robotics Research* **22**, 229–239
- [47] Loughlin PJ, Pitton J, Atlas L (1994). Construction of positive time-frequency distributions. *IEEE Transactions on Signal Processing* **42**, 2697–2705
- [48] Magnusson M, Enbom H, Johansson R, and Pyykko I (1990). Significance of pressor input from the human feet in anterior-posterior postural control. The effect of hypothermia on vibration-induced body-sway. *Acta Otolaryngologica* **110**, 182–188
- [49] Mahboobin A, Beck C, Moeinzedah M, and Loughlin PJ (2002). Analysis and validation of a human postural control model. *Proceeding of the American Control Conference*, 4122–4128
- [50] Mahboobin A, Loughlin PJ, Redfern MS, and Sparto PJ (2005). Sensory re-weighting in human postural control during moving-scene perturbations. *Experimental Brain Research* **167**, 260–267
- [51] Mahboobin M, Loughlin P, and Redfern M (2006a). A model-based approach to attention and sensory integration in postural control of older adults. *The 28th Annual International Conference IEEE Engineering in Medicine and Biology Society (EMBS)*, New York City, August 30-September 3
- [52] Mahboobin A, Loughlin P, and Redfern M (2006b). Modeling attention and sensory integration in postural control of older adults. *American Society of Biomechanics (ASB) Annual Meeting*, Blacksburg, Virginia, September 6-9

- [53] Mahboobin A, Loughlin PJ, and Redfern MS (2007a). Modeling attentional influence on postural control in young and older adults. *International Society for Gait and Posture 18th International Conference*, Burlington, Vermont, July 14th–18th, 64–65
- [54] Mahboobin A, Loughlin PJ, and Redfern MS (2007b). A model-based approach to attention and sensory integration in postural control of older adults. *Neuroscience Letters* **429**, 147–151
- [55] Mahboobin A, Loughlin PJ, Redfern MS, Anderson SO, Atkeson CG, and Hodgins JK. Sensory adaptation in human balance control: Lesson for biomimetic robotic bipeds. *Neural Networks Special Issue on Neuroscience and Robotics* (accepted)
- [56] Maki BE (1986). Selection of perturbation parameters for identification of the posture control system. *Medical & Biological Engineering & Computing* **24**, 561–568
- [57] Maki BE, Norrie RG, Zecevic A, Quant S, Kirshenbaum N, Bateni H, and McIlroy WE (2001). Initiation and execution of rapid postural reactions and stepping movements: Which phases require visuospatial attention? in *Control of Posture and Gait*, Ed: Duysens J, Smits-Engelsman B, and Kingma H. Symposium of the ISPG, 573–576
- [58] Marchand AR and Amblard B (1984). Locomotion in adult cats with early vestibular deprivation: visual cue substitution. *Experimental Brain Research* **54**, 395–405
- [59] Marsh AP and Geel SE (2000). The effect of age on the attentional demands of postural control. *Gait & Posture* **12**, 105–113
- [60] Maurer C, Mergner T, and Peterka RJ (2006). Multisensory control of human upright stance. *Experimental Brain Research* **171**[2], 231–250
- [61] Mehra RK (1970). On the identification of variances and adaptive Kalman filtering. *IEEE Transactions on Automatic Control*
- [62] Mehra RK (1972). Approaches to adaptive filtering. *IEEE Transactions on Automatic Control*
- [63] Mergner T, Maurer C, and Peterka RJ (2003). A multisensory posture control model of human upright stance. *Progress in Brain Research* **142**, 189–201
- [64] Mergner T, Schweigart G, Maurer C, and Blümle A (2005). Human postural responses to motion of real and virtual visual environments under different support base conditions. *Experimental Brain Research* **167**, 535–556
- [65] Moghaddamjoo A and Kirlin RL (1989). Robust adaptive Kalman filtering with unknown inputs. *IEEE Transactions on Acoustics, Speech, and Signal Processing*
- [66] Morasso PG, Baratto L, Capra R, and Spada G (1999). Internal models in the control of posture. *Neural Networks* **12**, 1173–1180

- [67] Myers KA and Tapley BD (1976). Adaptive sequential estimation with unknown noise statistics. *IEEE Transactions on Automatic Control*
- [68] Nagasaka K, Kuroki Y, Suzuki S, Itoh Y, and Yamaguchi J (2004). Integrated motion control for walking, jumping and running on a small bipedal entertainment robot. In *Proceedings of IEEE International Conference on Robotics & Automation*
- [69] Nashner LM (1971). A model describing vestibular detection of body sway motion. *Acta Otolaryngologica* **72**, 429–436
- [70] Nashner LM and Wolfson P (1974). Influence of head position and proprioceptive cues on short latency postural reflexes evoked by galvanic vestibular simulation of the human labyrinth. *Brain Research* **67**, 255–268
- [71] Nashner LM (1979). Organization and programming of motor activity during posture control *Reflex Control of Posture and Movement, Progress in Brain Research*, Ed: R. Granit and O. Pompeiano. Elsevier, North Holland: Biomedical Press
- [72] Nashner LM, Black FO, and Wall C III (1982). Adaptation to altered support and visual conditions during stance: Patients with vestibular deficits. *Journal of Neuroscience* **2**[5], 536–544
- [73] Nishiwaki K, Kagami S, Kuffner JJ, Inaba M, and Inoue H (2002). Humanoid ‘jsk-h7’: Research platform for autonomous behavior and whole body motion. *Proceedings of the Third IARP International Workshop on Humanoid and Human Friendly Robotics*, 2–9
- [74] Ogura Y, Aikawa H, Lim H, and Takanishi A (2004). Development of a human-like walking robot having two 7-dof legs and a 2-dof waist. *Proceedings of IEEE International Conference on Robotics & Automation*, 134–137
- [75] Oie KS, Kiemel T, and Jeka JJ (2002). Multisensory fusion: simultaneous re-weighting of vision and touch for the control of human posture. *Cognitive Brain Research* **14**, 164–176
- [76] Oie KS, Kiemel T, and Jeka JJ (2001). Human multisensory fusion of vision and touch: detecting nonlinearity with small changes in the sensory environment. *Neuroscience Letters* **315**, 113–116
- [77] Oppenheim AV, Schaffer RW, and Buck JR (1989). Discrete-Time Signal Processing. *Prentice Hall*
- [78] Park S, Horak FB, and Kuo AD (2004). Postural feedback responses scale with biomechanical constraints in human standing. *Experimental Brain Research* **154**, 417–27
- [79] Paulus WM, Straube A, and Brandt T (1984) Visual stabilization of posture. Physiological stimulus characteristics and clinical aspects. *Brain* **107**, 1143–1163

- [80] Peterka RJ and Benolken MS (1995). Role of somatosensory and vestibular cues in attenuating visually induced human postural sway. *Experimental Brain Research* **105**, 101–110
- [81] Peterka RJ (2000). Postural control model interpretation of stabilogram diffusion analysis. *Biological Cybernetics* **82**, 335–343
- [82] Peterka RJ (2002). Sensorimotor integration in human postural control. *Journal of Neurophysiology* **88**, 1097–1118
- [83] Peterka RJ (2003). Simplifying the complexities of maintaining balance. *IEEE Engineering in Medicine and Biology* **22**[2], 63–68
- [84] Peterka RJ and Loughlin PJ (2004). Dynamic regulation of sensorimotor integration in human postural control. *Journal of Neurophysiology* **91**, 410–423
- [85] Prieto T, Myklebust J, Hoffmann R, Lovett E, and Myklebust B (1996). Measures of postural steadiness: Differences between healthy young and elderly adults. *IEEE Transactions on Biomedical Engineering* **43**, 956–966
- [86] Rankin J, Woollacott M, Shumway-Cook A, and Brown L (2000). Cognitive influence on postural stability: a neuromuscular analysis in young and older adults. *Journal of Gerontology* **55**, M112–119
- [87] Redfern MS and Furman JM (1994). Postural sway of patients with vestibular disorders during optic flow. *Journal of Vestibular Research* **4**, 221–230
- [88] Redfern MS, Jennings JR, Martin C, and Furman JM (2001). Attention influences sensory integration for postural control in older adults. *Gait & Posture* **14**, 211–216
- [89] Redfern MS, Muller ML, Jennings JR, and Furman JM (2002). Attentional dynamics in postural control during perturbations in young and older adults. *The Journals of Gerontology. Series A: Biological Sciences and Medical Sciences* **57**, B298–303
- [90] Redfern MS, Talkowski ME, Jennings JR, and Furman JM (2004). Cognitive influences in postural control of patients with unilateral vestibular loss. *Gait & Posture* **19**, 105–114
- [91] Romero DH and Stelmach GE (2003). Changes in postural control with aging and Parkinsons disease. *IEEE Engineering in Medicine and Biology Magazine* **22**[2], 27–31
- [92] Salthouse TA (2004). What and When of Cognitive Aging. *Current Directions in Psychological Science* **13**[4], 140–144
- [93] Shumway-Cook A and Woollacott M (2000). Attentional demands and postural control: the effect of sensory context. *The Journals of Gerontology. Series A: Biological Sciences and Medical Sciences* **55**, M10–6

- [94] Soames RW and Atha J (1982). The spectral characteristics of postural sway behaviour. *European Journal of Applied Physiology* **49**, 169–177
- [95] Soechting JF and Berthoz A (1979). Dynamic role of vision in the control of posture in man. *Experimental Brain Research* **36**, 551–561
- [96] Sparto PJ, Jasko JG, and Loughlin PJ (2004). Detecting postural responses to sinusoidal sensory inputs: a statistical approach. *IEEE Transactions on Neural Systems and Rehabilitation Engineering* **12**[3], 360–366
- [97] Spong MW and Vidyasagar M (1989). Robot Dynamics and Control. *John Wiley & Sons*
- [98] Stelmach GE, Zelaznik HN, and Lowe D (1990). The influence of aging and attentional demands on recovery from postural instability. *Aging (Milano)* **2**, 155–161
- [99] Sundermier L, Woollacott MH, Jensen JL, and Moore S (1996). Postural sensitivity to visual flow in aging adults with and without balance problems. *The Journals of Gerontology. Series A: Biological Sciences and Medical Sciences* **51**, M45–52
- [100] van Asten WN, Gielen CC, and Denier van der Gon JJ (1988). Postural adjustments induced by simulated motion of differently structured environments. *Experimental Brain Research* **73**, 371–383
- [101] van der Kooij H, Jacobs R, Koopman B, and Grootenboer H (1999). A multisensory integration model of human stance control. *Biological Cybernetics* **80**, 299–308
- [102] van der Kooij H, Jacobs R, Koopman B, van der Helm F (2001). An adaptive model of sensory integration in dynamic environment applied to human stance control. *Biological Cybernetics* **84**, 103–115
- [103] Vuillerme N, Nougier V, and Teasdale N (2000). Effects of a reaction time task on postural control in humans. *Neuroscience Letters* **291**, 77–80
- [104] Winter DA, Prince F, Frank JS, Powell C, and Zabjek KF (1996). Unified theory regarding A/P and M/L balance in quiet stance. *Journal of Neurophysiology* **75**, 2334–2343
- [105] Winter DA. Biomechanics and motor control of human movement. *New York: Wiley*
- [106] Winter DA, Patla AE, Prince F, Ishac M, and Gielo-Perczak K (1998). Stiffness control of balance in quiet standing. *Journal of Neurophysiology* **80**, 1211–1221
- [107] Winter DA, Patla AE, Rietdyk S, and Ishac MG (2001). Ankle muscle stiffness in the control of balance during quiet standing. *Journal of Neurophysiology* **85**, 2630–2633
- [108] Young LR and Meiry JL (1968). Revised dynamic otolith model. *Aerospace Medicine* **39**, 606–608